

# THE APPLICATION OF 3D ANTHROPOMETRY FOR THE DEVELOPMENT OF HEADGEAR

A case study on the design of ergonomic brain-computer interface devices

DANIËL LACKO



Department of Product Development  
Faculty of Design Sciences  
University of Antwerp

Department of Neurosciences  
Faculty of Medicine  
KU Leuven

March 2017

## **Supervisors:**

Prof. Stijn Verwulgen (UAntwerp)  
Prof. Jan Sijbers (UAntwerp)  
Prof. Marc M. Van Hulle (KU Leuven)

"De toepassing van 3D antropometrie voor de ontwikkeling van hoofddeksels - een onderzoek naar het ontwerp van ergonomische brein-computer interface toestellen."

Proefschrift voorgelegd voor het verkrijgen van de graad van doctor in de Productontwikkeling en de graad van doctor in de Biomedische Wetenschappen.

Daniël Lacko: *The application of 3D anthropometry for the development of headgear*, A case study on the design of ergonomic brain-computer interface devices, © March 2017

*Dedicated to my grandfather, Drago Lacko. His perseverance and his  
patience will always be an inspiration.*



## FOREWORD

---

Back in 2010, my fellow engineering students and I were presented with the choice to either do a traditional master thesis in one of the ongoing research topics within electronics-ICT, or to join a multidisciplinary team and perform the master thesis as part of a larger project at Product Development. I had never even heard of Product Development at that point, but I decided to go for the latter option. (I had a habit of picking the unconventional or unpopular options at the time.) I never imagined I would find it so interesting that I would eventually decide to stay at Product Development to pursue a PhD. I'm happy to say that -although the past four years have been anything but easy- in the end I don't regret that decision. Product Development offers a unique blend of creative and scientific disciplines, as well as a strong focus on the end user, which I had unknowingly missed in all my engineering projects. If there is one thing I've learned during my PhD that I value above all others, it is the ability to apply my analytical and technical skills to solve human problems instead of purely technical ones.

One of such problems, presented to me at the start of my PhD, is the fact that EEG caps (used to position and fixate electrodes on a user's head during brainwave measurement) are unfashionable, uncomfortable, and practically unusable by the average person. In order to create brain-computer interfaces that work well at home, a new method or device needed to be conceived. Of course, 'simply' designing a new product is not an academic pursuit. However, brain-computer interfacing is a relatively new field and the design of such a device presents a number of challenges, a lot of which were already being addressed by various research groups (e.g. dry electrodes, better signal processing) and companies (e.g. non-stigmatising aesthetics). Luckily, there was one crucial element of the BCI headset design that received less attention: making the device fit a wide variation of human head shapes. An especially challenging element, because of the requirements for electrodes to be positioned at predefined locations and make electric contact with the skin surface.

Upon researching this problem, it soon became clear that the traditional approach to making products fit -basing the design on the variation in one-dimensional head measurements- would not work. The values derived from a limited set of measurement might offer a reasonable interpretation of overall head size, but do not contain any information on the local shape variation at electrode locations. A new design approach was required, and thus I ended up collecting a large number of 3D images of the human head, creating a statistical

shape model and evaluating whether it accurately represented local and global shape changes.

Before I could get around to celebrating the results, a new question arose: how should these kind of 3D models be used in product development? I've spent the most part of my PhD on finding an answer to this question. Throughout my work, I've mainly focused on EEG electrode placement, both as a use case and for verification of the new design method. Unfortunately, I've never finished a working BCI prototype, though I am convinced that this design method will lead to development of more ergonomic BCI headsets. Furthermore, the design method can also be expanded to other types of headgear (e.g. helmets or respirators), or other near-body products as soon as new 3D shape models of become available.

Since my PhD seems to have led me to a different field of study almost every year (neuroscience, medical and 3D image processing, product development), I admit that it was quite a challenge to present all my research projects as a coherent whole. I've considered various approaches, but ultimately decided that it was best to structure this thesis in the same order as the work was performed. I hope I've managed to fit all of it together properly.

## ABSTRACT

---

In this doctorate, the possibilities of 3D anthropometry for product development were explored by applying a statistical shape model of the human scalp to the design of more ergonomic brain-computer interface (BCI) headsets. First, a statistical shape model of the human scalp was created from a set of 100 MRI scans. This model was parametrized by intuitive anthropometric measurements and evaluated in terms of its ability to predict complete scalp surfaces given a set of anthropometric measurements. Using eight anthropometric measurements resulted in an average prediction error of only  $1.60 \pm 0.36$  mm, indicating the model accurately represents the underlying population. The choice of parametrization measurements should be based on their combined prediction errors, their sensitivity to variation in input measurements and a minimum population percentage that remains below a predetermined prediction error threshold. Next, the use of the statistical shape model for comparing the morphological differences between subpopulations and the application to the design of BCI headsets were briefly discussed. After this, the shape model of the scalp was used for the design of one-size-fits-all BCI headset with 14 electrode channels. Electrode placement, stability and reliability of the prototype headset were evaluated and compared to current EEG practices, as well as to a commercial BCI headset. The prototype met all design standards and performed well within EEG practices. It also offered 10% improvement in electrode placement according to the international 10-20 system and a 15% increase in reliability. A functional headset of this type would therefore be more consistent in longitudinal BCI studies and between studies of different research groups. The results prove that 3D anthropometry is a feasible design method for a one-size-fits-all BCI headset. Following this observation, the application of 3D anthropometry for product sizing was considered. Whereas sizing systems are usually based on statistical clustering of one-dimensional head measurements, a new method for 3D head shape clustering was proposed, taking into account the need for intuitive sizing and simple sizing tables. The method was labeled "constrained clustering" and was compared to clustering of traditional anthropometric features as well as unconstrained k-medoids clustering of the 3D shapes. Intra- and inter-cluster scalp shape variability and within-cluster point-to-point distances were used as criteria. The results of constrained clustering were similar to those of unconstrained k-medoids clustering of head shapes and offered a 20.69% improvement in cluster validity index and a decrease of size-weighted variances by 6.6% compared to traditional feature-based

clustering. This research resulted in three journal publications that form the main part of this thesis. This doctorate proves that head-based products that require accurate shape and size fit would benefit from a design process in which 3D shape models are included, and that 3D anthropometry has a place in the product design process. Compared to traditional anthropometry, the use of 3D anthropometry will result in devices that are better fitting, more comfortable and potentially even more functional.

## SAMENVATTING

---

*In dit doctoraat werden de mogelijkheden van 3D antropometrie binnen productontwikkeling onderzocht door de toepassing van statistische vormmodellering voor het ontwerp van meer ergonomische en gebruiksvriendelijke brein-computer interface (BCI) headsets. Allereerst werd er een statistisch vormmodel van de menselijke scalp gemaakt aan de hand van 100 MRI scans. Aan dat model werden intuïtieve antropometrische metingen gekoppeld, en er werd vervolgens onderzocht met welke nauwkeurigheid het model hoofdvormen kon voorspellen en hoe gevoelig het was voor meetfouten. Het gebruik van acht antropometrische metingen als parameters zorgde voor een gemiddelde voorspellingsfout van slechts  $1.60 \pm 0.36$  mm. Hoewel dit model op zichzelf gebruikt zou kunnen worden voor antropometrische studies (bijvoorbeeld om verschillende populaties met elkaar te vergelijken), werd in dit werk voornamelijk onderzocht hoe het binnen productontwikkeling gebruikt zou kunnen worden voor het ontwerp van hoofddeksels die betere aansluiten op de variatie in vorm en grootte van menselijk hoofd. Daarom werd in het tweede deel van het onderzoek een methode voorgesteld om een one-size-fits-all BCI-headset te maken, waarbij de elektroden goed contact maken met de schedel op vooropgestelde locaties. Om deze methode te verifiëren werd een (niet-functionele) 3D-geprinte BCI-headset vergeleken met een klassieke EEG-kap en met een commerciële BCI-headset. Het prototype presteerde 10-15% beter dan het commerciële equivalent op vlak van plaatsing van elektrodes en herhaalbaarheid, wat bewijst dat de voorgestelde methode een goed alternatief is voor traditioneel antropometrisch ontwerpen. In een derde deel van het werk werd het statistische vormmodel gecombineerd met k-medoids clustering om een nieuwe methode voor maatvoering te bieden. De nieuwe clustering-methode werd theoretisch geverifieerd door de Ray-Turi index, size-weighted variance en gemiddelde intra-cluster punt-tot-punt-afstanden te vergelijken met die van maatvoering gebaseerd op traditionele antropometrische metingen. De methode scoorde beter dan traditionele maatvoering op vlak van zowel de Ray-Turi index (verlaging van 20.69%) als op size-weighted variance (verlaging van 6.6%). Intra-cluster punt-tot-punt-afstanden waren vergelijkbaar voor alle methodes, wat erop wijst dat de nieuwe methode geen negatieve impact zou mogen hebben op de werklust van de ontwerper. Tenslotte werd een methode gepresenteerd om deze clustering*

*methode op basis van 3D antropometrie toe te passen op de maatvoering van BCI-headsets. Deze drie onderwerpen zijn verwerkt in drie wetenschappelijke publicaties, waar deze thesis uit is samengesteld. Dit doctoraat bewijst dat hoofddeksels die een nauwkeurige pasvorm nodig hebben, zoals BCI-headsets, baat zouden hebben bij een ontwerpproces waarin 3D vormmodellen worden gebruikt. Vergeleken met traditionele antropometrie, zal het gebruik van 3D antropometrie resulteren in toestellen die beter passen, comfortabeler zijn en mogelijk zelfs beter werken.*



## PUBLICATIONS

---

This doctorate has resulted in the following conference publications:

- [1] **Daniël Lacko**. „Smart Textiles: From Creative Engineers to Practical Product Developers.” In: *Research Lounge #3*. 2012, pp. 24–25.
- [2] Sarah Rohaert, **Daniël Lacko**, and Chris Baelus. „Project Work on Wellbeing in Multidisciplinary Student Teams: A Triple Testimonial on EPS at Artesis.” In: *Design Education for Future Wellbeing*. 2012, pp. 543–548.
- [3] **Daniël Lacko**, Toon Huysmans, Stijn Verwulgen, Paul M. Parizel, Marc M. Van Hulle, and Jan Sijbers. „Statistical shape modelling in support of user-centred BCI headset design.” In: *BBCI Workshop 2012 on Advances in Neurotechnology*. 2012.
- [4] Jan Steckel, Frank Goethijn, Guido De Bruyne, Vincent Nulens, **Daniël Lacko**, Samuel Bey, and Stijn Verwulgen. „A Research Platform using Active Local Cooling directed at Minimizing the Blood Flow in Human Fingers.” In: *7th International Conference on Pervasive Computing Technologies for Healthcare*. 2013.
- [5] Femke Danckaers, Toon Huysmans, **Daniël Lacko**, A. Ledda, Stijn Verwulgen, Stefan Van Dongen, and Jan Sijbers. „Correspondence Preserving Elastic Surface Registration with Shape Model Prior.” In: *International Conference of Pattern Recognition*. Vol. 22. 2014, pp. 2143–2148. DOI: [10.1109/ICPR.2014.373](https://doi.org/10.1109/ICPR.2014.373).
- [6] Stijn Verwulgen, **Daniël Lacko**, Guido De Bruyne, Femke Danckaers, Naomi Christis, Jan Sijbers, and Toon Huysmans. „Anthropometrics 2.0: Enrichment of Classical Anthropometry through Multidisciplinary Collaboration.” In: *6th International Conference on Engineering & Product Design Education*. 2014.
- [7] **Daniël Lacko**, Toon Huysmans, Annelies Claeskens, Stijn Verwulgen, Peter Aerts, Jan Sijbers, and Guido De Bruyne. „An Anthropometric Shape Model for the Design of Sports Helmets.” In: *European Conference on Protective Clothing (ECPC)*. 2014.
- [8] Jochen Vleugels, **Daniël Lacko**, Guido De Bruyne, Toon Huysmans, and Stijn Verwulgen. „Physical Evaluation of an Anthropometric Shape Model of the Human Scalp.” In: *Proceedings of the 6th International Conference on 3D Body Scanning Technologies, Lugano, Switzerland, 27-28 October*. Hometrica Consulting. Hometrica Consulting, 2015. DOI: [10.15221/15.161](https://doi.org/10.15221/15.161). URL: <http://dx.doi.org/10.15221/15.161>.

- [9] Femke Danckaers, Toon Huysmans, **Daniël Lacko**, and Jan Sijbers. „Evaluation of 3D Body Shape Predictions Based on Features.” In: *6th International Conference on 3D Body Scanning Technologies*. Lugano, Switzerland, 2015, pp. 258–265. DOI: [10.15221/15.258](https://doi.org/10.15221/15.258).

And the following journal publications:

- [1] **Daniël Lacko**, Toon Huysmans, Paul M. Parizel, Guido De Bruyne, Stijn Verwulgen, Marc M. Van Hulle, and Jan Sijbers. „Evaluation of an anthropometric shape model of the human scalp.” In: *Applied Ergonomics* 48 (2015), pp. 70–85. DOI: [10.1016/j.apergo.2014.11.008](https://doi.org/10.1016/j.apergo.2014.11.008).
- [2] **Daniël Lacko**, Jochen Vleugels, Erik Fransen, Toon Huysmans, Guido De Bruyne, Marc M. Van Hulle, Jan Sijbers, and Stijn Verwulgen. „Ergonomic design of an EEG headset using 3D anthropometry.” en. In: *Applied Ergonomics* 58 (Jan. 2017), pp. 128–136. DOI: [10.1016/j.apergo.2016.06.002](https://doi.org/10.1016/j.apergo.2016.06.002).
- [3] **Daniël Lacko**, Jochen Vleugels, Toon Huysmans, Guido De Bruyne, Marc M. Van Hulle, Jan Sijbers, and Stijn Verwulgen. „Product sizing with 3D anthropometry and k-medoids clustering.” en. In: *submitted to Computer-Aided Design* ().

Of this list, those publications that are referred to in the rest of the thesis have also been added to the bibliography section. Whenever a work is referenced in the thesis, the reader should always refer to the bibliography and not to the list of publications above.

## DANKWOORD

---

Waar begin ik? Hoewel het vaak zo aanvoelt, is een doctoraat nooit een individueel werk. Er zijn altijd enorm veel mensen betrokken bij het tot stand brengen van zo'n project; teveel om in een dankwoord op te sommen. In dit specifieke geval heeft het weinig gescheeld of ik had het document dat voor u ligt nooit geschreven. Het feit dat de volgende honderdtal pagina's niet blanco zijn, is onder andere aan de volgende mensen te danken.

Eerst en vooral bedank ik mijn promotoren prof. Stijn Verwulgen, prof. Marc Van Hulle en prof. Jan Sijbers om mij de kans te geven om aan dit doctoraat te werken, en voor het geduld wanneer de deadline telkens verder vooruit werd geschoven. Ik wil ook prof. Guido de Bruyne bedanken om me de laatste maanden de nodige ruimte te geven deze thesis af te werken.

Vervolgens dank ik Dr. Toon Huysmans voor al zijn hulp, zowel voor het maken van het vormmodel waarop deze thesis is gebaseerd als voor de begeleiding bij de niet-wetenschappelijke uitdagingen van het doctoraatsleven (ik heb nog altijd ergens die presentatie over de "second year slump" staan).

Zonder Jochen Vleugels zou mijn doctoraat beperkt zijn gebleven tot theoretische simulaties en zou ik wellicht nooit helemaal hebben begrepen wat Productontwikkeling inhoudt. Ik ken niemand die zo praktisch is ingesteld als Jochen. Bedankt voor de vele gesprekken en de verhelderende discussies. Oh ja, en voor het ontwerpen, CAD-tekenen en 3D-printen van alle prototypes.

Ik dank mijn vader Dado, moeder Ivančica (Eva) en zus Mathea voor hun steun en bemoediging. Bedankt om in mij te blijven geloven op de momenten dat ik dat zelf niet meer deed, en voor alle "nog efkens!".

Ik heb bovendien het geluk gehad om eenentwintig jaar na mijn geboorte een tweede paar ouders bij te hebben gekregen. Bedankt, Kurt en Marleen, voor al die jaren dat ik bij jullie een tweede thuis heb gehad.

En zoals gebruikelijk heb ik de laatste plaats bewaard voor de meest bijzondere persoon. Opnieuw: waar begin ik? Bedankt, schat, voor alles. Jij hebt me, meer dan wie anders, op mijn allerslechtste

gezien de afgelopen jaren. Bedankt voor je onvoorwaardelijke liefde. Ik kijk enorm uit naar ons leven samen.

Voilà. Aan allen die vernoemd zijn, proficiat. Aan allen die niet vernoemd zijn, ook proficiat, want ik ben ongetwijfeld nog belangrijke mensen vergeten. Aan iedereen die na het lezen van deze pagina denkt "hoe, en ik dan?": ook al heb ik het niet opgeschreven, ik weet wat ik aan je heb gehad. Bedankt!

Daniël Lacko, 7 augustus 2016

# CONTENTS

---

<b>I</b>	<b>INTRODUCTION</b>	<b>1</b>
1	INTRODUCTION	3
1.1	Basic principles of brain-computer interfacing	4
1.1.1	Measuring bioelectric brain activity	5
1.1.2	The 10-20 system for electrode positioning	5
1.1.3	Components of brain-computer interfacing devices	7
1.1.4	An example of currently available BCI devices	7
1.2	Usability and ergonomics aspects of BCI devices	11
1.2.1	A comparison of the usability of three types of BCI devices	11
1.2.2	Literature survey of BCI usability and ergonomics	16
1.2.3	Essential design requirements for consumer-grade BCI headgear	17
1.3	Designing products that fit the human head	19
1.3.1	Definition of anthropometry and ergonomics	19
1.3.2	Anatomy and anthropometry of the human head	20
1.3.3	The distinction between traditional anthropometry and 3D anthropometry	26
1.3.4	General design methods for physical ergonomics	29
1.3.5	Example of headgear design: sports and motorcycle helmets	32
1.3.6	The need for more detailed head models	35
1.4	Research questions	35
<b>II</b>	<b>RESEARCH PAPERS</b>	<b>37</b>
2	EVALUATION OF AN ANTHROPOMETRIC SHAPE MODEL OF THE HUMAN SCALP	39
2.1	Abstract	39
2.2	Introduction	40
2.3	Methods	41
2.3.1	Building the shape model	41
2.3.2	Extending the shape model with anthropometric measurements	45
2.4	Experiments	50
2.4.1	Determining the distribution of the prediction errors	50
2.4.2	Evaluating the data set size	52
2.4.3	Sensitivity Analysis of Mapping Algorithm	53
2.5	Results and Discussion	53
2.5.1	Data Set and ROI Selection	54
2.5.2	Selecting an appropriate shape model	54

2.5.3	Application for anthropometric research: comparison of male and female population	60
2.5.4	Application for industrial design: design of a brain-computer interface	65
2.6	Conclusion	68
2.7	Acknowledgments	69
3	ERGONOMIC DESIGN OF AN EEG HEADSET USING 3D ANTHROPOMETRY	71
3.1	Abstract	71
3.2	Introduction	72
3.2.1	Brain-computer interfacing	72
3.2.2	BCI headsets	73
3.2.3	3D anthropometry and ergonomics	75
3.3	Methods	77
3.3.1	Prototype design	77
3.3.2	Experiment design	79
3.4	Results	83
3.4.1	Verification of design specifications	83
3.4.2	Comparison to commercial reference	83
3.5	Discussion	85
3.5.1	3D anthropometry in product design	86
3.5.2	Choice of variables	86
3.5.3	Fit to 10-20 electrode positions	87
3.5.4	Stability	87
3.5.5	Repeatability	88
3.5.6	Limitations of current study	88
3.6	Conclusion	89
4	PRODUCT SIZING WITH 3D ANTHROPOMETRY AND K-MEDOIDS CLUSTERING	91
4.1	Abstract	91
4.2	Introduction	93
4.2.1	Product sizing based on anthropometric features	93
4.2.2	Product sizing based on 3D anthropometry	94
4.3	Methods	97
4.3.1	Data acquisition	97
4.3.2	Statistical analysis of shape variation	97
4.3.3	Dissimilarity between 3D shapes	100
4.3.4	Mathematical clustering of 3D shape model using k-medoids	101
4.3.5	Constrained clustering	103
4.3.6	Evaluating clustering quality using cluster validity indices	108
4.3.7	Product-related clustering metrics	109
4.4	Results	112
4.4.1	Comparison of clustering methods using cluster validity indices	112

4.4.2	Point-to-point distances and minimum-maximum envelopes in k-medoids constrained clustering	114
4.4.3	Selecting features for sizing and constraints	116
4.4.4	Varying the number of constraints in constrained clustering	117
4.5	Discussion	117
4.5.1	The effect of the statistical shape modeling characteristics	118
4.5.2	Performance of clustering methods	119
4.5.3	Interpretation of cluster metrics	120
4.5.4	Selecting features for sizing and constraints	121
4.5.5	Selecting the optimal number of sizes and creating representative manikins	121
4.5.6	Creating intuitive sizing tables	125
4.5.7	The disadvantages of shape-based clustering	126
4.5.8	Future work	127
4.6	Conclusion	128
III	DISCUSSION	129
5	DISCUSSION	131
5.1	Summarized answers to the research questions	131
5.1.1	How well can the global and local shape variation of the human scalp be quantified in a statistical shape model?	131
5.1.2	Does the use of shape models have an impact on the geometric fit, stability and repeatability of EEG sensors in BCI-equipment?	131
5.1.3	How can 3D anthropometry be implemented in product sizing to create better fitting headgear?	132
5.2	Shape variation of the human scalp	133
5.3	The use of 3D anthropometry in the product design process	138
5.4	Case study: simplified design process for BCI headset in three sizes	143
5.4.1	Analysis phase	144
5.4.2	Synthesis phase	145
5.4.3	Simulation phase	148
5.4.4	Evaluation phase	150
5.5	Evaluation of prototype BCI headsets according to essential design requirements	152
5.6	Expected impact of shape models on the design of BCI headgear	154
5.7	Suggestions for future research	155
IV	CONCLUSION	159
6	CONCLUSION	161

xviii CONTENTS

BIBLIOGRAPHY 165

## ACRONYMS

---

AL Arc Length

ALS Amyotrophic Lateral Sclerosis

API Application Programming Interface

ASIC Application-Specific Integrated Circuit

AW Arc Width

BCI Brain-Computer Interface

BNCI Brain/Neural Computer Interfacing

BW Bitracion Width

CAD Computer-Aided Design

CDF Cumulative Distribution Function

CEN European Committee for Standardization (Comité Européen de Normalisation)

CF Circumference

CT Computed Tomography

CVA Cerebro-Vascular Accident

CVI Cluster Validity Index

DOT Department Of Transport

EH Ear Height

ECE Economic Commission for Europe

EEG Electroencephalography

ERP Event-Related Potential

FW Face Width

HE Horizontal position of the Ear

HL Head Length

I Inion

ICBM International Consortium for Brain Mapping

- ISO International Organization for Standardization
- LPA Left Pre-Auricular point
- MRI Magnetic Resonance Imaging
- MS Multiple Sclerosis
- N Nasion
- NASA National Aeronautics Space Administration
- NEN NEDerlandse Norm
- PC Principal Component
- PCA Principal Component Analysis
- PE Projected Ear Height
- PLS Primary lateral sclerosis
- POI Point(s) Of Interest
- ROI Region Of Interest
- RPA Right Pre-Auricular point
- SSM Statistical Shape Model
- SSVEP Steady-State Visually Evoked Potential
- SVD Singular-Value Decomposition
- SWV Size-Weighted Variance
- URL Uniform Resource Locator
- US United States
- UZA University Hospital of Antwerp (Universitair Ziekenhuis Antwerpen)
- VE Vertical position of the Ear
- VLSI Very-Large-Scale Integration

Part I

INTRODUCTION



## INTRODUCTION

---

"At the moment BCIs are almost exclusively used in lab settings. In order for BCIs to be successful interaction paradigms, the top level challenge is: successfully migrating BCI out of the lab, into the everyday and working lives of people." This was one of the conclusions drawn from the Future BNCI project in 2012 [1], in which the state of the brain-computer interfacing (BCI) field was analyzed and suggestions for future research were formulated. The aim of BCI is to directly or indirectly connect the human brain to digital devices through the use of electrodes that measure brainwave activity, in order to bypass muscular pathways and to provide new opportunities for human-machine interaction and diagnostics. The field has gathered an increasing amount of interest, credibility [2], and even a new academic journal [3] since the report was published. Furthermore, an increasing number of companies has put commercial BCI devices on the market [4] with various degrees of (commercial) success. Yet despite the enthusiasm, not much has been done with the observations in the BNCI 2012 report. Although numerous applications and algorithms are reported in scientific journals, including alternative communication for physically disabled people, rehabilitation for stroke patients, epilepsy detection, sleep therapy or even new gaming interfaces, most BCI applications to date are still only tested in research labs, using classic electrode caps [2, 3].

Of course, this was just one of many recommendations made in the report and only so much can be done in the course of four years. Still, BCI research continues to remain focused on electric components, signal processing, and applications; and usability and user-centered design are usually considered an afterthought or future research theme. The field of industrial design, as opposed to pure science or engineering, originated from the need for user-centred devices and could provide a solution to this problem. Even though it is sometimes associated with art rather than science, there is a growing demand for evidence-based design in the industry [5, 6]. Clearly, there are key shortcomings in design process of brain computer interfaces that results in sub-optimal BCI hardware. The goal of this thesis is to pinpoint those steps in the design process that need to be reconsidered in order to achieve user friendly BCIs, and to develop the required design tools and techniques to make them usable outside of laboratory settings.

Overall, the structure of this dissertation follows the chronology of the research that preceded it. First, in section 1.1, the basic concepts and terminology of BCI are explored. Section 1.2 discusses the usability issues that were found with a selection of current BCI devices, resulting in a set of user requirements for future devices. One of the major challenges in transitioning BCI devices from the lab to the real world is to create a device that fits the heads of the entire population. General practice involves deriving product dimensions from statistical distributions of head measurements such as circumference. While, under the right conditions, this can result in product models with the proper global size variation, local shape variations of the head at custom electrode positions are impossible to predict using traditional anthropometry. Section 1.3 is about traditional design methods to make products fit, the anatomy and anthropometry of the human head, and the introduction of 3D anthropometry, that theoretically makes it possible to create digital human models that capture shape variations more accurately. The exploration of the usability of BCI devices and of the ergonomics of head products was translated in a number of research questions, which are stated in section 1.4.

Because 3D anthropometry of the human head is still under development, it is important to explore how exactly shape models could be used to create more ergonomic headgear. Chapters 2, 3 and 4 contain three journal publications that were written in the course of this doctorate, with each of the publications addressing one of the research questions. While the presented design methods can be generalized to all kinds of near-body products, BCI devices and electrode fit are the main use case throughout this dissertation. In this way, the work brought out of the theoretical realm, making it possible to discuss the design method concretely and to gather evidence for its added value.

Finally, the implications of the proposed methods to the design of BCI headgear are presented in chapter 5, and, as is customary, chapter 6 concludes the work and provides a summarized answer to the research questions.

### 1.1 BASIC PRINCIPLES OF BRAIN-COMPUTER INTERFACING

Brain activity causes small electric potentials, a measure of which can be recorded non-invasively with electrodes placed on the scalp. These so called electroencephalographic (EEG) components can be evoked in response to internal and external stimuli or events (i.e., EEG paradigms) and can be extracted by signal processing techniques [7]. Jacques Vidal was the first to demonstrate a Brain Computer Interface (BCI), a technique that allows subjects to communicate with their environment without the need for speech, gestures, or any voluntary muscular activity [8]. By virtue of this, BCIs have raised great hopes to improve the quality of life of patients suffering from severe

muscular disorders such as amyotrophic lateral sclerosis (ALS), multiple sclerosis (MS) and cerebrovascular accidents (CVA or stroke) by assisting in their communication needs [1, 2, 9]. While most BCI applications rely on non-invasive electrodes placed on the scalp, invasive EEG electrodes implanted on the brain surface have also been developed. However, as invasive electrodes require surgery and are prone to signal deterioration due to gliosis and scarring, non-invasive BCIs have gained much interest. BCI is a big and multidisciplinary field that is already adequately reviewed in other works (e.g. [1]). Therefore, this chapter is limited to a brief introduction of those aspects of BCI that are required to understand the rest of the thesis.

### 1.1.1 *Measuring bioelectric brain activity*

In the past years, characteristic EEG signals relating to specific events and human behavior have been described in literature. The most extensively studied of these are the Steady State Visual Evoke Potential or SSVEP [9] and the Event-Related Potentials (ERP) P300 and N400 [10]. In an SSVEP BCI paradigm, several targets are simultaneously displayed, each one with a different stimulation frequency, and the target onto which the subject's gaze is directed is decided from the EEG recorded from the subject's scalp by verifying the presence of the corresponding stimulation frequency, after which the associated action is executed or a physiological conclusion is drawn. Deviations in the SSVEP characteristics have since long been used for diagnostics [11], selecting items on a screen [12, 13] and for mentally typing text (mind spelling, see [14]). In a P300 ERP paradigm, the P300 peak can be detected while a subject is shown two types of stimuli with one occurring much less frequently than the other ("rare event"). The rare event elicits an ERP consisting of an enhanced positive-going signal component with a latency of about 300 ms after stimulus onset. This paradigm is mainly used for mind spelling, in which a user spells words by selecting letters on a computer screen using a BCI device [15–20]. Lastly, the N400 ERP is a cognitive EEG component consisting of a negative going wave that reaches its peak around 400 ms after stimulus onset. In clinical assessment studies [21], the N400 potential has been used for diagnosing patients with semantic comprehension deficits, for elucidating the nature and extent of their disorder, and for guiding therapeutic interventions [22].

### 1.1.2 *The 10-20 system for electrode positioning*

Generally, electrode positions for EEG measurements are distributed on the subject's scalp along the classical international 10-20 reference system, in which electrodes are placed at 10% and 20% increments on surface curves on the scalp between four anatomical reference

points: nasion, inion, left and right preauricular point, respectively named Nz, Iz, T9 and T10 in the 10-20 system [23]. A depiction of the anatomical reference points can be found in section 1.3.2. For a detailed discussion on how electrodes are placed in the 10-20 system, please see chapter 3. The electrode locations according to the 10-20 system are shown in figure 1 (black circles). The so-called Modified Combinatorial Nomenclature is used in this figure, meaning that the names of some electrodes are different than presented in the original 10-20 system: T7, T8, P7 and P8 were originally named T3, T4, T5 and T6, respectively [24].

Different paradigms require different spatial configurations and a different number of electrodes, usually 6-32 for P300 [25]. For example, in the Lab of Neurophysiology of prof. M. Van Hulle the following electrode positions are used as a minimum: FCz, Cz, CP1, CP2 and Pz for the P300; F3 on the temporal lobe for the N400; Cz, Pz, O1, Oz and O2 for the SSVEP. TP9 and TP10, the mastoids, are used as reference.

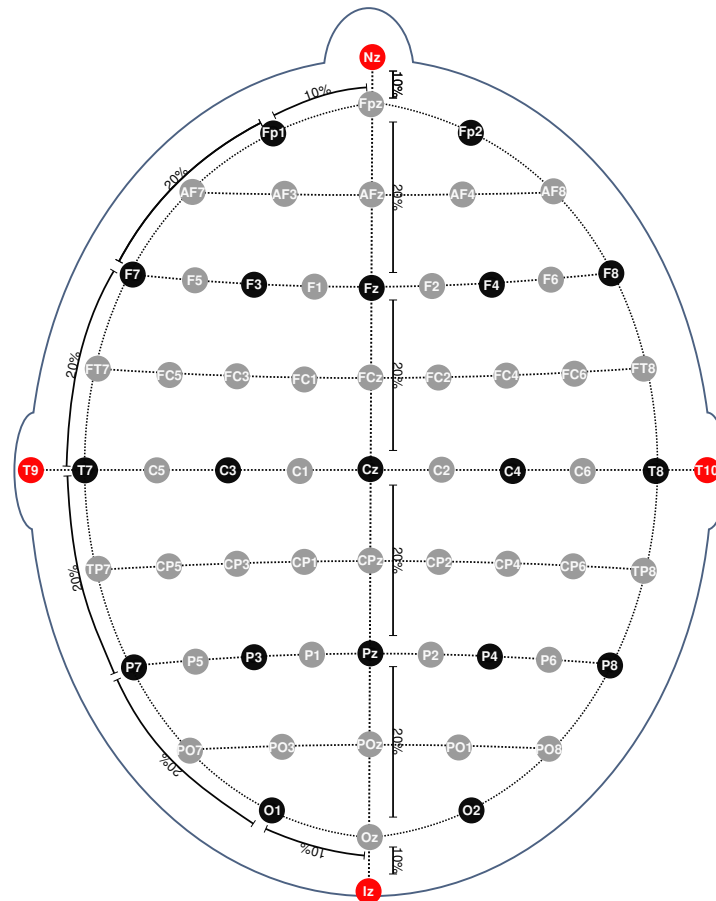


Figure 1: 10-20 electrode placement layout, with anatomical reference points Nz, Iz, T9 and T10 shown as red circles. Black circles represent electrode locations according to the original 10-20 layout, grey circles are part of the 10-10 system.

While the 10-20 system is essential in order to be able to compare EEG and BCI research studies, it does have a number of limitations. Firstly, it only covers a very limited number of electrodes, which is not sufficient for all BCI paradigms. Because of this, it has since been expanded into the 10-10 and 10-5 systems, which offer a much higher spatial resolution. Some electrodes of the 10-10 system are shown in figure 1 in grey. Secondly, it depends on the correct identification of a number of anatomical reference points. In many cases, this will be done by a trained specialist such as a nurse or an EEG technician. However, electrode positions tend to vary depending on the training and experience of the person placing the electrodes, and on their interpretation of the ambiguous descriptions of the anatomic reference points [26]. This inter-observer variability affects the ability to detect the targeted EEG patterns without retraining the detection algorithm, although in general EEG practice an electrode displacement (radius) of 2 cm is accepted in exchange for a loss in detection accuracy (without retraining).

### 1.1.3 *Components of brain-computer interfacing devices*

A BCI device roughly consists of the following components [1], depicted in figure 2:

- The electrodes are used to capture the EEG signals from a user's scalp. These electrodes can be of the active wet- (gel-based or water-based) or dry type.
- The frame of the headset holds the electrodes and the electronics and is ideally designed in such a way that when the user puts on the headset the electrodes make immediate contact with the scalp at preselected locations, usually according to the 10-20/10-10/10-5 system (depending on the EEG paradigm).
- The headset uses various types of electronic components and circuits. The signals first pass through an active readout circuit and are then acquired by an application specific integrated circuit (ASIC: for example [27]) that amplifies, filters, and possibly samples the EEG signals before they are transmitted through a microcontroller for transmission to the receiver.

### 1.1.4 *An example of currently available BCI devices*

In laboratory settings, it is customary to use electrode caps with gel-based Ag/AgCl electrodes, as in figure 3. The advantage of the cap is its flexibility and elasticity, ensuring that it can be perfectly formed around the user's head and tightened so the electrodes are sure to

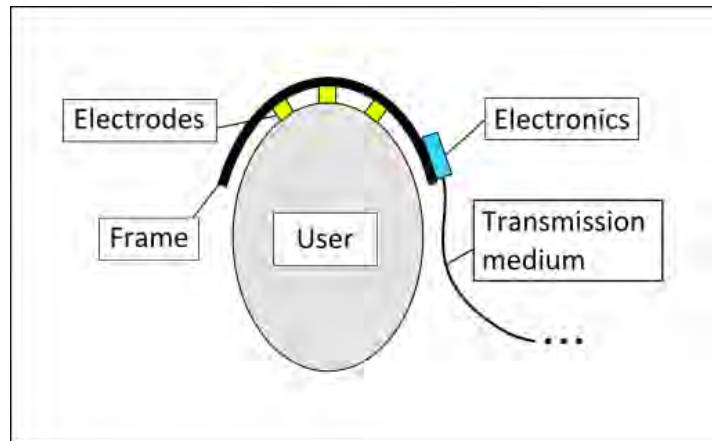


Figure 2: Basic components of a brain-computer interface (BCI).

make contact. Another advantage is that EEG caps contain holes (to attach electrodes) at predefined locations, usually following the 10-20 system or its derivatives. This means that there is no need to manually take measurements and locate a number of physical landmarks by palpation (although the nasion and inion are still required), decreasing the set-up time and spreading the electrodes evenly across the subject's scalp. An innovative alternative to traditional EEG caps that does not require the electrodes to be placed one-by-one, nor any preparation of the skin or usage of conducting gel, is Geodesic Sensor Nets (GSNs) [28]. These products work on the same principle as EEG caps by placing the electrodes in a flexible net and stretching it over the user's head, thereby automatically receiving correct relative electrode placement and coverage for as much as 256 electrode channels, provided that the right product size is chosen.

Although EEG caps as of yet provide the best accuracy (after manual placement by a specialist [31]) and GSNs significantly reduce the set-up time, it is easy to see that they are not usable in a home setting by non-specialists, or even outside research laboratories. Therefore, a number of alternatives has been put on the market, with various intended applications. One of the most popular of these is Neurosky's Mindwave. The biggest advantage of this device is that it looks like a regular headset, decreasing the threshold for user acceptance [32]. However, the Neurosky only offers three EEG channels that are always at the same locations, making it a lot less suitable for scientific research. A similar device with a pleasing design but limited electrode channels is the Melon headband. A number of applications exist for both of these devices (especially for the Mindwave), but due to the limited amount of EEG signals that can be captured, only very basic applications such as measuring user attention can be provided. So far, the available applications have seemingly not enticed many developers or users.



Figure 3: EEG cap with gel-based electrodes inserted. Photo by Chris Hope, made available by Tim Sheerman-Chase at [29] through CC BY 2.0 license [30]

A device that has been more extensively covered both in media and in scientific literature is Emotiv's Epoc, shown in figure 4 (a). While the design looks less appealing than that of most other commercial headsets, it does have more electrode channels than any other other commercial EEG device, and the flexible arms on which the electrodes are mounted allow for a decent accommodation to local shape variation on the user's head. However, because Emotiv only offers the hardware and a software application programming interface (API), applications are left to developers. So far, the device has been primarily successful with BCI researchers [4, 33], because it can be used to test and demonstrate a number of basic BCI applications. Contrary to the other headsets shown, electrode-skin contact is ensured through small sponges soaked in a saline solution and that can theoretically

maintain signal quality for 8 hours. Still, apart from early adopters and proof-of-concepts, the author knows of no successful home applications currently available on the market. Recently, Emotiv has created a second headset with dry electrodes, called the Insight (see figure 4 (b)). Similar to most other commercial headsets, this one offers only three electrode channels. As of yet, it is unclear how successful it will be compared to the original one, especially now that the Epoc (recently renamed Epoc+) is targeted specifically at scientific research [34].



Figure 4: Emotiv’s research-grade Epoc+ headset (a) and consumer-grade Insight headset (b). Both images were made available by Wikimedia user Chrisshe at [35] (a) and [36] (b) through the CC BY-SA 4.0 license [37].

Finally, OpenBCI, a company that develops open-source Arduino-based electronic boards for brain-computer interfacing, has also been experimenting with its own 3D printable headsets. Their second version, the "SpiderClaw" model is shown in figure 5. While it was an interesting concept due to the modularity of the device, it had a number of problems regarding fit and fixation [38] and has been discontinued [39]. A new version, called the Ultracortex was recently released.

While this is by no means a comprehensive overview of all commercial BCI devices on the market, it exemplifies the most common design architectures that are followed by all BCI headgear developers: cap, headband, headset-like and custom BCI headsets. While the cap and custom BCI headsets have been more popular in research contexts, devices resembling headbands or headphones are less alien to potential general users and might be more suited for home applications, provided that a sufficiently large number of electrode channels for non-trivial applications can be incorporated.



Figure 5: OpenBCIs second 3D-printed "SpiderClaw" headset prototype.

## 1.2 USABILITY AND ERGONOMICS ASPECTS OF BCI DEVICES

While BCI is a very promising technology for various applications, it is still a relatively new field. As such, most BCI-related research over the past decade has focused on the technical aspects of EEG measurement, mainly signal processing techniques and electronics. There has not yet been much research on the ergonomic and usability-related aspects. As briefly mentioned in section 1.1.4, this results in most commercial BCI devices having complications with headset preparation, electrode locations, head shape and size variation, stability during movement and/or consistency in electrode placement over multiple sessions [1, 26]. This chapter describes a preliminary study on the usability of commercial BCI devices, discusses ergonomic issues that have been raised in existing literature and concludes with a list of user needs for commercial BCI devices.

### 1.2.1 *A comparison of the usability of three types of BCI devices*

At the start of this doctoral project, a preliminary experiment was conducted in order to define the usability issues of several types of BCI devices (manuscript in preparation). 21 people (15 males, 6 females) were asked to play a brain-controlled game using three different BCI headsets: a traditional Biosemi EEG-cap similar to the one in figure 3, the Emotiv EPOC headset (figure 4), and a prototype BCI headset with dry electrodes developed by Imec, shown in figure 6. They wore each headset for a period of 15 minutes and were asked to report on their experience in a questionnaire at the end of each session. Furthermore, any comments they made by either test subject or EEG

technician were noted, and the whole experiment was videotaped to make sure no comments were missed. Finally, the preparation and clean-up time for each headset was also measured.



Figure 6: A prototype BCI headset with dry electrodes, created by Imec for research purposes. Image from NeuroGadget [40].

The results of this experiment can be seen in table 1. Overall, the Imec prototype headset took the least preparation and cleaning time, only 17" combined, yet was deemed to be the most uncomfortable. One participant even asked to terminate the experiment early (after 4'36") because he found the headset too painful. Upon examination, the pressure on the pins of the dry electrodes was indeed such that it caused indentations in the skin, as seen in figure 7.

The outcome of the experiment was somewhat surprising in several regards. For example, while the researchers expected the Biosemi cap to be the most comfortable one based on prior experience and research (e.g. [41]), the participants rated it as less comfortable than the Epoc because of the requirement for wires and conductive gel. Several people also remarked that the chin strap was uncomfortable. One person even decided to withdraw from the experiment when they learned gel was involved. While the electrode calibration did not take long because of good skin contact, placing the electrodes was inconvenient both for the test subject and the EEG technician.

Headset	Avg. set-up time	Avg. clean-up time	Discomfort	User preference
Epoc	8'08"	1'25"	1.36	15/22 (68%)
Imec pro-prototype	0'13"	0'04"	6.64	6/22 (27%)
Biosemi cap	8'31"	7'19"	2.91	1/22 (5%)

Table 1: Results from preliminary EEG usability experiment conducted in 2012. Discomfort was rated on a scale of 0-9, with 1 being no discomfort and 9 being severe pain.

Headset	EEG operator comments
Epoc	<ul style="list-style-type: none"> <li>• Impedance measurement not reliable. Electrode indicators turn green without proper contact.</li> <li>• Difficult to use for people with thick hair.</li> <li>• Electrodes keep falling out of their sockets during set-up.</li> </ul>
Imec prototype	<ul style="list-style-type: none"> <li>• Seems very painful, right from the start.</li> <li>• Incredibly easy to set-up and clean.</li> </ul>
Biosemi cap	<ul style="list-style-type: none"> <li>• Difficult to determine whether enough gel is used.</li> <li>• Not comfortable for people with glasses.</li> <li>• Adjusting the headset and electrodes often requires being in the personal space of test subjects.</li> </ul>

Table 2: Summary of most noticeable EEG operator comments.

Headset	Test subject comments
Epoc	<ul style="list-style-type: none"> <li>• I don't think I would be able to put it on correctly myself.</li> <li>• Takes long to set up with thicker hair.</li> </ul>
Imec prototype	<ul style="list-style-type: none"> <li>• (Very) painful/uncomfortable.</li> <li>• Too much pressure on the headset fixation points, becomes uncomfortable after a while.</li> <li>• Makes it difficult to concentrate.</li> </ul>
Biosemi cap	<ul style="list-style-type: none"> <li>• I don't like the gel.</li> <li>• Chinstrap becomes very uncomfortable after a while.</li> <li>• I don't feel the sensors at all.</li> <li>• Works well, but it takes a long time before all cables are connected.</li> </ul>

Table 3: Summary of most noticeable test subject comments.



Figure 7: Skin indentations and irritation caused by the pressure of the I Mec prototype's bristle electrodes. Photo published with permission of subject.

Therefore, the Biosemi headset scored the worst on all aspects related to usability. That being said, it did fit all user's heads very well.

The Epoc was the preferred EEG-device among the three, with 68% of the user votes. Most users found it very comfortable and did not mind the slightly longer set-up times compared to the I Mec headset. However, from the EEG technician's point of view there were some important usability issues. For example, while it's possible to mount the headset in a matter of seconds, a lot of time is lost adjusting the flexible arms so the electrodes make proper skin contact. In people with thick hair, the technician needs to manually manipulate the sponge containing the saline solution that enables electric contact between the hair. The electrodes or sponges would also often fall out of their sockets, in which case replacing them added to the set-up time. Furthermore, the EEG technician noted that whereas the flexible electrode arms fit local head shape variation very well, for people with larger heads the back brace of the headset needed to be stretched further than intended. Their concern proves valid a couple of years later, as both Epoc devices which were regularly used for experiments or demonstrations have had their back braces break on multiple occasions. The Epoc, therefore, does not accommodate for head size variation well.

Finally, the I Mec prototype headset was rated as the most uncomfortable one. Multiple people described it as painful, and one participant asked to terminate the experiment early because the bristle electrodes caused them too much pain. Even so, contrary to the expectation, almost a third of the participants preferred this headset over

the others. Reasons stated were mainly the design, the simplicity and the fact users felt like they could set it up themselves without any prior EEG knowledge (possibly due to the fact that it resembles common devices such as headphones).

### 1.2.2 *Literature survey of BCI usability and ergonomics*

Several papers from other research institutes mention similar concerns for usability. The FBNCI report from 2012 report states that one of the main requirements for BCI is to shift the focus on usability and user experience, and to elucidate what these are determined by [1]. According to the consortium, it is important to bring BCI out of the lab by creating more reliable, convenient BCI headsets that can be used without expert help. Ekendam et al. state that too much BCI research is focused on data acquisition, signal processing and theoretical foundations, and that there is a need for studies that explore the ergonomic aspects of BCI design in order to reduce usability issues such as comfort during prolonged use or reduced performance for people with long or coarse hair [33]. They reiterate that current commercial devices often suffer from low signal quality, and -similar to the work described above- they found that preparing and adjusting the 14 active electrodes of the EPOC headset to make contact with the scalp takes too long (which they attribute to the sensitivity of sensor placement to hair), and they report that comfort is an important factor in BCI headsets. Hairston et al. also start their work by stating that little objective research is dedicated to the physical features and usability of BCI headsets, even though these have an important impact on the user acceptance [26]. While evaluating the usability of four commercially available BCI systems, they found that participants experience discomfort due to unevenly distributed pressure on the scalp, due to weight or constriction of the BCI system, and/or due to difficulty of application or clean up. Furthermore, they also mention that if more objective studies on BCI headsets are to be performed, consistent electrode placement across different systems is a major challenge and that the intended 10-20 locations of the examined BCI systems were not accurate across participants because the device dimensions could not properly accommodate variability in head sizes and shapes. Nijboer et al. agree that the usability of BCIs is of the utmost importance to ensure that the technology is not abandoned [42]. They performed a survey about BCI perception on sample consisting of rehabilitation professionals and found that none of the participants perceived an added value of BCIs over existing alternatives for augmented and alternative communication. Participants noted that the usability of BCI systems should improve significantly. Nijboer et al. provide a list of 21 requirements to improve BCI usability, many of

which relate to correct fit and electrode placement. Finally, Ahn et al. [4], in reviewing the use of commercial BCI devices by researchers, game developers and users, state that there is a need for simple and precise devices, and that researchers look forward to the development of a convenient BCI device with a high signal quality.

A number of conclusions can be drawn from these publications:

- Firstly, it seems like the main reason many BCI headsets are uncomfortable is because most of the pressure is localized on individual electrodes, depending on the user's head shape. Headsets that use flexible materials to distribute the pressure more evenly tend to score higher in terms of user comfort [26]. Therefore, a uniform distribution of pressure over all electrodes is advisable. This is also confirmed in [41], in which Guger Technology Sahara dry bristle electrodes were tested in an electrode cap, and none of the test subjects mentioned discomfort.
- Secondly, it is vital for a fixed material BCI headset to accommodate for both size (linear scaling) variation and shape variation. In order to better anticipate on both kinds of variation, BCI manufacturers should consult representative anthropometric data for their intended populations.
- Finally, the headset should ideally be designed in such a way that users without prior knowledge can mount the headset with minimal instruction, at least for commercial BCI purposes. Wireless solutions are also preferable to wired ones, and if possible, the design should mimic similar devices which are already known to users.

To summarize, current medical-grade BCI devices are too complex, uncomfortable, and time-consuming. FBNCI lists 20 minutes of preparation for EEG caps, and for applications with 128 electrodes a minimum of 40 minutes is not exceptional. Commercial BCI devices, on the other hand, are inaccurate, often lack functionality and cause discomfort because they do not fit the human head shape and size variation. For the advancement of BCI, it is essential that new commercial BCI devices are created, which can function in real world scenarios and still offer adequate signal quality.

### 1.2.3 *Essential design requirements for consumer-grade BCI headgear*

Based on the above experiment, and on research from [1], [26] and [42], the key requirements for a commercial BCI headset have been defined in table 4. The importance of each need will vary depending on the application (e.g. gaming, alternative communication, research).

<b>ID</b>	<b>primary need</b>	<b>secondary need</b>
1	The sensors are at the correct measurement locations according to the international 10-20 system, with at least the same accuracy as currently used EEG caps.	
2.1		The electrode locations are configurable by the user.
2.2	The device is usable for multiple paradigms.	Multiple software packages can be used with the device.
2.3		Multiple kinds of electrodes can be used with the device.
3	The acquisition cost is low enough for consumers and small laboratories.	
4	The headset can be applied on the user's head by the user.	
5.1		There is only one way to mount the headset correctly.
5.2	The headset makes it possible to perform repeatable measurements and	The sensors are at the same anthropometric locations every time it is put on.
5.3	experiments.	There is an indication of electrode impedance.
5.4		There is an indication of contact pressure.
6.1		Users should not experience discomfort for the duration of experiments.
6.2	The headset fits the shape of user's head optimally.	Users are not distracted by the headset during experiments.
6.3		The sensors constantly make contact with the skin during the experiment.
7.1		It is easy to clean the headset.
7.2	The device does not require a lot of maintenance.	The headset does not take long to set up (< 2 min).
7.3		The device is robust, wires and other components can last multiple sessions without breaking.

Table 4: Requirements for a user-friendly BCI headset that works outside of controlled environment such as a research laboratory.

According to the observations from the experiment described in section 1.2.1 and to the literature survey in section 1.2.2, no commercial BCI device exists at this time that meets all (or even most of) these requirements. The hypothesis is that this is at least partly due to the fact that current BCI headsets do not fit the head properly. On the one hand, this results in electrodes losing contact with the skin and decreases the efficiency of BCI devices, since the electrode pressure should be enough to lower the electrode-skin impedance to 20 – 40k $\Omega$  [43, 44]. On the other hand, electrodes that exert too much pressure on the head cause discomfort or pain, as confirmed by the experiment described above. This work will focus on providing BCI manufacturers and designers with a better understanding of the shape variation of the human head. Once more accurate 1D and 3D anthropometric data of the head is available, this can be used as a basis to improve the ergonomic aspects and a number of functional aspects of BCI headsets (and other products). The scope of this work is therefore limited to improving the physical product fit of BCI headgear (user need 1, 5.1, 5.2 and 6.1 in table 4).

### 1.3 DESIGNING PRODUCTS THAT FIT THE HUMAN HEAD

This section deals with the statistical study of human head shape, and how this knowledge is employed in the process of product development. The head presents an ideal case to explore the added value of 3D anthropometry in product development: dynamic properties such as movement or compression, which would increase the complexity and the level of the models and would introduce a larger level of uncertainty in results, need not be taken into account initially due to the scalp's static morphology. The work can therefore be focused purely on the geometrical properties of the head, i.e. the size and shape.

#### 1.3.1 *Definition of anthropometry and ergonomics*

Anthropometry is the science of measuring the human body and generating insight on the static and dynamic measurements (e.g. body height and reach, respectively) using applied statistics [45, 46]. Traditionally, descriptive measurements such as average and standard deviation have been favoured. While they are still in use in many applications, the rise of 3D scanning devices and more performant image processing algorithms have made it possible to perform much more detailed analyses on the complete shape of the body [47].

The International Ergonomics Association defines Ergonomics as: "the scientific discipline concerned with the understanding of interactions among humans and other elements of a system, and the profession that applies theory, principles, data and methods to design in order to optimize human well-being and overall system perfor-

mance." [48] While it was initially focused on methods, tools, and spaces related to human work, as well as the related psychosocial aspects [46], the field has expanded to cover wellbeing in all aspects of human activity [48]. The goal is to create products and environments so as to minimize health-related issues that arise from their use [49]. Ergonomics follows the user-centered design principle: if an object, a system or environment is intended for human use, its design should be based upon the physical and mental characteristics of its human users inasmuch as these may be determined by the investigative methods of the empirical sciences. Broadly speaking, two types can be distinguished: physical ergonomics, cognitive ergonomics, and organizational ergonomics [48]. This thesis deals with the former kind, in which apparel and environments are made to fit humans as well as possible. For this purpose, physical ergonomics is heavily based on anthropometry, and the two are often thought about and discussed together. Another way to look at it is to say that ergonomics translates insights from anthropometry into product design, as will be explained in the next chapters.

### 1.3.2 *Anatomy and anthropometry of the human head*

In general, the human head can be said to consist of three parts from which anatomical traits can be derived: the brain, the bone layer or skull and the skin layer. The upper (dorsal) region of the head, above the forehead and ears, is commonly referred to as the scalp. The brain itself has already been briefly mentioned in chapter 1.1. While the shape of the brain will determine at which locations EEG electrodes should ideally be placed, it does not appear to have a direct effect on the outer shape of the head. Therefore, this chapter will focus on the skull and scalp layers. The anatomical reference points that are used by designers are derived from medical literature, and thus carry medical nomenclature. The top part of the skull (or cranium) is divided into 8 separate parts, related on the underlying cerebral structure: frontal bone, temporal bone, occipital bone, parietal bone, etc. [50], see figure 8. The anatomical reference points on the skull are either distinct morphological landmarks or intersections between bones. The medical practitioner is able to intuitively identify these points based on descriptions such as "nasion", "ophistocranium" or "gnathion".

However, for the product designer, the only relevant anatomical reference points are those that can be defined by palpation and that can be measured externally, e.g. to be used as reference or fixation points to mount products. Unfortunately, anatomical literature is more commonly oriented towards the medical field than towards the anthropometrist or designer. Still, a number of reference works are available, most of them from the US, such as NASA's Anthropometric

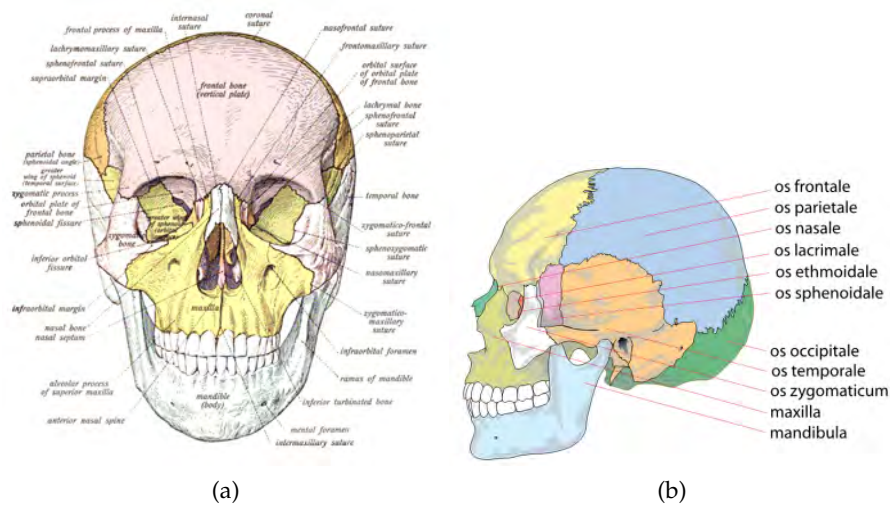


Figure 8: Regions of the human skull. (Images are in the public domain.)

Source Book [51]. Thus, a different method of recognizing anatomical landmarks is commonly used for design purposes, in which the landmarks are defined according to externally visible or palpable features. First, a number of reference planes is defined, the most important of which is the Frankfurt (or Frankfort) plane: if the subject is standing with the back of his head against a wall, the plane formed by the lowest points of its eye sockets (orbitale) and its tragi (tragus being the eminence of cartilage anterior to the opening of the external ear canal) should be perpendicular to this wall, as shown in figure 9. Note: the lowest point of the eye socket can only be correctly determined by palpation. For most anthropometric measurements, the head needs to be oriented so that it is aligned with the Frankfurt plane.

Once the head is oriented in this manner, a number of anthropometric points can be defined either by palpation or by sight. In order to understand the descriptions of various anatomical points, a basic familiarity with anatomical nomenclature is required. For example, when a point is described as being "lateral", it lies on the sides of studied body part, or when it is "dorsal", it lies on the back (see figure 10 (a)). The anatomical directions of the head are slightly different from those of the body and are shown in figure 10 (b). When describing the 3D locations of the human body, the coordinate planes are referred to as the (mid)sagittal plane, the coronal plane and the transverse (or transversal) plane, also shown in figure 10 (c). For example, the ophistocranium can be described as the most dorsal point on the midsagittal plane, i.e. the point that is the furthest to the back when viewed from the side. A number of such anthropometric points and measurements is described in chapter 2.

Anthropometric measurements are specified as linear or surface (curve) distances between anatomic reference points. Two of the most

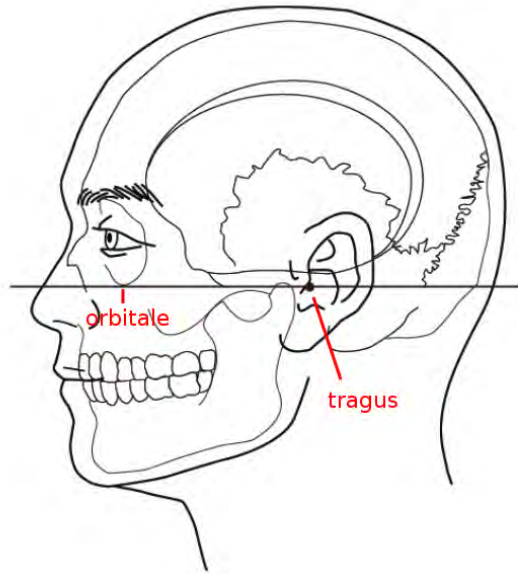


Figure 9: Head alignment according to the Frankfurt plane.

commonly used tools are tape measures and outside calipers [47, 53], shown in figure 11. Although these tools have been the standard in anthropometry for many years, they have two important drawbacks. Firstly, anatomic landmark and measurement descriptions are sometimes vague and can be difficult to locate, even for specialized anthropometrists. This results in high inter- and intra-observer variability especially when the work is performed by non-experts such as graduate students [54–57]. Secondly, performing anthropometric measurements can take a lot of time, depending on the sample size and the number of repeated measurements.

Alternatively, performing the measurements on digital images (e.g. CT, MRI or 3D scans) provides a solution to both of these problems: the 3D image can be viewed from all directions and at any magnification level before placing a landmark. When working with bone layer surfaces, underlying morphological characteristics can be easily determined, as shown in figure 12. Furthermore, measurements can be automated, speeding up the measurement process significantly.

However, when deriving anthropometric measurements from skin layer surfaces (as in figure 13), localization of landmark positions is more difficult. Because palpation can no longer be used to find morphological structures on the underlying bone, extra caution should be exercised in the selection, collection and analysis of these measurements. Alternatively, the landmarks could be placed on a model in which both layers are visualized at the same time for visual assessment or benchmark.

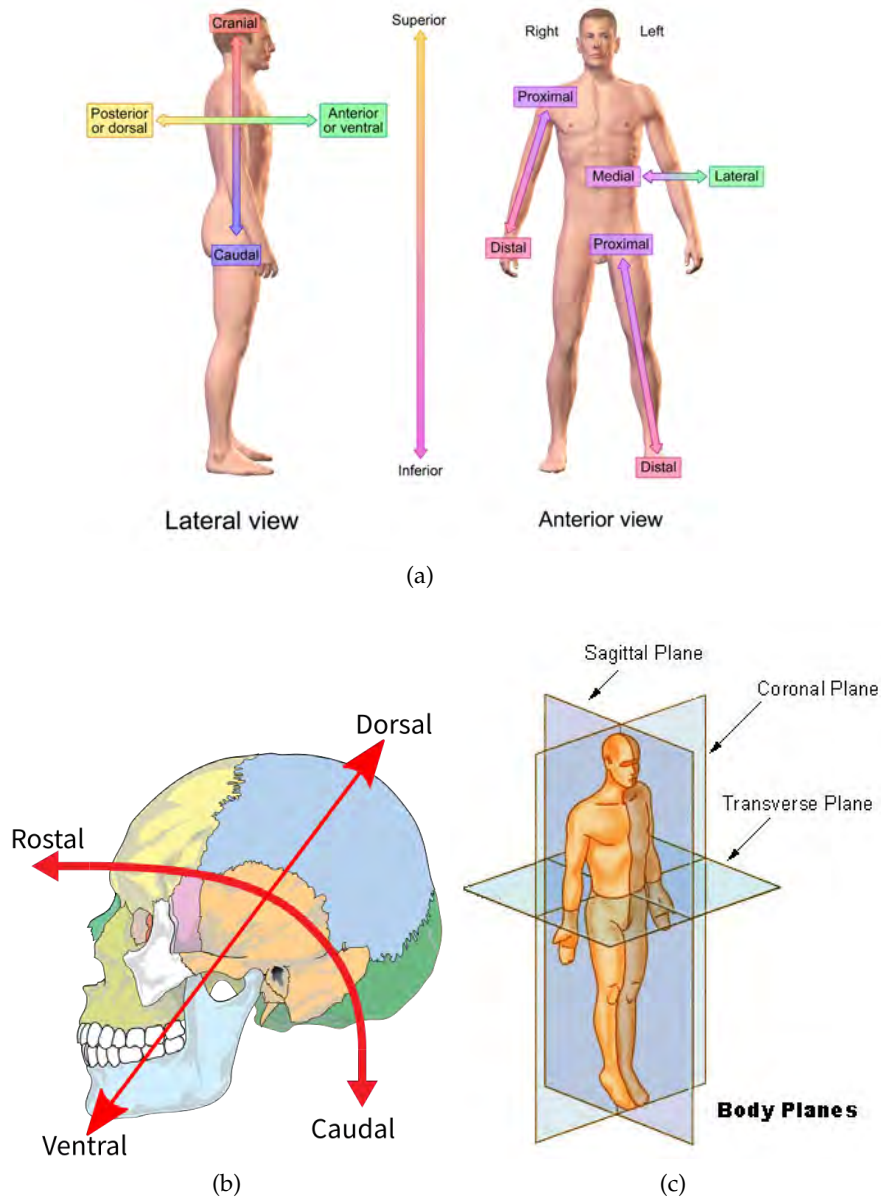


Figure 10: Anatomical directions on the human body (a), directions on the head (b) and anatomical coordinate planes (b). (a) was made available by Bruce Blausen [52], (b) and (c) are public domain images. (b) was slightly adapted to also show the dorsal direction.

Still, in both cases, the selected landmarks can be more easily visualized, shared and verified. Only a single measurement session needs to be organized in which the participant's images are captured, making subsequent measurement of replication of studies much easier. In many cases, the advantages of using digital images for anthropometric measurement often outweigh the disadvantages.



Figure 11: Common anthropometric tools: a tape measure (a) and outside calipers (b).

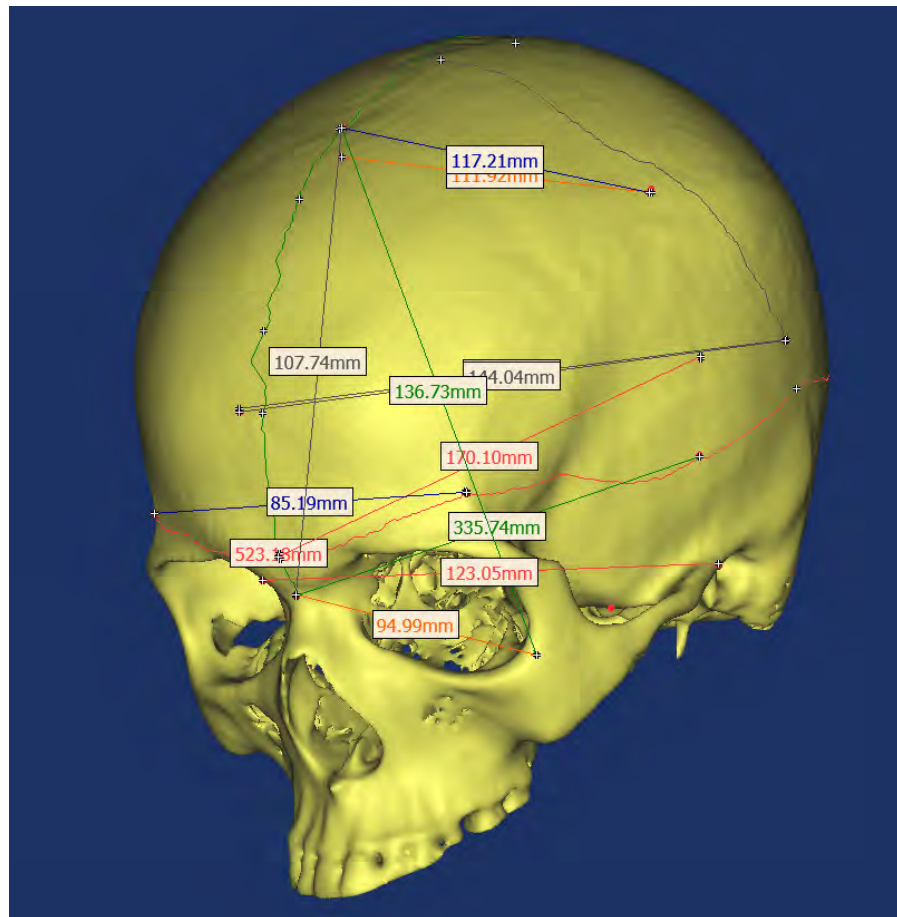


Figure 12: Anthropometric measurements on a cranium bone surface (Mimics).

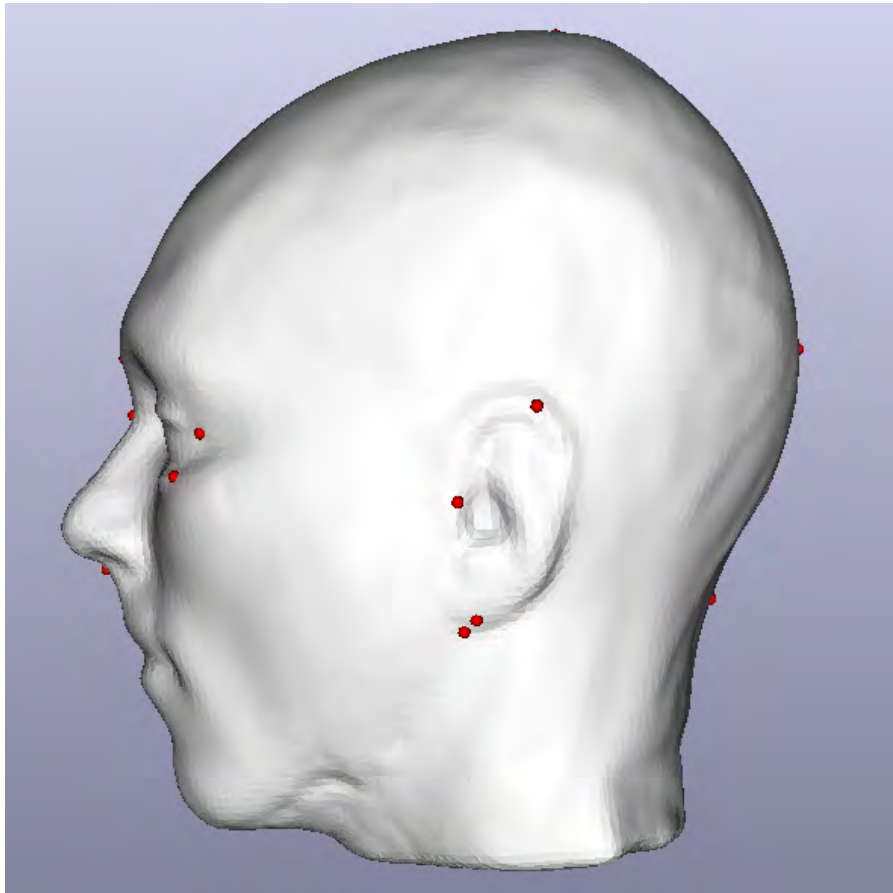


Figure 13: Annotation of anthropometric landmarks on cranium skin surface. 3D scan published with permission from subject.

### 1.3.3 *The distinction between traditional anthropometry and 3D anthropometry*

Traditional anthropometry deals with descriptive statistics performed on a subset of measurements of a representative sample of a population. Measurements are collected in anthropometric data tables and the average and standard deviation of each measurement is calculated, as discussed in section 2. A statistic concept that is vital to anthropometry is population percentiles. A percentile is a measurement value above or below which a given percentage of the population is included. For example, if the 5th percentile of head length for a given population is 181 mm, 5% of that population has a head length lower than or equal to 181 mm. The 5th and 95th percentiles of measurements are often included in anthropometric data tables [46]. For an anthropometric study to be valid, all descriptive statistics should be included, as well as meta-information on the population sample that was used, e.g. age, ethnicity, and gender.

One-dimensional anthropometric measurements (as described in section 1.3.2) and correlation analysis between them have been the standard in ergonomic design for many years. Even so, a significant disadvantage of anthropometric measurements for ergonomics is that shape variation can only be studied in terms of the included measurements, which often leads to incomplete or incorrect conclusions because only the variation of a set of pairs of anthropometric points can be studied. Because it is not known how this variation affects the areas outside of the studied points, these areas are usually interpolated and assumed to scale linearly with the measurements. In reality, this is not always the case, resulting in products that do not fit large parts of the population. To give a simple example from personal observation, many L-size shirts are simply upscaled versions of M-shirts. Tall, skinny people therefore often have trouble finding fitting shirts, because M shirts will be too short whereas L-shirts are much too wide.

Instead of analyzing tables of anthropometric measurements, there is an increasing interest in studying the shape by analyzing collections of 3D surface meshes of the human body or of certain body parts. When anthropometric studies are based on 3D data sets of body shapes, this is referred to as 3D anthropometry. An increasing number of 3D scanners exist to capture 3D shapes. They can be broadly divided into two categories: contact and non-contact scanners [58]. Contact scanners such as the Microscribe MX [59] are referred to as coordinate measuring machines (CMMs), and involve manually touching reference points on the scanned object with a probe [60]. Because this is time-consuming and usually results in low-resolution images, it is not often used for taking body scans.

Non-contact scanners can be further subdivided in active or passive scanners, with active scanners that rely on sending out ionizing radiation, electromagnetic fields [61], laser light triangulation and time-of-flight [62], or structured light [63] being the largest category. For example, in medical practice it is increasingly common to take 3D images of various body parts, either using computed tomography (CT), which is cheaper and more suited to visualizing dense structures [64], or magnetic resonance imaging (MRI), which does not require ionizing radiation and is more suited for soft tissues [65]. See figure 14 for an example of an MRI scan and scanner.

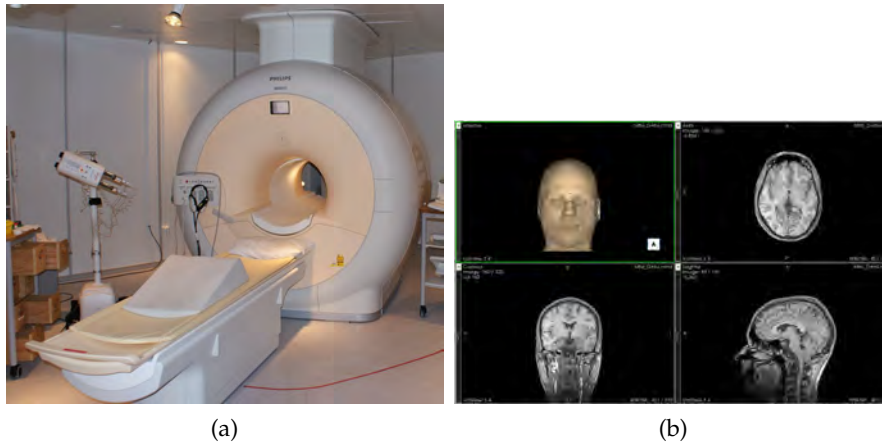


Figure 14: Example of an MRI scanner (a) and the resulting image (b). (a) was made available by Wikimedia user Jan Ainali at [66] through the CC BY 3.0 license [67].

A second type of active 3D scanners that is often used in 3D anthropometry is structured light. Half a decade ago, size was a limiting factor, and these scanners were mostly used in specialized environments such as ergonomics labs or certain clothing stores [63]. However, at the time of writing various hand-held 3D scanners are available at relatively low prices and these are becoming a common sight in ergonomic research labs and fab-labs. An example of a 3D-scanned head surface is shown in figure 15 (b), and the hand-held device that was used to capture is shown in figure 15 (a). In contrast, techniques based on laser light triangulation or depth-of-field are less common in anthropometric studies (with the exception of the TC2 body scanner [68]), because they are more reliable at large distances and thus more suitable for subjects such as statues, architecture or geography [62].

Finally, a commonly used passive scanning technique is stereophotogrammetry, in which a subject is photographed from multiple angles and/or with multiple camera's and the images are superimposed to create a 3D surface [69]. An example of an image captured in this way is shown in figure 16.

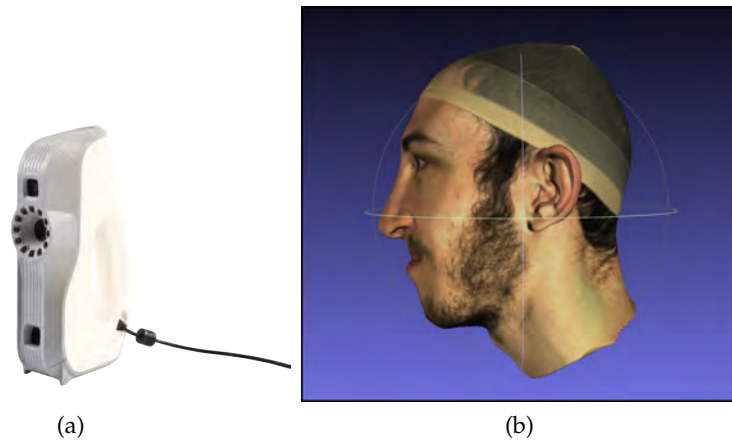


Figure 15: Example of a hand-held structured light scanner (Artec Evo) (a) and the resulting image (b). 3D scan printed with permission of subject.

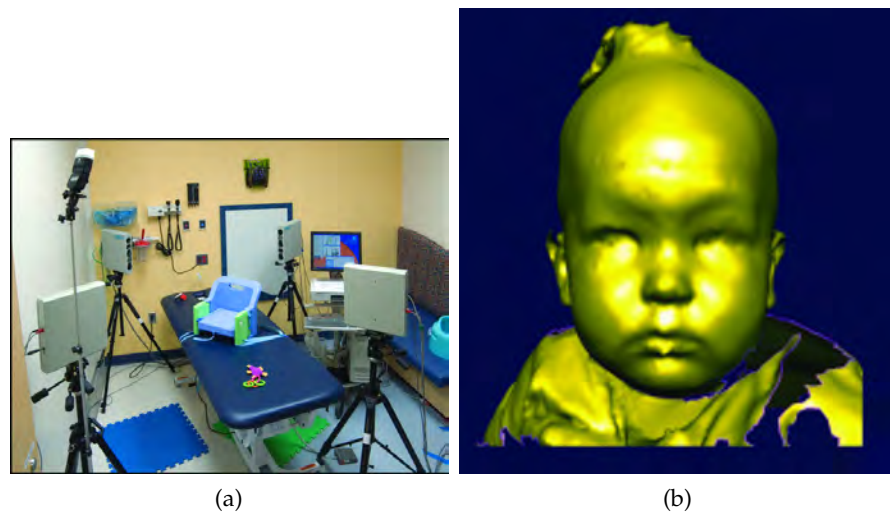


Figure 16: Example of an stereoscopic imaging set-up (a) and the resulting image (b). These images were made available by Heike et al. [70] on BioMed Central through the CC BY 2.0 license [30]

In theory, all of these 3D images can be used to study shape variation. Of course, they all have their advantages and limitations, which should be considered on a case-by-case basis. For example, while 3D-scans using hand-held structured light scanners offer an easy and fast way to capture 3D images without a specialized set-up or environment, they have a comparatively long scanning and processing time, which make them less suitable for anthropometric studies. Furthermore, hair is often a problem in this kind of scans: either because it cannot be captured efficiently or -when studying the shape of the scalp- it obscures the actual head surface. Medical images contain much more information, including underlying structures which are

not visible to the naked eye or to other types of 3D scanners. They do require expensive and complex machinery which is usually only available in hospitals. It is much more difficult and expensive to set up studies with even a small number of test subjects. Luckily, a number of medical image database is openly accessible on the internet, e.g. the LONI image archive [71] (a comprehensive list of these can be found online at [72]). However, these databases are presently intended for medical studies instead of anthropometric research, and it can be challenging or even impossible for an anthropometrist to find a database containing the right body parts with the right field of view and in sufficiently large samples. Furthermore, medical images need to be preprocessed by a specialist in order to extract the required structures (e.g. bone or skin layers). Even so, the flexibility of selecting the desired layers and the high spatial resolution make medical images highly suitable for shape studies, especially of static surfaces such as the human head (excluding the hair). Therefore, the models that were used in this doctoral research were all based on medical images.

After obtaining a 3D data set that represents a desired population, the surface meshes can be matched to each other using image processing techniques for further statistical analysis. A set of corresponding 3D shapes (i.e. same size, orientation and corresponding vertices) on which shape analysis can be performed is called a statistical shape model. Shape modeling is further discussed in chapter 2.

#### 1.3.4 *General design methods for physical ergonomics*

This chapter provides an overview of several design methods that can be used to make products fit their intended users. The methods were taken from current design practice and education (at Product Development, University of Antwerp) and are mostly based on traditional anthropometry. They will be extrapolated to 3D anthropometry in the remainder of this thesis.

##### 1.3.4.1 *Individual design*

Individual design is, as the name implies, custom-made design for a single individual. It is the most expensive type of design, but it results in the best possible fit. Individual design was commonplace before the Industrial Revolution, but has been on the decline since mass-production has become the standard way to produce goods and products. For example, whereas buying clothes from a tailor used to be a common occurrence, it is now expensive and focused on specific niches such as custom-tailored business clothing or people with deviating physical dimensions for whom mass-produced clothing does not fit.

However, there is a different method to allow nearly individual design: mass-customization. The term is combination of mass-production and customization, in which a product is comprised of several mass-produced or 3D-printed parts of various sizes that can be put together in such a way as to fit (almost) everyone. Mass-customization is a lot cheaper than individual design, although it is still not that common in apparel or clothing design. Even so, it is an acceptable and often appropriate design method to achieve a better fit at the expense of some extra effort from the user or an intermediary.

#### 1.3.4.2 *Sizing systems*

Product sizing is the art of creating a minimal number of different versions of a product to fit a maximal number of people [73, 74].

In traditional anthropometry, creating a sizing system is a subjective process that is highly dependant on a designer's experience and skill. Although -to the author's knowledge- few standardized methods are described in scientific literature [73], the following approach is taught at Product Development, University of Antwerp.

First a so called "ego-design" is made: a mock-up of the product concept that fits the designer. This is done to ensure that the required fit and functionality can be achieved by the design.

The next step is to find out the design plasticity, meaning how much the shape, size or flexibility of the device may vary before it no longer performs its intended function. For example, when designing a respirator mask, the respirator's size is incrementally increased or decreased until there's no longer a tight seal with the designer's (or test subjects) face. From the minimum and maximum increments, the total maximum size variation that can be accounted for in a single product size can be determined. The process can also be repeated for shape variation and material properties.

When design plasticity is known, the population's measurements are consulted, usually from an anthropometric data table that gives averages, standard deviations and percentile values for each measurement. First, the total desired population coverage should be determined (for each measurement) in order to find the minimum and maximum measurement values. For example, the designer might decide to target the P5 to P95 region and not take into account the smallest or largest 5% of the population. The values that correspond with these percentiles are drawn from the anthropometric table, and product sizes are created by subdividing the measurement range in parts with the maximum variation found in the plasticity test. See figure 17 for a visualization of this process.

At the end of this process, the product dimensions are known for each measurement, for a discrete number of product sizes. The anthropometric data tables can now be consulted again to find what

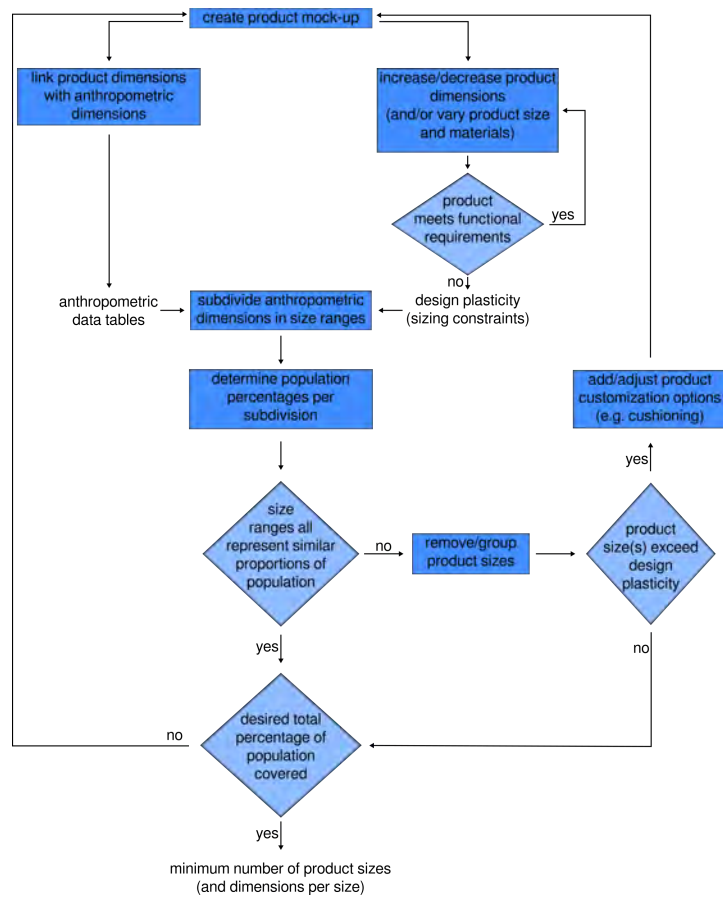


Figure 17: Visualization of product sizing using traditional anthropometry.

percentage of the population that is included in each product size. To determine which percentage of the population is covered by a product size, an inverse approach of finding population percentile values is followed. First, the designer checks how far the upper and lower values of the measured dimension are from the population mean of that dimension. This value is then expressed in a number of standard deviations by dividing it by the population's standard deviation for that dimension. Because this corresponds to the z-value, the z-table can be consulted to find which population percentage corresponds to the product size's upper and lower values (for this specific dimension). The difference between these percentage values is the percentage of the population covered by this product size. Of course, this becomes slightly more complicated when multiple anthropometric dimensions are used, because the correlation between all dimensions needs to be taken into account. For this procedure, as well as a more detailed explanation of population percentile calculations in product design, the reader is referred to [45], [75] and [46]. Depending on the population percentages, small modifications can still be made to each product size if this results in a better population distribution. Alternatively, a product size might be dropped from the product range if

it turns out it would only fit a minor percentage of the population.

Finally, in most cases, some overlap is allowed in the dimensions of neighboring product sizes. By enforcing a strict separation between the dimensions, people that have measurements on the boundary between two sizes might not get a comfortable fit from either of them. An overlap eliminates this problem and allows for more comfortable error margin during product design. Usually, the designer determines how large the overlap should be, based on previous experience and similar products.

Less experienced designers are bound to make mistakes the first time(s) they apply this method, regardless of how thoroughly they work, because the process is not purely algorithmic and highly depends on experience. Even though they would greatly benefit from a heuristic design method that is proven to result in acceptable product sizes, it is challenging to find a standardized method for a subject that is so designer-, product- (or concept) and population-specific.

#### 1.3.4.3 *One-size-fits-all*

One-size-fits-all (1SFA) design is very similar to sizing systems, with the difference that only one product size is created. While it is usually desirable to have as few product sizes to cover a large population, 1SFA puts a number of constraints and challenges on the materials and the creativity of the designer. In order to fit every individual in a population, either a flexible material should be used (e.g. sweat band), a minimum level of customization be incorporated (e.g. head phones), or both. If no flexibility or customization is allowed, this leads to products that do not properly fit any user in the best case, or in the worst case cause discomfort, pain and even injury [76]. On the other hand, it is important that customization does not come at the cost of usability; if the product is too difficult to customize, the user will get frustrated with it and might not buy similar products again in the future [77].

#### 1.3.5 *Example of headgear design: sports and motorcycle helmets*

In this chapter, the practice of headgear design is briefly illustrated through the example of helmets. As most readers will likely know, helmets are used to protect the human head from injury and exist in various shapes and sizes. Safety helmets protect construction workers from falling objects, motorcycle helmets protect their user's head from impact due to falls, and bicycle helmets not only protect the head from impact, but also improve aerodynamics and help the user cycle faster. Each helmet has three main parts: an inner lining that

fits the head and provides user comfort, an outer shell from a shock-absorbing material to absorb the impact and disperse energy, and a retention system that ensures the helmet stays on the user's head. Some helmets contain additional parts to protect the face and eyes. An example is of the various parts of motorcycle helmet is shown in figure 18.

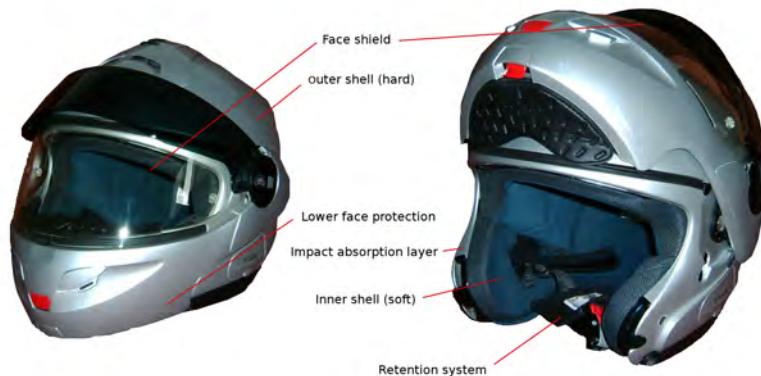


Figure 18: Basic components of a helmet. Photo in the public domain, adapted to remove background and add component labels.

Apart from being made of shock-absorbing materials and having a retention system that sufficiently fixates the helmet during use, the helmet should properly fit the human head in order to be effective [78]. The helmet should be fixed on the frontal and occipital regions, because the skull is thicker in these areas and they are less likely to fracture [79, 80]. As little pressure as possible should be placed on the thinner temporal and fontanel regions [80, 81]. Various organizations publish standards for the characteristics, design and testing of different types of helmets [78, 82]. The most well-known are the US-based DOT (Department of Transport) and Snell Memorial Foundation, and the European Committee for Standardization (CEN) and the United Nations Economic Commission for Europe (ECE) [83]. While most of the standards revolve around the functionality and testing of the headset, helmet coverage -the surface area of the head that is covered by the helmet- is also an important factor. One of the internationally most often used headform for helmet coverage testing is EN960 [50, 84]. The EN960 headforms come in a set of 13 sizes based on the head circumference, starting from 500 mm and increasing in size for each 100 mm. The increase in size is linear: all anthropometric dimensions are assumed to increase by the same relative amount as the circumference. Only the size of the headform changes, not the shape. After a manufacturer has finished a set of helmets, they are compared against the EN960 headforms (either digitally or physically) to determine whether they cover the correct head surface, which differs between applications.

One problem with this approach for helmet coverage, is that due to the fact that shape variation is not included in e.g. the EN960 headforms, these standards will not optimally represent their underlying populations. Helmets might pass every test and still fit the user poorly, possibly compromising their safety. For example, helmets designed in Europe or the United States often do not fit Asian users, which were found to have smaller and rounder heads than Westerners [50]. Another problem is that the standard headforms are often based on outdated anthropometric data. In the case of EN960, it is unclear from which population the measurements were originally derived, but it is well known that these measurements have not been updated much since its conception around 1900 [50]. 3D anthropometry could offer a solution for both of these problems. Dr. Roger Ball demonstrated the use of 3D anthropometric models for this purpose by creating a new set of physical and digital EN960 headforms specifically for the Chinese population. An example of the digital headforms can be seen in figure 19.



Figure 19: Example of a set of EN960 headforms (manikins). Image from "SizeChina: 3D anthropometric survey of the Chinese head" [50].

Even so, while the standards for helmet verification are well described, to the authors knowledge no standardized design methods or manikins exist for the initial design. Current standards are focused more on safety than on user comfort. However, research has shown that comfort might be at least equally important, especially in cases where helmets are not mandatory, as is the case for bicycle helmets in Belgium and the Netherlands. Many bicyclists choose not to wear a helmet due to issues related to lack of comfort caused by a bad physical fit, high weight or insufficient heat dissipation. Helmet users would therefore benefit from a standardized design and verification method for optimal helmet fit. However, as discussed in section 1.3.4, each manufacturer has their own method to create product fit, usu-

ally based on a set of traditional anthropometric measurements and depending on experience, designer intuition and sales numbers to determine helmet dimensions and sizes [46].

In most cases, helmet designers follow a sizing system approach. Most helmets exist in a minimum of three sizes (e.g. small, medium, large). Further customization within each helmet size is achieved through customizability of the retention system on the one hand, and the soft, flexible inner lining on the other. While the inner lining has few shock-absorbing capabilities, it can have a significant impact on fit and user comfort. As mentioned in section 1.3.4.2 and discussed in chapter 4, it is not always feasible to create a sufficient number of product sizes to perfectly fit a given population. Soft inner layers made from foam or rubber offer a solution in these cases. Even so, conventional helmet sizing is often inaccurate [85, 86].

While this chapter was focused on helmets, the same design approach is used for other head-based products, such as respirators, glasses or safety goggles [46].

#### 1.3.6 *The need for more detailed head models*

From the chapters above, it seems that there is still a lot of room for improvement in the design methods for headgear in general and BCI in specific. Firstly, better anatomical and anthropometric models are required in order to fully understand the shape variation of the human head. As discussed above, one-dimensional anthropometric measurement tables are often incomplete, outdated or unreliable. They offer only rudimentary information on the three-dimensional shape of the head. Designers and standards organisations alike would benefit from accurate and up-to-date 3D models of the head. These models could be used to improve the fit, functionality and safety of many head products by supporting standard headforms that much more closely resemble their intended populations. They could also be used to construct digital or physical 3D manikins to be used in the initial design of head products, thereby reducing the time and material costs that would normally be spent on trial-and-error prototyping. Finally, in the case of BCI product development, a 3D anthropometric model of the human scalp would make it possible to correctly predict how a BCI headset's electrodes and fixation points should be placed, increasing the possibility of designing commercial BCI headsets that can be used outside of laboratory settings.

### 1.4 RESEARCH QUESTIONS

The remainder of this thesis will focus on the creation and evaluation of such a 3D model, as well as on its implementation in product

design. This will be done by considering the following research questions:

- *How well can the global and local shape variation of the human scalp be quantified in a statistical shape model?*
- *Does the use of shape models have an impact on the geometric fit, stability and repeatability of EEG sensors in BCI-equipment?*
- *How can 3D anthropometry be implemented in product sizing to create better fitting headgear?*

The structure of the performed research and its correspondence to the research questions is shown in figure 20.

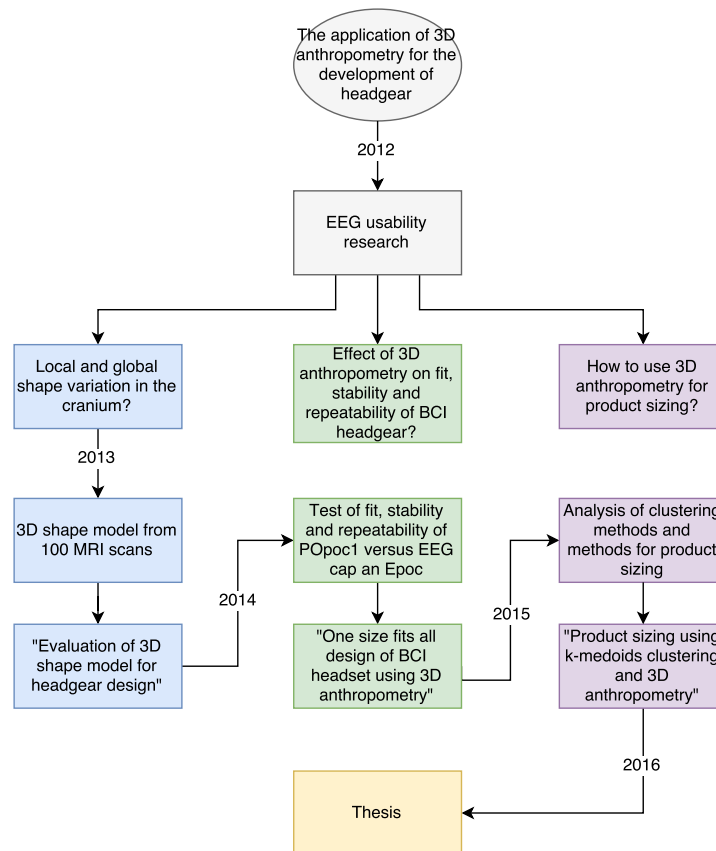


Figure 20: Research structure.

## Part II

### RESEARCH PAPERS

This chapter contains research papers that were published in (or in one case submitted to) international peer-reviewed journals during the course of this doctorate. Each paper answers one of the research questions posed in section 1.4. Chapter 2, "Evaluation of an anthropometric shape model of the human scalp", addresses the creation and evaluation of a shape model to quantify the global and local variation in the human scalp shape. In chapter 3, "Ergonomic design of an EEG headset using 3D anthropometry", a method is presented to use the shape model for the design of a one-size-fits-all BCI headset frame, and the electrode placement and stability of the frame is examined. Chapter 4, "Product sizing with 3D anthropometry and k-medoids clustering", discusses and evaluates a method to combine k-medoids clustering and statistical shape models to improve product sizing. The papers are presented as they were published, although the tables were slightly modified in order to maintain a unified look throughout the document. Some remaining typographical errors were also corrected, and the reference sections of the papers were combined in the thesis bibliography. Some overlap with the previous chapters was unavoidable, although it was kept to a minimum.



## EVALUATION OF AN ANTHROPOMETRIC SHAPE MODEL OF THE HUMAN SCALP

---

Daniël Lacko<sup>a,b,c</sup>, Toon Huysmans<sup>b</sup>, Paul M. Parizel<sup>d</sup>, Guido De Bruyne<sup>a</sup>, Stijn Verwulgen<sup>a</sup>, Marc M. Van Hulle<sup>c</sup>, Jan Sijbers<sup>b</sup>.

<sup>a</sup> *Product Development, Faculty of Design Sciences, University of Antwerp, Antwerp, Belgium*

<sup>b</sup> *iMinds-Vision Lab, University of Antwerp, Antwerp, Belgium*

<sup>c</sup> *Laboratorium voor Neuro- en Psychofysiologie, KU Leuven, Leuven, Belgium*

<sup>d</sup> *Department of Radiology, Antwerp University Hospital & University of Antwerp, Antwerp, Belgium*

Original research article published in *Journal of Applied Ergonomics*, vol. 48, p. 70-75, 2015.

### 2.1 ABSTRACT

This paper presents the evaluation a 3D shape model of the human head. A statistical shape model of the head is created from a set of 100 MRI scans. The ability of the shape model to predict new head shapes is evaluated by considering the prediction error distributions. The effect of using intuitive anthropometric measurements as parameters is examined and the sensitivity to measurement errors is determined. Using all anthropometric measurements, the average prediction error is  $1.60 \pm 0.36$  mm, which shows the feasibility of the new parameters. The most sensitive measurement is the ear height, the least sensitive is the arc length. Finally, two applications of the anthropometric shape model are considered: the study of the male and female population and the design of a brain-computer interface headset. The results show that an anthropometric shape model can be a valuable tool for both research and design.

## 2.2 INTRODUCTION

Parametric shape modeling is a popular technique to describe a population of 3D shapes with a limited set of parameters [87]. When applied to the human body, it enables medical doctors, product designers and researchers to study the human body through high-quality 3D representations [88]. For the sake of simplicity, people working in these fields will be referred to as 'ergonomists' throughout the remainder of this article. The parameters that yield the most accurate shape predictions of the body are usually found by statistically analyzing a sample of 3D polygonal surfaces. Although the resulting statistical shape models (SSM) accurately describe the object's shape, these statistics are often difficult to interpret and non-intuitive for design specialists. Therefore, several methods have been proposed to compute a new set of parameters to characterize the human body shape. Most of them were focused on the full body [87, 89–92], the face [93] or head [94]. This research shows that head shapes can indeed be predicted from either semantic parameters such as age, gender and ethnicity or from various body size measurements.

While more recent techniques were suggested as solutions for industrial designers [91, 94–96], it is not clear how they should interpret and use the results. Custom GUI applications have been suggested, in which the model can be varied according to statistical parameters [97, 98]. However, statistical parameters are not intuitive enough to be used by ergonomists. Other suggestions include generating 3D models based on anthropometric measurements and then using these static shapes in 3D software [99], which is not far off from traditional anthropometry. Furthermore, only the average geometric (i.e. vertex-to-vertex) fit of the shape models to the scanning data was usually validated. While this is a valuable parameter, it only gives a very limited indication of the predictive capabilities of the models. Finally, despite the advent of head-centered products such as EEG-recording devices [100], to the best of the authors' knowledge no parametric models to date focus on the scalp.

In this work, the hypothesis is that a statistical shape model can be created that accurately represents the human scalp and that can be modified by parameters that are intuitive to designers or ergonomists. A statistical 3D shape model of the human scalp is created and a linear mapping is made between statistical parameters and ten anthropometric measurements. The prediction accuracy of the model is examined by using three different error metrics, i.e. vertex-to-vertex, normal and tangential error. Both the average and point-to-point errors are evaluated for several combinations of anthropometric measurements. Cross-validation is used to verify both the statistical and the anthropometric shape model. The sensitivity the prediction to measurement errors for individual parameters is shown and the ef-

fect of measurement errors on the prediction is evaluated. This extensive analysis will allow ergonomists to select the minimal required set of anthropometric measurements, determine the influence of measurement errors and accurately locate shape variation.

The remainder of this paper is organized as follows. Section 2.3 describes how the shape model is built, including the segmentation and parametrization of the MRI scans, the principal component analysis (PCA) of the 3D scalp geometry, the selection of the anthropometric measurements, and the correlation between these measurements and the PC weights. In section 2.4, the shape model is evaluated in terms of prediction accuracy, the data set size is verified for the statistical as well as the anthropometric model, and the sensitivity of the prediction to measurement errors is discussed. The results are shown in section 2.5, as well a discussion on how to select the right anthropometric measurements and an application for anthropometric research and for industrial design. Finally, the conclusion is formulated in section 2.6.

## 2.3 METHODS

This section presents the workflow of the methodology that was used to create the anthropometric shape model (see Fig. 21). Because the input MRI scans contain more information than just the skin surface, they first need to be preprocessed to remove all artefacts and to extract the cranium surface as a geometric surface mesh. This process is described in section 2.3.1.1. The surfaces then need to be aligned to each other and be projected into a simpler parameter space for further analysis. This ensures that corresponding points are used throughout the remainder of the methodology, instead of possibly comparing e.g. the tip of the nose with the tip of the earlobe. Section 2.3.1.2 describes how this was done. The surfaces are then sampled so as to obtain a uniform set of corresponding points on which PCA can be performed to examine the shape variation, as explained in section 2.3.1.3. However, as will be discussed in section 2.3.2.1, PCs are not intuitive enough to be used as parameters for the model. Therefore, section 2.3.2.2 concludes the methodology by showing how ten intuitive measurements can be used instead to analyze the head geometry and predict new head shapes.

### 2.3.1 *Building the shape model*

#### 2.3.1.1 *Segmentation of MRI Scans*

100 MRI T1-FFE-weighted MRI scans (50 male, 50 female aged between 20 and 30 years, Western population) were used as input for the shape model. The scans were acquired using a Philips ACS III 1.5

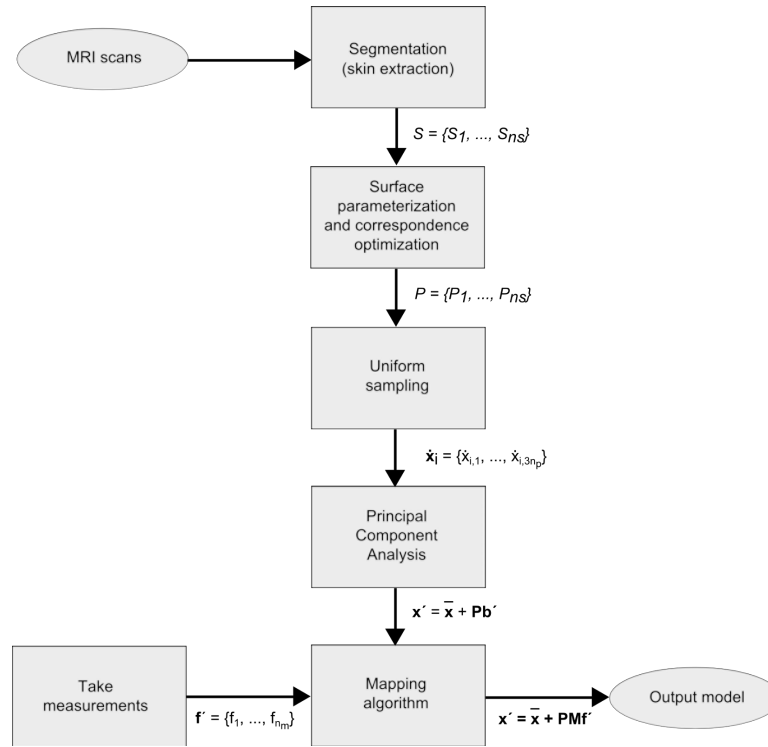


Figure 21: **Workflow.** The skin layer is first extracted from MRI scans, then the scalp surfaces are parametrized and corresponded to one another. After sampling the images using uniform landmark locations, PCA is performed on the resulting point cloud. Finally, the anthropometric measurements are acquired from the scalp surfaces and are correlated with the respective PC weights to create a mapping. This mapping results in an anthropometric model that can be used to predict new scalp surfaces based on anthropometric measurements.

T scanner in the sagittal acquisition plane, with a slice thickness of 1 mm, an echo time of 10 ms, a repetition time of 18 ms and a flip angle of 30 degrees. These scans were obtained from the International Consortium for Brain Mapping (ICBM) database [101].

The first step in the processing pipeline was to segment the skin layer. Hereto, the MR images were debiased by Lloyd-Max quantization [102] and thresholded for grayscale intensity between 300 and 1800. Connected components labeling [103] was used to separate the head from smaller noise artifacts and head fixation braces. Finally, a morphological closing operation was applied to fill cavities such as the ear canals and nostrils. The ensuing surface was then extracted using marching cubes [104] and any remaining holes were interpolated using Poisson surface reconstruction [105].

The skin surface of the cranium was extracted as the region of interest, because the aim of this work was to mainly examine the variability of the scalp. To that end, each surface was cut by the shortest path connecting four consecutive points that were manually annotated on each surface: the subnasale (sn), both otobasia inferia (obi1 and obi2) and the inion (i) (see Fig. 22). The shortest path was determined using fast marching, in which a distance map is first calculated from the one boundary point to the next, followed by gradient descent interpolation from the latter to former [106]. This resulted in a set of surfaces of the same topology  $\mathcal{S} = \{\mathcal{S}_1, \dots, \mathcal{S}_{n_s}\}$ , with  $n_s$  the number of surfaces.

### 2.3.1.2 Surface Parametrization and Correspondence Optimization

The next step was to correspond the 3D coordinate points of the surfaces to each other, enabling statistical analysis of the 100 scans. The surfaces  $\mathcal{S}$  were mapped to a simpler parameter space by a process called surface parametrization. Many parametrization methods exist: if the corresponding surface is disc-like or spherical, a disc or sphere is often taken as the parameter space, while other domains are used for more complex topologies [107]. In this paper, the approach of [107] was used, with the exception that the head surfaces were mapped to a planer (two-dimensional) rectangle with sides of length 1. The set of parametrizations is  $\mathcal{P} = \{\mathcal{P}_1, \dots, \mathcal{P}_{n_s}\}$ ; where  $\mathcal{P}_j$  is a parametrization for a surface  $\mathcal{S}_j$  only if its nodes, edges and faces are embedded in the rectangular planar domain and have a one-to-one correspondence to those of  $\mathcal{S}_j$ . The mapping  $\phi : \mathcal{S} \rightarrow \mathcal{P}$  between the parameterizations  $\mathcal{P}$  and surfaces  $\mathcal{S}$  was calculated by defining each point in  $\mathcal{P}_j$  as a linear combination of its neighbours [108]. The resulting system of linear equations only has a unique solution if  $\phi$  satisfies the Laplace equation  $\Delta\phi = 0$  on the interior of  $\mathcal{S}$ . Once  $\phi$  is defined on the boundary of  $\mathcal{S}$ , the system can be solved using finite element analysis as in [109].

With the parameterizations well defined, point-to-point correspondence is the next step. A group-wise correspondence optimization

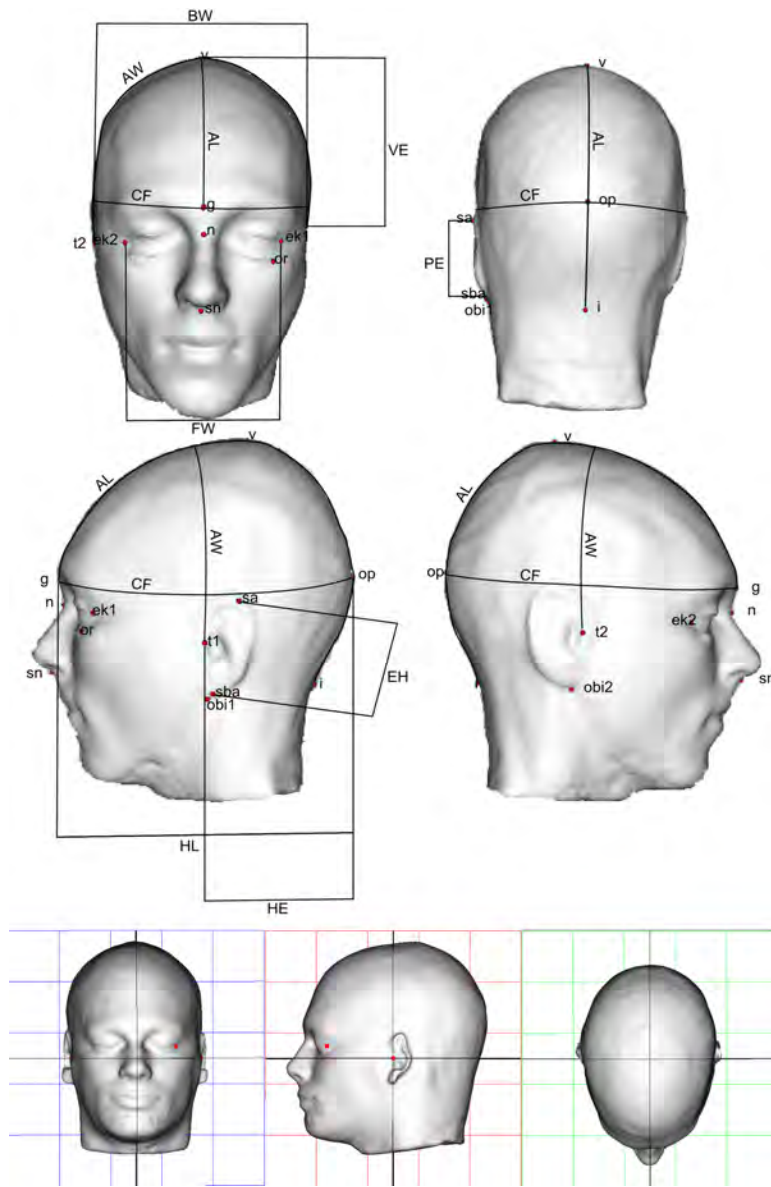


Figure 22: **Annotation points and coordinate system.** Anthropometric measurements and annotation points (top) and example of coordinate system used for anthropometric measurements showing the transversal (bottom left), midsagittal (bottom middle) and Frankfurt plane (bottom right), respectively, facing the front.

was performed [107], resulting in high-quality correspondences and a compact model. This method consisted of two steps: a rigid optimization in which the surfaces were aligned, and a non-rigid optimization in which the parameterizations were locally deformed while the surfaces were kept optimally aligned, resulting in new parametrizations  $\mathcal{P}$  and transformed surfaces  $\mathcal{S}$ . Fig. 23 shows the parametrization process and the correspondence optimization in more detail. Since there are no points to correspond below the boundary, the surfaces are aligned mainly according to the scalp region. The corresponded surfaces of all 100 scans used in this paper can be downloaded from [http://www.visielab.ua.ac.be/sites/default/files/research\\_topic\\_files/shape-matrix\\_29910-coordinates\\_x\\_100-surfaces\\_0.xlsx](http://www.visielab.ua.ac.be/sites/default/files/research_topic_files/shape-matrix_29910-coordinates_x_100-surfaces_0.xlsx).

### 2.3.1.3 Modeling the Shape of the Scalp

The corresponding parametrizations were used for statistical analysis of the underlying shapes. Each surface was sampled in the parameter space  $\mathcal{P} \equiv [0, 1]^2$  with a set of landmarks that resulted in a uniform distribution of landmarks over the average scalp. The 3D coordinates of these landmarks were concatenated into a vector  $\dot{\mathbf{x}}_i = [\mathbf{v}_{i,1}, \dots, \mathbf{v}_{i,n_p}] = [x_{i,1}, y_{i,1}, z_{i,1}, \dots, x_{i,n_p}, y_{i,n_p}, z_{i,n_p}]$  with  $n_p$  the number of landmarks. A  $3n_p \times n_s$  shape matrix  $\mathbf{X}$  was then defined as  $[\dot{\mathbf{x}}_1^T, \dots, \dot{\mathbf{x}}_{n_s}^T]$  (with  $n_s$  the number of shapes) and zero-centered by subtracting the row-wise mean  $\bar{\mathbf{x}}$  from each element for each respective surface:

$$\mathbf{X}_c = [\dot{\mathbf{x}}_1^T - \bar{\mathbf{x}}^T \dots \dot{\mathbf{x}}_{n_s}^T - \bar{\mathbf{x}}^T] \quad (1)$$

After applying PCA, each scalp can be represented as follows:

$$\mathbf{x}' = \bar{\mathbf{x}} + \sum_{j=1}^{n_s-1} \mathbf{P}_j \mathbf{b}'_j = \bar{\mathbf{x}} + \mathbf{P} \mathbf{b}' \quad (2)$$

where  $\mathbf{x}'$  is a column vector containing the vertex coordinates of the scalp,  $\mathbf{P}$  a  $3n_p \times (n_s - 1)$  orthonormal matrix containing the principal component vectors as columns, and  $\mathbf{b}'$  a  $(n_s - 1) \times 1$  column vector of weights of the respective PCs. By modifying the principal component weights  $\mathbf{b}'$ , new scalp surfaces can be constructed. Hence, Eq. 2 represents a shape model that is parametrized by the PC weights.

### 2.3.2 Extending the shape model with anthropometric measurements

#### 2.3.2.1 Performing anthropometric measurements on the human scalp

The first five PCs are shown in Fig. 24. Unfortunately, PC weights do not provide an intuitive description of the shape of the scalp because

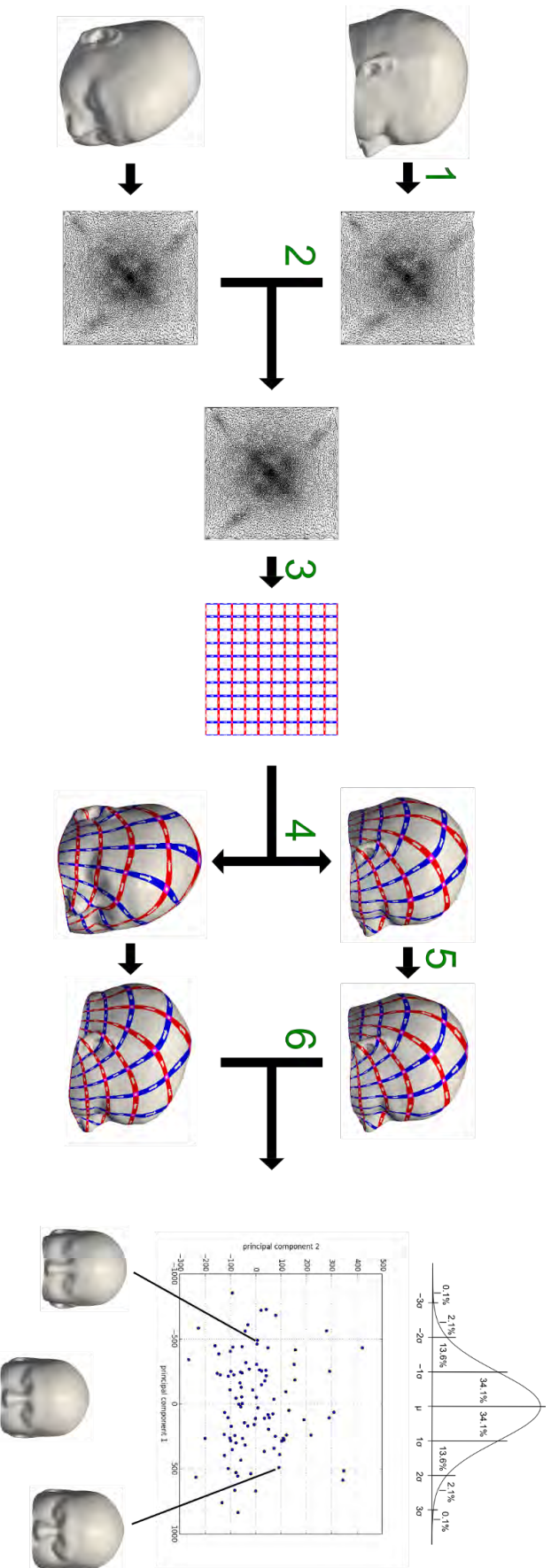


**Figure 23: Visualization of parametrization and correspondence optimization** First, all segmented surfaces are mapped onto a planar rectangle with sides of length 1 (step 1). The area distortion of the planar map is calculated for each surface and an average distortion map is derived in the rectangular domain (step 2). A dithering algorithm is performed on the average triangle area distortion, resulting in a resulting in a set of 10000 points that are approximately uniformly distributed over the surface of the scalp (step 3). This grid is projected back on the original surfaces (step 4). The surfaces are translated, rotated and locally deformed in order to optimize the point correspondence to obtain a compact PCA model (step 5). This step ensures that equivalent anatomical landmarks on different surfaces, e.g. the tip of the nose or the earlobes, are closely located to each other in the planar parameterization domain. Without this step, resulting variations might be due to misalignment instead of actual shape variation. Finally, statistical analysis can be performed on the corresponding surfaces (step 6).

the principal components have no clear physical interpretation (e.g., 'volume' or 'size'). This leads to ambiguous definitions and clearly shows the need for a new set of intuitive parameters, i.e. anthropometric measurements. NEN-EN-ISO 7250.

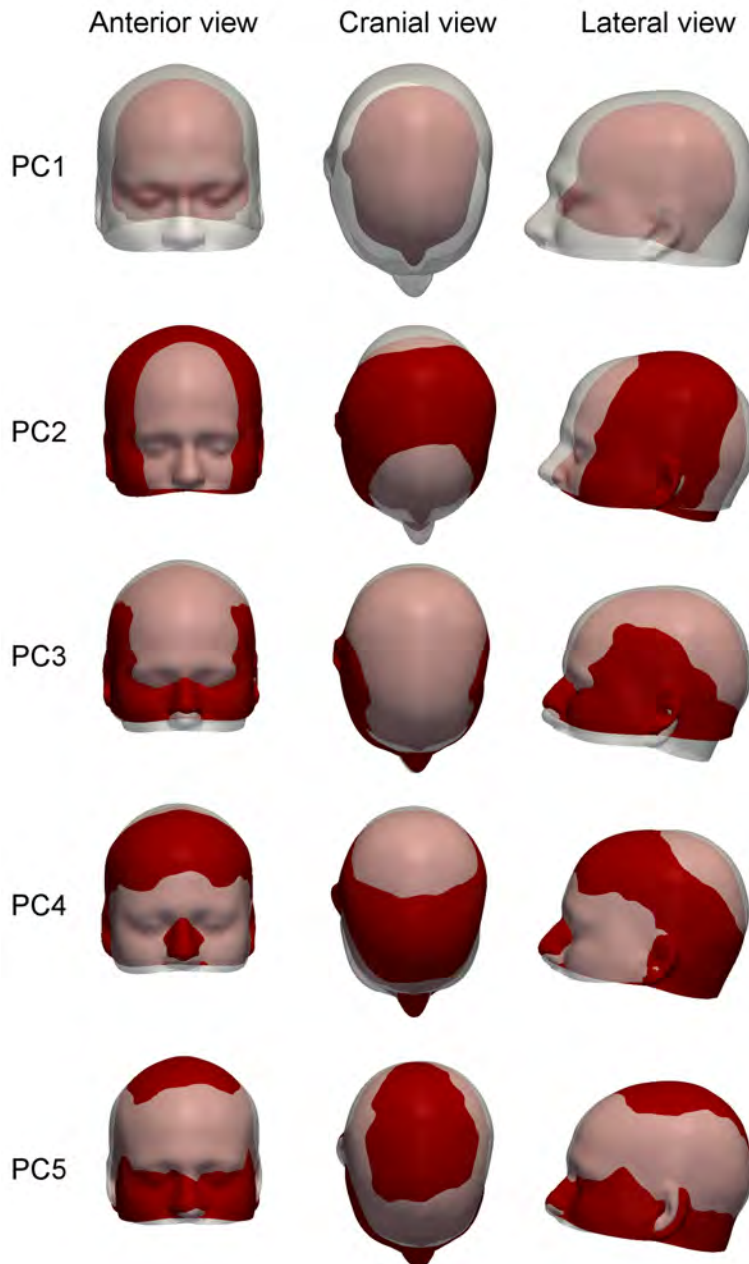


Figure 24: **Visualization of principal components.** Principal component 1 to 5 shown as the average head -3 (red) and +3 (white) standard deviations of the respective PC.

Anthropometric measurements are usually defined according to standards which are based on the work of Rudolf Martin [110] in Europe, e.g. The measurements are taken with respect to the Frank-

furt plane, which is defined as the plane passing through the lower points of both eye sockets (in this work, the lowest point of the left eye socket (or) is used) and both tragia (t1 and t2) [111]. The other reference planes, the midsagittal and the transversal planes, are perpendicular to this plane (see Fig. 22).

The following measurements were selected (see Fig. 22):

*Head length (HL)*: glabella (g) to ophistokranion (op) distance.

*Face width (FW)*: left ektokanthia (ek1) to right ektokanthia (ek2) distance.

*Bitracion width (BW)*: left tracion (t1) to right tracion (t2) distance.

*Ear height (EH)*: sub-aurale (sba) to super-aurale (sa) distance.

*Projected ear height (PE)*: sub-aurale (sba) to super-aurale (sa) distance, projected on the midsagittal plane.

*Vertical position of the ear (VE)*: left tracion (t1) to vertex (v) distance, projected on midsagittal plane.

*Horizontal position of the ear (HE)*: left tracion (t1) projected on midsagittal plane to ophistokranion (op) distance, projected on Frankfurt plane.

*Head circumference (CF)*: the length of the intersection of the head surface and the plane perpendicular to the midsagittal plane and going through the glabella (g) and ophistokranion (op).

*Arc length (AL)*: measured over the surface of the head, from glabella (g) to inion (i) on the midsagittal plane.

*Arc width (AW)*: measured over the surface of the head, from tracion (t1) to tracion (t2) and perpendicular to the transversal plane (see below).

The measurements were performed on the input surfaces and concatenated into a vector  $\mathbf{f}_i = [f_{i,1}, \dots, f_{i,n_m}]$  for each surface  $\mathcal{S}_i$ , with  $n_m$  the number of measurements, and combined into a  $n_m \times n_s$  measurement matrix  $\mathbf{F} = [\mathbf{f}_1^T, \dots, \mathbf{f}_{n_s}^T]$ . The results of the measurements for the population head scans are summarized in Table 5. The full measurements for all 100 scans can be downloaded as a labeled spreadsheet from [http://www.visielab.ua.ac.be/sites/default/files/research\\_topic\\_files/anthropometric\\_measurements\\_0.xlsx](http://www.visielab.ua.ac.be/sites/default/files/research_topic_files/anthropometric_measurements_0.xlsx), and as the data matrix used throughout this work from [http://www.visielab.ua.ac.be/sites/default/files/research\\_topic\\_files/feature-matrix\\_10-measurements\\_x\\_100-surfaces\\_0.xlsx](http://www.visielab.ua.ac.be/sites/default/files/research_topic_files/feature-matrix_10-measurements_x_100-surfaces_0.xlsx).

Measurement	<i>head length</i>	<i>face width</i>	<i>bitr. width</i>	<i>ear height</i>	<i>hor. pos. ear</i>
Max	222	108	167	70	114
Min	168	77	131	47	82
Mean	199	94	148	55	101
St. dev.	10.6	5.8	8.0	4.4	6.1

Measurement	<i>ver. pos. ear</i>	<i>proj. ear height</i>	<i>circ.</i>	<i>arc length</i>	<i>arc width</i>
Max	150	69	626	342	389
Min	109	47	511	262	298
Mean	133	55	565	304	346
St. dev.	7.2	4.4	25.7	16.5	17.5

Table 5: Summary of anthropometric measurements for a population of 100 individuals (50 male, 50 female, ages between 20 and 40).

### 2.3.2.2 Correlating anthropometric measurements and PCs

Next, the correlation between the anthropometric measurements and the PCs was studied. For this purpose, the multivariate regression approach of Allen et al. [89] was used. A linear method was chosen because it can be implemented using linear matrix operations, which are easy to calculate and allow for low delay dynamic interaction with the resulting shape model. An  $(n_s - 1) \times (n_m + 1)$  mapping matrix  $\mathbf{M}$  was calculated as follows:

$$\mathbf{M} = \mathbf{B}\mathbf{F}^+ \quad (3)$$

$\mathbf{B}$  is a  $(n_s - 1) \times n_s$  matrix containing the weight vectors corresponding to the measurements for each PC, as calculated in section 2.3.1.3. To account for y-intercepts in the regression, a row of ones was appended to the measurement matrix  $\mathbf{F}$ , represented as  $(n_m + 1) \times n_s$  matrix  $\mathbf{F}$ , with pseudo-inverse  $\mathbf{F}^+$ . For the purpose of this paper,  $n_s = 100$ ,  $n_p = 10000$  and  $n_m = 10$ . Once the mapping matrix was obtained, it was possible to calculate a weight vector  $\mathbf{b}'$  for a new set of measurements  $\mathbf{f}' = [f'_1, \dots, f'_{n_m}, 1]$ :

$$\mathbf{b}' = \mathbf{M}\mathbf{f}'^T \quad (4)$$

In order to create a new surface using custom anthropometric measurements, the new  $\mathbf{b}'$  is simply inserted into Eq. (2) to obtain a new shape  $\mathbf{x}' = [\mathbf{v}'_{i,1}, \dots, \mathbf{v}'_{i,n_p}] = [x'_{i,1}, y'_{i,1}, z'_{i,1}, \dots, z'_{i,3n_p}]$ :

$$\mathbf{x}' = \bar{\mathbf{x}} + \mathbf{P}\mathbf{b}' = \bar{\mathbf{x}} + \mathbf{P}\mathbf{M}\mathbf{f}'^T \quad (5)$$

Thus, the shape model can now also be parametrized according to the anthropometric measurements and will be further referred to as the anthropometric model.

## 2.4 EXPERIMENTS

In this section, the anthropometric shape model built in section 2.3 is evaluated. First, a number of error metrics are introduced in section 2.4.1.1 that will be used throughout the rest of the work to determine the accuracy of each prediction. The overall prediction quality is assessed in section 2.4.1.2, for anthropometric models built with single measurements or with combinations of them. In order to examine the generalization ability of the models, cross-validation analysis is performed on the PCA model from section 2.3.1.3 and the anthropometric model from section 2.3.2.2 in sections 2.4.2.1 and 2.4.2.2, respectively. Finally, since errors due to human error or due to equipment properties sometimes occur when measuring subjects, section 2.4.3 discusses the sensitivity of each of the anthropometric measurements to measurement errors.

### 2.4.1 Determining the distribution of the prediction errors

#### 2.4.1.1 Prediction Quality Measures

To assess the accuracy of the prediction of a given shape model, three distance metrics were introduced: the geometric  $d_g$ , the normal  $d_n$ , and the tangential error  $d_t$ , between a point  $\mathbf{v}$  on the original surface and the corresponding point  $\mathbf{v}'$  on the mapped surface (see Fig. 25):

$$d_g(\mathbf{v}, \mathbf{v}') = |\mathbf{v} - \mathbf{v}'| \quad (6)$$

$$d_n(\mathbf{v}, \mathbf{v}') = |(\mathbf{v} - \mathbf{v}') \cdot \mathbf{n}_v| \quad (7)$$

$$d_t(\mathbf{v}, \mathbf{v}') = \sqrt{d_g(\mathbf{v}, \mathbf{v}')^2 - d_n(\mathbf{v}, \mathbf{v}')^2} \quad (8)$$

To assess the quality of a shape model prediction, the errors need to be combined into a single meaningful number. To this end, the vertex errors are averaged into the shape geometric errors  $D_g(\mathcal{S}_i)$  as follows:

$$D_g(\mathcal{S}_i) = \frac{1}{n_p} \sum_{\mathbf{v} \in \mathcal{S}_i} d_g(\mathbf{v}, \mathbf{v}') \quad \forall i = 1, \dots, n_s \quad (9)$$

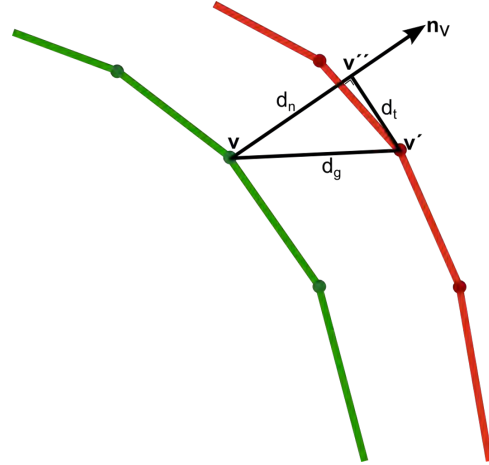


Figure 25: **Error metrics.** Visualizations of the error metrics used. The green line represents the original surface, the red line represents the prediction. Vertex  $\mathbf{v}'$  on the predicted surface corresponds to  $\mathbf{v}$  on the original surface.  $\mathbf{n}_v$  is the normal of vertex  $\mathbf{v}$ , and  $\mathbf{v}''$  is the projection of  $\mathbf{v}'$  on  $\mathbf{n}_v$ . The geometric error between these points is the norm of vector  $\mathbf{v}' - \mathbf{v}$ , the normal error the norm of  $\mathbf{v}'' - \mathbf{v}$  and the tangential error the norm of  $\mathbf{v}'' - \mathbf{v}'$ .

Finally, the average of the shape geometric errors for a set of shapes  $\mathcal{S}$  is calculated for each mapping, resulting in the model geometric error  $E_g(\mathcal{S})$ :

$$E_g(\mathcal{S}) = \frac{1}{n_s} \sum_{\mathcal{S}_i \in \mathcal{S}} D_g(\mathcal{S}_i) \quad (10)$$

Furthermore, the error metrics were also calculated per point, resulting in a vector  $\mathbf{e}_g = [e_g^{(1)}, \dots, e_g^{(n_p)}]$  of average point geometric errors, which can be used to visually locate the prediction errors of the model:

$$e_g^{(j)} = \frac{1}{n_s} \sum_{\mathcal{S}_i \in \mathcal{S}} d_g(\mathbf{v}_{i,j}, \mathbf{v}'_{i,j}) \quad \forall i = 1, \dots, n_s; j = 1, \dots, n_p; \mathbf{v}_i \in \mathcal{S}_i \quad (11)$$

Two approaches were considered for the calculation of the standard deviation. By taking the standard deviation over all  $D_g(\mathcal{S}_i)$ , one can gain insight on how the prediction errors vary across the entire population. The standard deviation over all vertex errors instead gives more information on the local error variation. The former was deemed to be of more use in evaluating the feasibility of a shape model for design purposes and was therefore used throughout most of this paper.

The model, shape, and point normal error  $E_n(\mathcal{S})$  and tangential error  $E_t(\mathcal{S})$  are calculated analogously.

#### 2.4.1.2 Analysis of Anthropometric Model Prediction

Apart from the sensitivity for each anthropometric measurement, the prediction errors of the mapping using several combinations of measurements were also taken into account. First, an anthropometric shape model was built for the entire input population, using only one individual measurement to calculate the mapping (Eq. 3). The scalp shapes of the entire population (Eq. 4) were predicted with this mapping. Each of the 100 predicted shapes was calculated by creating a model using the 99 remaining shapes and predicting the shape based on the measurements. The average geometric, tangential and normal errors 2.4.1.1 over all 100 scalp shapes were used to compare the prediction accuracy of each anthropometric measurement. In the same way, predictions were calculated for anthropometric models using all 1022 possible combinations of anthropometric measurements. This supports the creation of an anthropometric shape model with a minimal number of parameters.

#### 2.4.2 Evaluating the data set size

##### 2.4.2.1 Verification of PCA Model by Repeated Random Sub-sampling

To verify the robustness of the PCA model of section 2.3.1.3, repeated random sub-sampling was applied. Subsets of 10, 20, ..., 90 scans were randomly selected from the 100 scans. PCA was performed on each subset (see section 2.3.1.3), resulting in a PC matrix  $\mathbf{P}_t^T$  and an average surface  $\bar{\mathbf{x}}_t$ . One additional surface  $\mathbf{x}_v$  was randomly selected from the original data set (excluding the scans in the subset) to serve as validation data. The PC weights  $\mathbf{b}_v$  for  $\mathbf{x}_v$  were calculated as follows:

$$\mathbf{b}_v = \mathbf{P}_t^T(\mathbf{x}_v - \bar{\mathbf{x}}_t) \quad (12)$$

A new surface was then created by inserting the PC weights  $\mathbf{b}_v$  in Eq. (2). The resulting surface is a restriction of the original shape to the space spanned by the PCs of the trained PCA model. The shape geometric errors (see section 2.4.1.1) between this restricted surface and the validation surface  $\mathbf{x}_v$  were then calculated. The above procedure was repeated for 1000 iterations. Finally, the average and standard deviation of all 1000 shape geometric errors were calculated for each of the subsets. Since the projection error contributes to the mapping error, it was important to ensure that it was in the range of the original resolution of the MRI scans (1 mm).

#### 2.4.2.2 *Verification of Anthropometric Model by Repeated Random Sub-sampling*

Next, the generalization ability of the anthropometric model using the mapping of section 2.3.2.2 was examined. This was done in a similar way to section 2.4.2.1, with the exception that a mapping was constructed between the PC weights and the measurements using Eq. (3) of the training data. This mapping was then used to predict the shape of a randomly selected scalp surface (excluded from the training data). The geometric error between the predicted surface and the original surface was used to assess the robustness of the mapping.

#### 2.4.3 *Sensitivity Analysis of Mapping Algorithm*

The prediction error of the anthropometric model is influenced by the skills of the practitioner [112, 113], the precision of the equipment and the measurement method (direct measurement, measurement from 2D images or from 3D images) [114]. Therefore, the sensitivity of the prediction to measurement errors ought to be examined. In this section, a distinction is made between the anthropometric measurement (e.g. *head length*) and the measurement value (e.g. 190 mm). In order to obtain a single factor to express the sensitivity for each anthropometric measurement, a Monte Carlo analysis was performed on a full anthropometric model. Assuming that physical measurement errors follow a normal distribution, a range of normally distributed errors were added to the value of each anthropometric measurement, and a number of surfaces was predicted using the aberrated measurements. The prediction errors for these surfaces were averaged over 1000 trials for each step in the error range and a regression line was fitted to the averages and standard deviations.

## 2.5 RESULTS AND DISCUSSION

In this section, the results are shown. First, the data set size and region of interest are discussed in section 2.5.1. A quantitative and qualitative analysis of the shape model is made in section 2.5.2, and the selection of the right anthropometric models for a desired prediction accuracy is discussed. Two applications are discussed at the end of the chapter, section 2.5.3 demonstrates a comparison between the male and female head shape, section 2.5.4 explores the design of the brain-computer interface using an anthropometric shape model.

### 2.5.1 Data Set and ROI Selection

#### 2.5.1.1 Discussion on the data set size

A data set of MRI scans was used as input because of several reasons. Firstly, the high availability of MRI data, e.g. in university hospitals, eliminates the need for volunteer recruitment and time-consuming scanning sessions. As opposed to CT, MRI does not operate with ionizing fields [115]. Furthermore, extracting the skin layer directly means that there is no image occlusion due to hair. If necessary, the hair could be modeled separately. Alternatively, one might want to examine the effect of ethnicity, e.g. by considering scans from the Chinese population [116]. As long as the data can be extracted as a polygon surface, the presented methodology can be extended to other input data sets.

#### 2.5.1.2 Verification of PCA Model and Anthropometric Model

Fig. 26 (left) shows the average and standard deviation of the geometric error for the PCA model, as defined in section 2.4.2.1. The geometric error levels at  $0.64 \pm 0.12$  mm for 100 shapes, indicating a proper approximation (around 1 mm) of the head shape for the given population. Furthermore, the fact that there is a linear correlation between the PCs and the anthropometric measurements is supported by the outcome of the procedure in section 2.4.2.2: when using the anthropometric shape model for prediction, the geometric error again levels for 100 shapes, this time at  $1.52 \pm 0.37$  mm. The results are plotted in Fig. 26 (right).

### 2.5.2 Selecting an appropriate shape model

#### 2.5.2.1 Applying the error metrics

The three error metrics provide distinctly different information that benefits the interpretation of the prediction. The geometric error  $d_g$  is the most obvious one, and is commonly used in geometric modeling to determine the linear distance between a original and a predicted point. As such, it offers information on the spatial location of points in the prediction. In general, the higher this distance, the worse the prediction is considered to be. However, it contains no information on the direction in which the point has moved between predictions. The normal error  $d_n$ , on the other hand, shows whether the predicted point has moved towards the inside or outside of the shape. This knowledge is useful for fixation purposes: a higher normal error means that it is uncertain whether the retention system system (e.g. a hinge or a spring system) will be able to provide the right amount of flexibility. A designer will then either have to choose other fixation

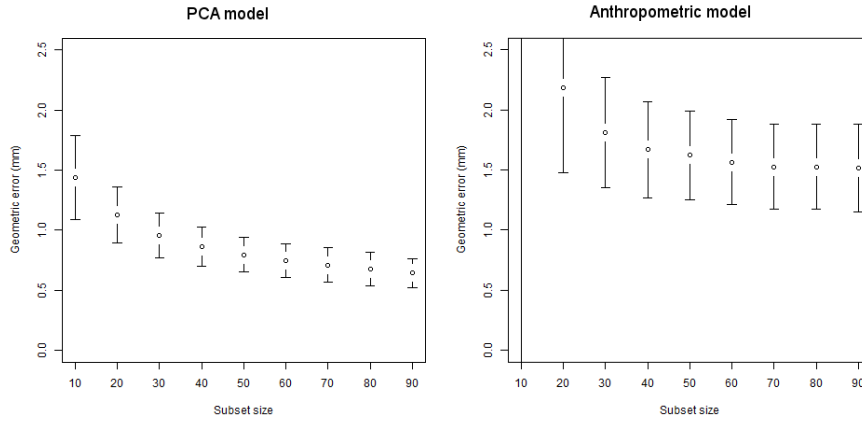


Figure 26: **Verification of PCA model and anthropometric model.** Average geometric error per subset size for shape model under repeated random sub-sampling and for 1000 iterations. Left: verification of PCA model with the first geometric error  $1.44 \pm 0.35$  mm (subset of 10 shapes) and the last one  $0.64 \pm 0.12$  mm (subset of 90 shapes). Right: verification for anthropometric measurement model with the first geometric error (out of range in the plot)  $18.6 \pm 27.5$  mm (subset of 10 shapes), and the last one  $1.52 \pm 0.37$  mm (subset of 90 shapes).

2

regions or another anthropometric model. Finally, the tangential error  $d_e$  expresses how much the point has moved along the surface of the shape. The higher this number, the larger the contact area between a product and the head will have to be. If it is too high, this requirement might result in overlapping contact areas. This is problematic for sensor application, e.g. for EEG-electrodes. The three measures combined provide information for a wide range of applications and can be used both to evaluate the feasibility of a given shape model and to assist in the determination of product specifications.

### 2.5.2.2 Quantitative Analysis of the Anthropometric model

As discussed in sections 2.2 and 2.3.2.1, there is a clear need for a shape model parametrized by simple, intuitive parameters when head product design is envisaged. The prediction errors (see section 2.4.1.1) for individual measurements are summarized in Table 6, the errors for various combinations in Table 7. The required number and combination of measurements will depend on the intended application. For example, if a geometric error of no more than  $2.5 \pm 0.1$  mm on average is acceptable, one might use the *head length*, *circumference* or *bitrignon width* individually to predict the three dimensional shape of a customer's head and create a 3D design.

Measurement	geom. error ( $E_g^S$ )	norm. error ( $E_n^S$ )	tan. error ( $E_t^S$ )
<i>all</i>	$1.61 \pm 0.36$	$1.40 \pm 0.32$	$0.20 \pm 0.03$
<i>head length</i>	$2.32 \pm 0.94$	$2.04 \pm 0.84$	$0.21 \pm 0.03$
<i>face width</i>	$3.06 \pm 1.41$	$2.74 \pm 1.30$	$0.21 \pm 0.03$
<i>bitragion width</i>	$2.46 \pm 0.99$	$2.17 \pm 0.90$	$0.21 \pm 0.03$
<i>ear heigh</i>	$3.28 \pm 1.65$	$2.97 \pm 1.53$	$0.21 \pm 0.03$
<i>hor. pos. ear</i>	$2.90 \pm 1.20$	$2.60 \pm 1.10$	$0.21 \pm 0.03$
<i>ver. pos. ear</i>	$2.64 \pm 1.06$	$2.40 \pm 0.99$	$0.19 \pm 0.02$
<i>proj. ear height</i>	$3.26 \pm 1.63$	$2.94 \pm 1.51$	$0.21 \pm 0.03$
<i>circumference</i>	$2.03 \pm 0.68$	$1.78 \pm 0.61$	$0.21 \pm 0.03$
<i>arc length</i>	$2.60 \pm 0.95$	$2.33 \pm 0.89$	$0.20 \pm 0.03$
<i>arc width</i>	$2.64 \pm 1.03$	$2.39 \pm 0.96$	$0.20 \pm 0.03$

Table 6: Average geometric, normal and tangential error for shapes predicted by the shape model using individual measurements (expressed in mm) for each shape in the data set (i.e. 100 shapes for this experiment).

Measurement	geom. error ( $E_g^S$ )	norm. error ( $E_n^S$ )	tan. error ( $E_t^S$ )
<i>HL, FW, BW, HE, VE, PE, CF, AL, AW</i>	$1.60 \pm 0.36$	$1.40 \pm 0.31$	$0.20 \pm 0.03$
<i>HL, FW, BW, HE, VE, CF, AL, AW</i>	$1.60 \pm 0.35$	$1.40 \pm 0.30$	$0.20 \pm 0.03$
<i>HL, FW, BW, EH, CF, AL, AW</i>	$1.63 \pm 0.37$	$1.43 \pm 0.30$	$0.20 \pm 0.03$
<i>HL, FW, BW, CF, AL, AW</i>	$1.63 \pm 0.36$	$1.42 \pm 0.30$	$0.20 \pm 0.03$
<i>HL, BW, CF, AL, AW</i>	$1.63 \pm 0.37$	$1.43 \pm 0.31$	$0.20 \pm 0.03$
<i>HL, BW, CF, AW</i>	$1.64 \pm 0.39$	$1.43 \pm 0.32$	$0.20 \pm 0.03$
<i>HL, CF, AW</i>	$1.70 \pm 0.45$	$1.49 \pm 0.39$	$0.20 \pm 0.03$
<i>HL, CF</i>	$1.80 \pm 0.52$	$1.54 \pm 0.44$	$0.21 \pm 0.04$

Table 7: Average pgeometric, normal and tangential error for shapes predicted by the anthropometric model using combinations of measurements, expressed in mm. HL = *head length*, FW = *face width*, BW = *bitragion width*, EH = *ear height*, HE = *horizontal position of ear*, VE = *vertical position of ear*, PE = *projected ear height*, CF = *circumference*, AL = *arc length* and AW = *arc width*.

Sometimes, an ergonomist will only have a limited set of physical measuring tools (e.g. calipers) at hand. In these cases, using a subset measurements would be preferred to finding the tools necessary to acquire all measurements. However, this advantage comes at a price: the average geometric prediction errors increase to  $1.80 \pm 0.47$  mm, as shown in Table 8 and 27.

Tool	Meas.	geom. error ( $E_g^S$ )	norm. error ( $E_n^S$ )	tan. error ( $E_t^S$ )
calipers	<i>HL, FW, BW</i>	$1.86 \pm 0.47$	$1.58 \pm 0.37$	$0.22 \pm 0.04$
calipers	<i>HL, BW</i>	$1.88 \pm 0.50$	$1.61 \pm 0.40$	$0.21 \pm 0.04$
tape measure	<i>CF, AL, AW</i>	$1.84 \pm 0.49$	$1.63 \pm 0.44$	$0.19 \pm 0.03$
tape measure	<i>CF, AW</i>	$1.87 \pm 0.52$	$1.66 \pm 0.46$	$0.19 \pm 0.03$

Table 8: Average geometric, normal and tangential error for shapes predicted by the anthropometric model using combinations of measurements that can be measured using a single tool, expressed in mm. HL = *head length*, FW = *face width*, BW = *bitracion width*, CF = *circumference*, AL = *arc length* and AW = *arc width*.

If the prediction error should be lower (e.g. for personalized EEG devices), more anthropometric measurements will be required, as shown in Table 7. A surprising fact from this table is that the best prediction, with a geometric error of  $1.38 \pm 0.27$  mm, a normal error  $1.27 \pm 0.26$  mm, and a tangential error  $0.15 \pm 0.03$  mm is achieved by using eight measurements, leaving out *ear height* and *projected ear height*. As of yet, it is not clear whether this is due to the segmentation process or because the anthropometry of the ear is actually not related to that of the head. Therefore, the current dataset cannot be used for designs that rely on detailed description of the ear geometry.

Another parameter to consider is the desired percentage of the population that the model should cover for a selected prediction error. This can be visualized by plotting the cumulative distribution function (CDF), as in Fig. 27. For example, while the combination of *head length* and *bitracion width* offers an average geometric error of  $1.88 \pm 0.50$  mm, Fig 27 (top left) shows that less than 70 percent of the population will actually have a geometric error lower than 2 mm. This might suffice for designs which aim to incorporate a higher amount of customizability, but it will not be enough for highly personalized products with fewer customization options. In the latter case, a combination covering a higher percentage will be preferred, e.g. *head length*, *bitracion width*, *circumference*, *arc length* and *arc width* (80 percent, see Fig. 27, top right).

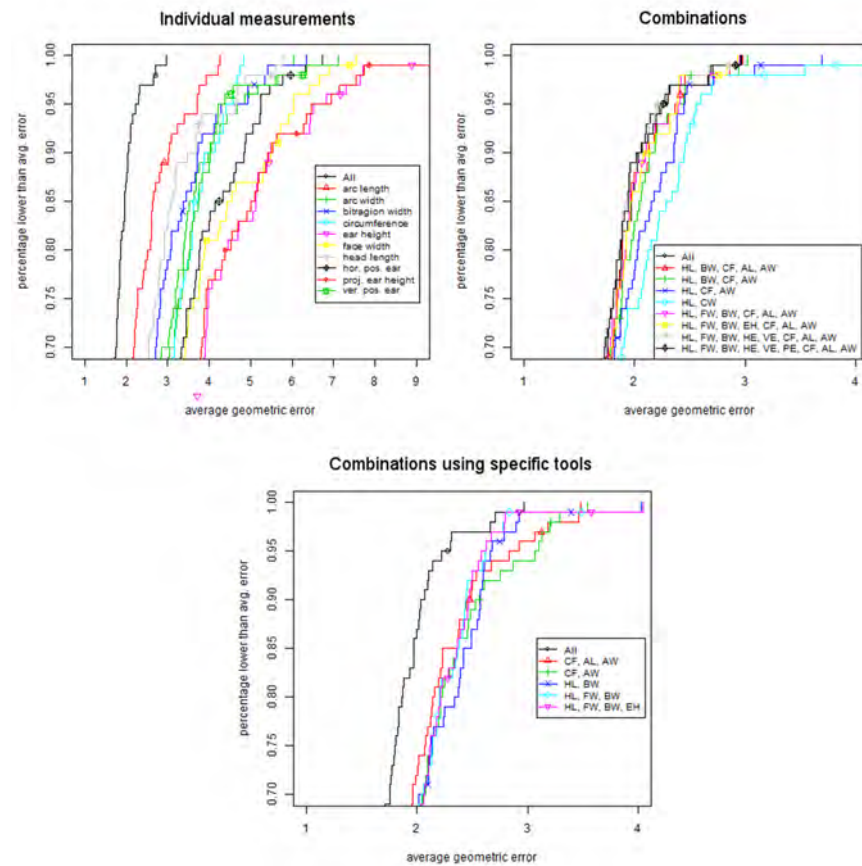


Figure 27: **CDF of average geometric error.** Cumulative distribution of average geometric error for an anthropometric model built using individual measurements (top left), combinations of measurements (top right), and combinations using specific anthropometric tools (bottom), including a full anthropometric model for comparison.

Finally, the sensitivity of the anthropometric model to measurement errors, as explained in section 2.4.3, should be taken into account. The results of the regression on prediction errors induced by measurement errors are listed in Table 9. Multiplying the slopes of these lines with an expected measurement error provides an estimate of the geometric error and standard deviation of the resulting shape model. While the *head length* and *circumference* both yield the very low individual prediction errors, *head length* is also more sensitive to measurement errors than *circumference*. Because the mapping was created using digital measurements, errors for measurements from digital surfaces will be smaller than those from physical measurements with calipers and measuring tapes. In this case, the sensitivity will be a less influential factor and a small number of anthropometric measurements can be used to build the anthropometric model (e.g. *head length* and *bitrignon width*). In contrast, when performing physical measurements, it is advisable to include anthropometric measurements with lower sensitivity and lower geometric errors in the anthropometric model (e.g. *circumference*, *arc length* and *arc width*). Again, *ear height* and *projected ear height* seem to be the most sensitive. Seeing as they also offer the worst individual prediction errors, the authors do not recommend using these as parameters for scalp-based designs.

Measurement	geom. error slope	Geom. st. dev. slope
<i>head length</i>	0.14	0.11
<i>face width</i>	0.04	0.03
<i>bitrignon width</i>	0.09	0.07
<i>ear height</i>	0.47	0.36
<i>hor. pos. ear</i>	0.06	0.05
<i>ver. pos. ear</i>	0.12	0.09
<i>proj. ear height</i>	0.50	0.38
<i>circumference</i>	0.07	0.05
<i>arc length</i>	0.02	0.02
<i>arc width</i>	0.05	0.04

Table 9: Sensitivity of the prediction to measurement errors. Slope of the regression line through the average geometric error and standard deviation for a Monte Carlo analysis performed for 1000 trials using the anthropometric model with all measurements. For anthropometric models using measurements with high slopes, measurement errors will have a larger impact on the resulting shape prediction.

### 2.5.2.3 Qualitative Analysis of Anthropometric Model

The average point geometric errors for all 100 predicted shapes are shown as a color map on the average head shape in Fig. 28. The figure shows the errors for the model using all measurements and for several combinations. The predictions on the forehead and the temporal regions seem to degrade when using less anthropometric measurements, which is especially clear for the combination of *head length* and *bitracion width*. The error metrics give a rough indication of the direction and magnitude of the prediction errors. The color map makes it possible to locate the measurement errors and to inform ergonomists which areas need extra attention and testing. For example, areas with a low normal error allow for product parts that fit closely to the skin, while areas with a high normal error might need additional cushioning.

The high errors at the boundary result from the fact that the surfaces are aligned using the corresponding points in the upper region of the head and more variation is expected at the lower side, as explained in section 2.3.1.2. Because the region of interest of the scalp, the bias is acceptable.

Fig. 29 shows some examples of shapes resulting from the mapping using all measurements. As long as the input range stays within three standard deviations of the mapped PC weights, realistic head shapes can be obtained. The variability of the underlying shapes can be visualized according to the tensor Frobenius norm of the landmark covariance matrix [117]. A color map of this norm overlaid on the average head shape is shown in Fig. 30.

### 2.5.3 Application for anthropometric research: comparison of male and female population

For this application, separate shape models were created for the male and female subgroups of the sample. The distribution of the PC weights for the entire population were separated into male and female subsets and statistically compared to find out which ones differ the most between the groups. The anthropometric measurements were also compared to discover which ones are best suited for characterizing male and female head shapes. A summary of the anthropometric measurements for the male and female parts of the population are shown in Table 10.

Table 11 shows that the most significantly different measurements (according to the Welch's t-test) are *head length*, *bitracion width* and *circumference*, which also offer the lowest individual prediction errors.

The first principal component seems to be the most significant one, see Table 12. This is supported by Fig. 31, where the average male and average female head are depicted, together with the distance be-

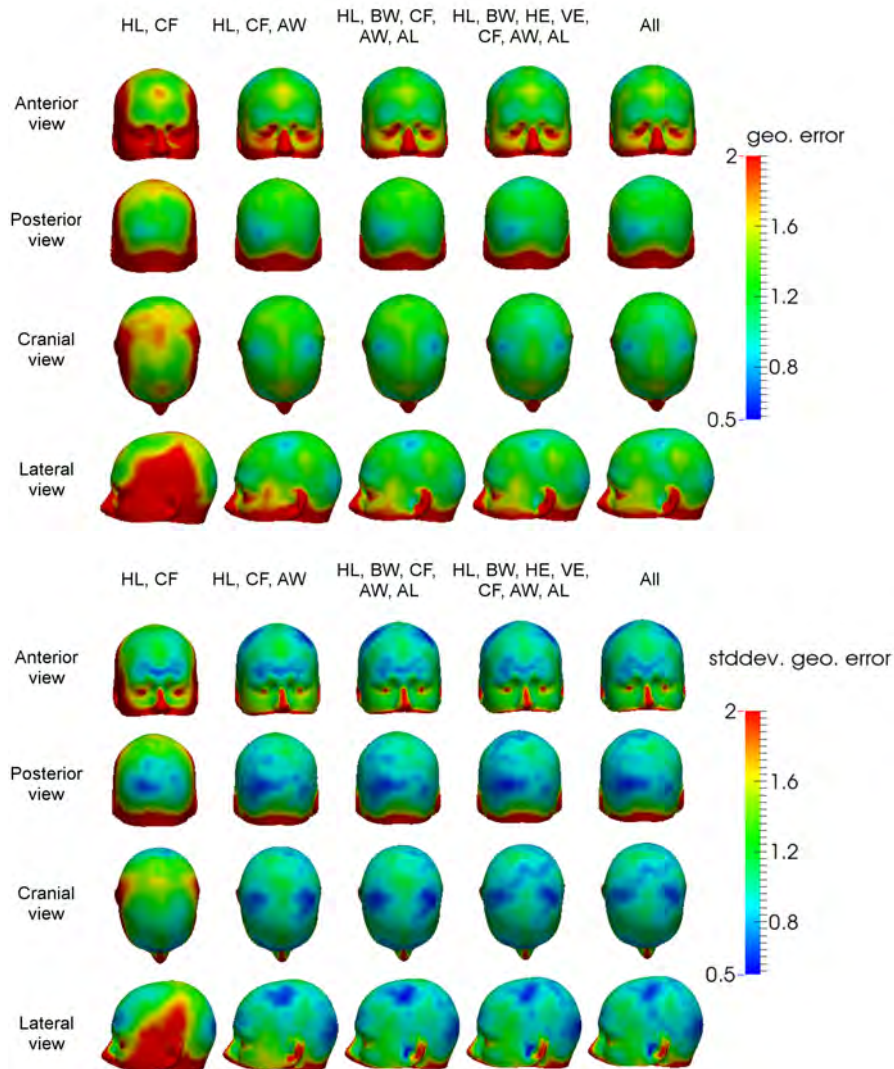


Figure 28: **Color map of geometric errors.** Average geometric error per point (top) and standard deviation of the geometric error (bottom) for the anthropometric measurement mapping in mm, shown on a 3D surface representing the average head for the model created with models using different combinations of anthropometric measurements. HL = *head length*, FW = *face width*, BW = *bitrignon width*, CF = *circumference*, AL = *arc length*, AW = *arc width*.

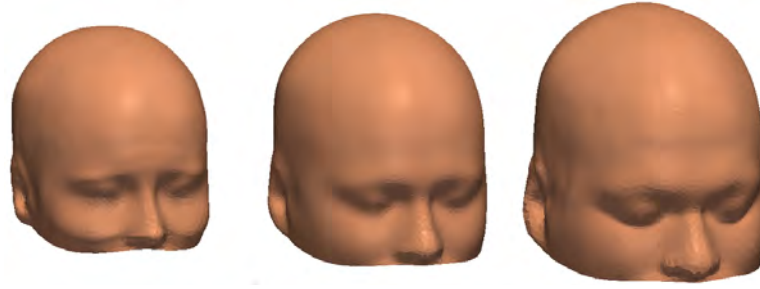


Figure 29: Example surfaces generated using the anthropometric model.

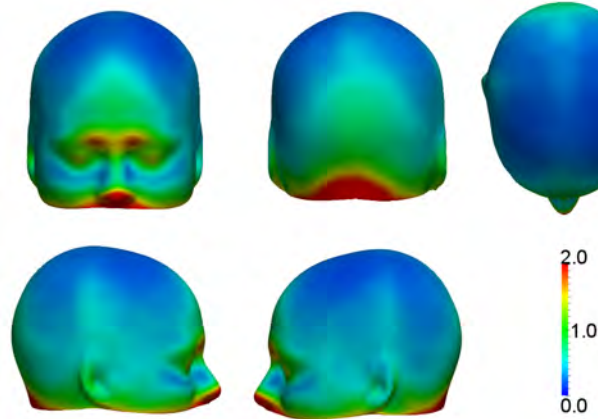


Figure 30: **Variability of the human scalp.** Variability of the scalp shape shown on the average 3D surface, expressed in terms of landmark covariance matrix Frobenius norm (in mm). High-variability regions are shown in red; low-variability regions are shown in blue.

Meas.	<i>head length</i>	<i>face width</i>	<i>bitr. width</i>	<i>ear height</i>	<i>hor. ear</i>	<i>pos. ear</i>
Male avg.	206 ± 7.9	96 ± 5.7	153 ± 6.3	57 ± 4.6	103 ± 5.2	
F avg.	191 ± 7.4	92 ± 5.1	142 ± 5.2	53 ± 2.8	98 ± 5.8	
p	1.26E-15	2.97E-04	1.47E-15	1.60E-07	2.97E-06	
Meas.	<i>ver. ear</i>	<i>pos. ear</i>	<i>proj. height</i>	<i>ear circ.</i>	<i>arc length</i>	<i>arc width</i>
Male avg.	137 ± 5.7	57 ± 4.6	584 ± 18.3	315 ± 13.0	356 ± 13.1	
F avg.	129 ± 6.5	52 ± 2.7	546 ± 16.1	293 ± 11.3	337 ± 16.5	
p	2.83E-08	3.14E-08	2.20E-16	1.32E-14	1.95E-08	

Table 10: Average anthropometric measurements for male (M) and female (F) population. The p-values for a Welch's t-test between both populations is also included. Only the measurements with p-value <0.05 are significantly different for the male and female populations.

Measurement	Geom. error ( $E_g^S$ )	Norm. error ( $E_n^S$ )	Tan. error ( $E_t^S$ )
Mixed	$1.59 \pm 0.50$	$1.36 \pm 0.43$	$0.21 \pm 0.03$
Mixed to F	$1.82 \pm 0.47$	$1.59 \pm 0.43$	$0.21 \pm 0.03$
F to F	$1.62 \pm 0.34$	$1.42 \pm 0.32$	$0.20 \pm 0.03$
Mixed to M	$1.89 \pm 0.47$	$1.65 \pm 0.43$	$0.21 \pm 0.03$
M to M	$1.71 \pm 0.38$	$1.49 \pm 0.33$	$0.20 \pm 0.03$

Table 11: Average geometric, normal and tangential error for prediction of the male and female population using various shape models. Mixed gender is a model containing 25 female and 25 male scalp shapes, F contains 50 female scalp shapes and M contains 50 male scalp shapes.

tween the respective shapes. For the sample means, the overall size of the head clearly seems to vary, which indeed corresponds to the first PC (see Fig. 24). Furthermore, the distance between the shapes seems to be the highest on the forehead, above the eyebrows. (As explained in section 2.5.2.3, the higher error at the boundary is due to the correspondence algorithm.)

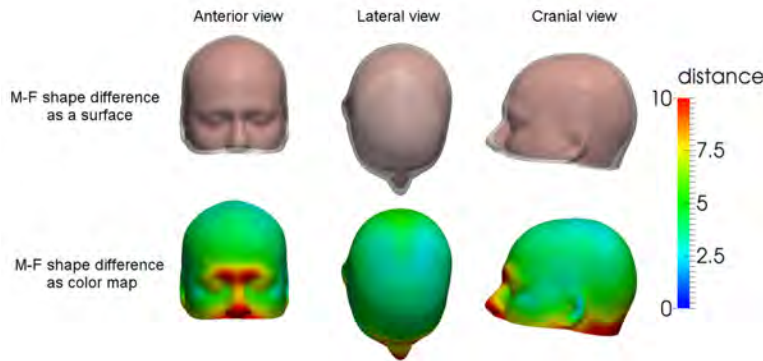


Figure 31: **Difference between male and female head.** The top row shows the difference between the average shapes of the male (white, transparent) and female (red) head. The bottom row shows the distance per point (in mm) as a color map on the average male head.

After this, the prediction errors for both models were first calculated separately as in section 2.4.1.2. Because using the full shape model of 100 shapes to predict the 50 male or female shapes would inevitably result in a better comparison, 25 male and 25 female scans were randomly removed from the full shape model to create a mixed gender shape model. The mixed gender model was used to predict the remaining 25 male and 25 female shapes. This procedure was then repeated using the latter shapes as training data and the for-

Statistic	PC <sub>1</sub>	PC <sub>2</sub>	PC <sub>3</sub>	PC <sub>4</sub>	PC <sub>5</sub>
p	6.89E-15	0.306	0.187	0.017	0.269
Statistic	PC <sub>6</sub>	PC <sub>7</sub>	PC <sub>8</sub>	PC <sub>9</sub>	PC <sub>10</sub>
p	0.068	0.254	0.992	0.257	0.232

Table 12: Significance of the first ten PCs, determined using a Mann Whitney U-test. U- and p-value is shown for each of the PCs. Only PCs with p-value <0.05 are significantly different for the male and female population.

mer ones for validation. The resulting predictions errors were then averaged. Finally, the predictions of the male shapes by a completely female shape model and the predictions of the female shapes by a male model were also calculated for comparison.

The results of the shape predictions are shown in Fig. 32 and Fig. 33. As expected, the prediction of the male shapes by the male models offers a lower geometric error ( $1.71 \pm 0.34$  mm) than the prediction of the male shapes by the mixed model ( $1.89 \pm 0.47$  mm), and the prediction of the female shapes by the female model a lower one ( $1.62 \pm 0.34$  mm) than that of the female shapes by the mixed model ( $1.82 \pm 0.47$  mm). Furthermore, Fig. 32 and Fig. 33 show that when using a mixed model to predict either gender, most of the errors are concentrated at the eyebrow ridge, around the glabella.

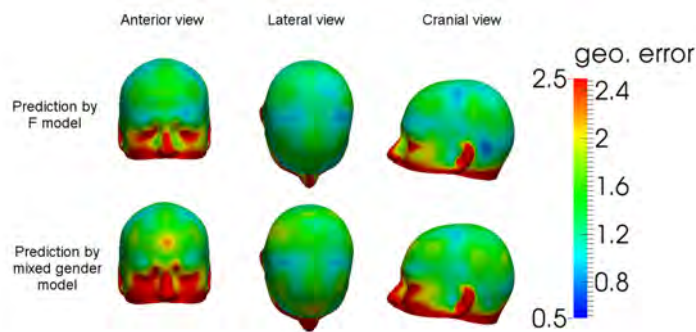


Figure 32: **Prediction error for female shapes.** Average point geometric errors for predictions of 50 female scalp shapes by a model consisting of 50 female shapes and a mixed model consisting of 25 female and 25 male shapes.

The observations in this chapter support earlier literature that concludes male and female head shape differ mostly in overall size [118] and in the size of supraorbital ridge [119, 120]. The same analysis could be performed to compare subsets of different ages and ethnicities. Unfortunately, the current data set does not contain information on the ethnicity of the subjects.

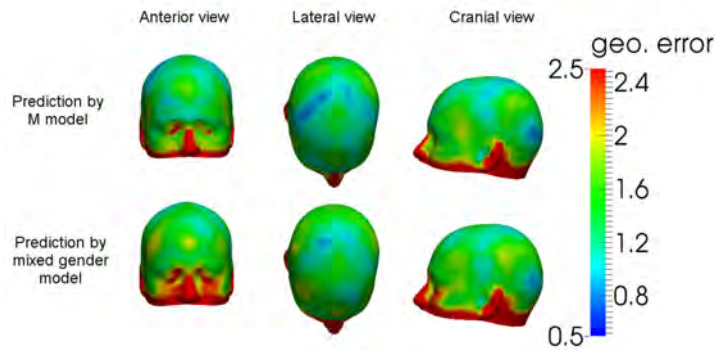


Figure 33: **Prediction error for male shapes.** Average point geometric errors for predictions of 50 male scalp shapes by a model consisting of 50 male shapes and a mixed gender model consisting of 25 female and 25 male shapes.

#### 2.5.4 *Application for industrial design: design of a brain-computer interface*

In this chapter, an application of the model for industrial design will be discussed. One product that would benefit from design using anthropometric shape models, is an EEG-monitoring headset for Brain-Computer Interfacing (BCI) [121]. One of the main challenges in BCI design is creating an EEG-monitor that is at the same time comfortable, easy to use, and accurate. These requirements can only be met if designers can properly accommodate for the variability of the head. An anthropometric shape model can be used to achieve the desired level of accuracy. To demonstrate this, a prototype headset was created using a custom plugin for SolidWorks [122]. This plugin allows importing a shape model as a B-spline surface and parametrizing it according to a number of anthropometric features [123]. Certain points of a CAD design can be linked to parametric head and will automatically adapt when it's dimensions are changed.

To create the BCI headset, the designer will first need to determine what the product should look like and how it should be fixated on the head. For instance, people generally do not prefer pressure on the temporal regions. Thus, a retention system that puts pressure on the frontal and occipital regions of the scalp is ideal. Using the color maps in Fig. 28, he can determine if a given shape model offers an accurate prediction on these regions of interest. For this purpose, he needs to know how much error is acceptable on individual predictions. Say the customer is paralysed and wishes to use a BCI for assisted communication. Seeing as the patient will wear the headset for extended periods of time, the comfort and the fit are very important. In this case, the lowest possible prediction error will need to be achieved. As discussed in the paper, the lowest prediction error occurs for shape models parametrized by all of the measurements

minus the *ear length* and *projected ear length*. While it will take some time to perform the remaining eight measurements, this process will only need to be performed once and thus speed is not as important as accuracy. The designer then predicts the user's individual head shape using the shape model and design a product using the head shape as a mannequin. An example of such a product is shown in Fig. 34 for three different shape predictions, with electrodes at locations Fpz1, Fpz2 and Oz according to the international 10-20 system [124]. While the shape of the headset is changed according to each individual prediction, the electrodes will remain at the proper positions. This is due to the fact that the electrode contact points have been linked with the shape model. The designer therefore does not have to realign the design for each new user. Instead, he has only to adapt the curvature of the headset's upper brace. Depending on the prediction error derived from Table 7, an extra layer of cushioning can be added to this product in order to ensure optimal fit and comfort.

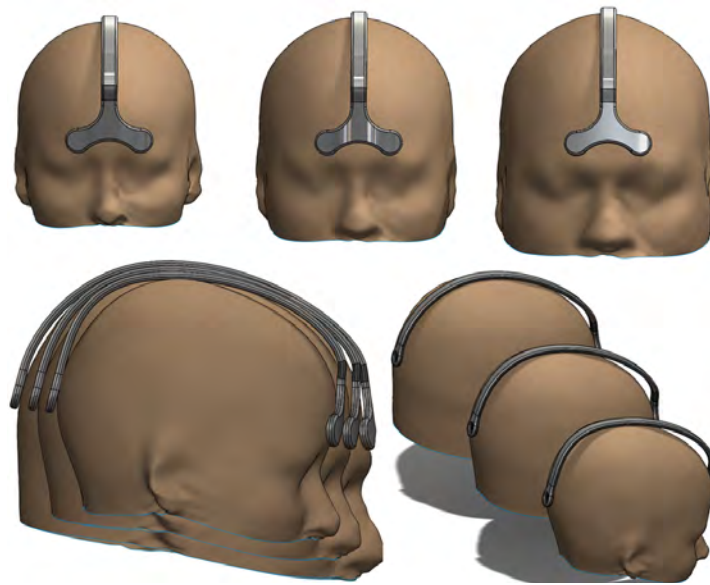


Figure 34: Example of an individualized brain-computer interface headset created with the anthropometric shape model.

Alternatively, a BCI headset might be required by a research lab in order to prototype BCI-software. In this case, a more generic product is preferable. The designer now needs to create an adjustable headset, using as few parameters as possible to predict the optimal size of the head. Based on the results in Table 6 and Table 7, the designer selects *head length* and *circumference* as parameters. Comfort or fit is not as important in this case as the subject will only be wearing the device for a short time, so a higher prediction error is allowed. However, researchers might be in a hurry to set up the experiment and be less precise when performing the measurements. It is therefore in

their best interest to select measurements that are not too sensitive to measurement errors. Upon considering Table 9, the designer decides to use *arc length* instead of *head length*. He then creates a 3D design by varying the two parameters within certain ranges and making sure the product offers the right amount of adjustability. Using Fig. 27, he knows this design will accommodate at least 75% of the population. An example of the final result is shown in Fig. 35. Customizability can be achieved by turning the knob on the back of the head. Even though certain parts of the headset do not make contact with all user's heads, the electrodes remain at the proper positions, so measurement accuracy is not compromised. Furthermore, markings can be made on the knob to indicate the position to which it should be adjusted for different head sizes. The researcher can thus simply use a look-up-table or computer program to instantly find the proper adjustment for a specific test subject. This eliminates the need to rely on trial-and-error and decreases the preparation time required for the experiment.

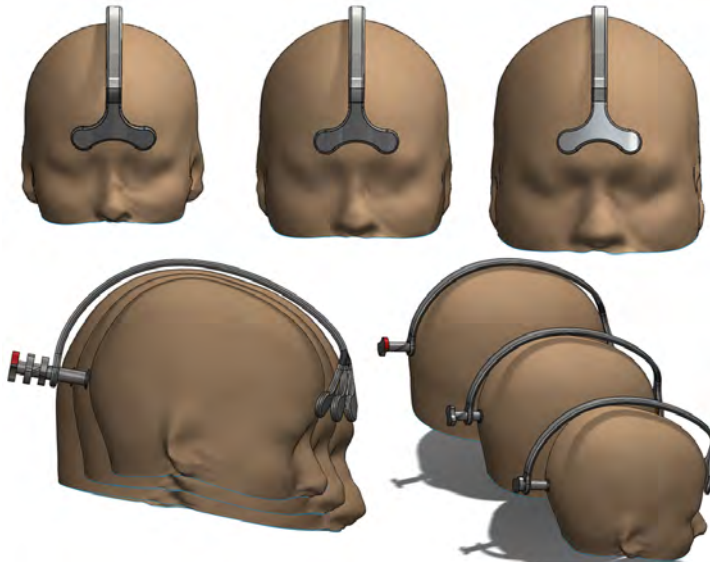


Figure 35: Example of an adjustable brain-computer interface headset created with the anthropometric shape model.

The above discussion gives a limited description of how the shape model can be used to design one type of products. Other products that might benefit from anthropometric model design are sports and safety helmets, glasses, smart textiles and near-body sensors. A complete description of the design process using anthropometric shape models is out of scope for this paper, but will be the theme of future work.

## 2.6 CONCLUSION

This work describes a method to create an anthropometric shape model from 100 MRI scans that can be used to accurately predict and analyze the shape of the human scalp for a Western population. The shape model was parametrized by the anthropometric features *head length*, *face width*, *bitragion width*, *ear height*, *horizontal position of the ear*, *vertical position of the ear*, *projected ear height*, *circumference*, *arc length* and *arc width*. Several combinations of these anthropometric measurements offer good predictions, but the best one is obtained by combining all of them except for the *ear height* or *projected ear height*:  $1.60 \pm 0.36$  mm. The sample size was verified using a cross-validation analysis on the anthropometric model, which revealed that the average geometric error levels at a sample size of 90 individuals. The sensitivity of the model to errors in input measurements was analyzed and it was shown that the *arc length measurement* is the least sensitive to measurement errors, while the *(projected) ear height* is the most sensitive one. Furthermore, the *ear height* seems to have no correlation with the overall shape of the head. It is not clear whether this is due to actual physical properties or due to the effect of the morphological operations that are applied to the input scans. It was shown that 3D scalp shapes generated with the proposed method look realistic and retain all information on the variability of the entire head. However, when the input measurements lie in extreme ranges or when an incompatible combination of values is used, realism is no longer guaranteed. Further research is needed to find the correlations between all anthropometric measurements values and to determine the correct input boundaries.

Two use cases were demonstrated for the model. The first case is an application for anthropometric research, discussing the shape variability between the male and female scalp. Using the anthropometric shape model, it was shown that the main difference between male and female head shapes is the overall size or volume of the head. Furthermore, when predicting a female scalp shape with a male shape model or vice versa, most errors seem to be located in the region of the forehead. A literature review confirmed that the main differences between male and female skull are indeed the size of the head and the size of the eyebrow ridge. This demonstrates that the anthropometric shape model can be used to accurately find variations in shape between different populations. A second use case was the CAD design of an elementary brain-computer interface (BCI) headset for two types of use cases: assisted communication and BCI research. A CAD design of a BCI headset was created for both cases using the data presented in this paper. Because the CAD design was linked to the shape model, it could automatically be adapted to various head sizes while retaining the correct electrode positions. This implies that the

anthropometric shape model can indeed be used to aid the design of BCI-headsets and other near-body products such as helmets or glasses.

The current results demonstrate the usability of a shape model parametrized by anthropometric measurements for ergonomic studies and design. In summary, to determine the optimal combination of anthropometric measurements for product design or analysis, the prediction accuracy, cumulative distribution and sensitivity should be taken into account. The importance of each of these factors depends on the intended application. By incorporating the anthropometric model into CAD software, digital designs can be directly driven and verified before prototyping. It is expected that the implementation of the proposed methodology will save time and significantly improve the design process.

## 2.7 ACKNOWLEDGMENTS

Data collection and sharing for this project was provided by the International Consortium for Brain Mapping (ICBM; Principal Investigator: John Mazziotta, MD, PhD). ICBM funding was provided by the National Institute of Biomedical Imaging and BioEngineering. ICBM data are disseminated by the Laboratory of Neuro Imaging at the University of California, Los Angeles.

This work was partially supported by Interuniversity Attraction Poles Programme - Belgian Science Policy (IUAP), Grant number: IUAP P7/11, Institute for Technology (iMinds), a research institute founded by the Flemish Government, URL: <http://www.iminds.be/en>.



## ERGONOMIC DESIGN OF AN EEG HEADSET USING 3D ANTHROPOMETRY

---

Daniël Lacko<sup>a,b,c</sup>, Jochen Vleugels<sup>a</sup>, Erik Franssen<sup>d</sup>, Toon Huysmans<sup>b</sup>,  
Guido De Bruyne<sup>a</sup>, Marc M. Van Hulle<sup>c</sup>, Jan Sijbers<sup>b</sup>, Stijn Verwulgen<sup>a</sup>.

<sup>a</sup> *Product Development, Faculty of Design Sciences, University of Antwerp, Antwerp, Belgium*

<sup>b</sup> *iMinds-Vision Lab, University of Antwerp, Antwerp, Belgium*

<sup>c</sup> *Laboratorium voor Neuro- en Psychofysiologie, KU Leuven, Leuven, Belgium*

<sup>d</sup> *StatUa Center for Statistics, University of Antwerp, Antwerp, Belgium*

Original research article published in *Journal of Applied Ergonomics*, vol. 58, p. 128-136, 2017.

### 3.1 ABSTRACT

Although EEG experiments over the past decades have shown numerous applications for brain-computer interfacing (BCI), there is a need for user-friendly BCI devices that can be used in real-world situations. 3D anthropometry and statistical shape modeling have been shown to improve the fit of devices such as helmets and respirators, and thus they might also be suitable to design BCI headgear that better fits the size and shape variation of the human head. In this paper, a new design method for BCI devices is proposed and evaluated. A one-size-fits-all BCI headset frame is designed on the basis of three digital mannequins derived from a shape model of the human head. To verify the design, the geometric fit, stability and repeatability of the prototype were compared to an EEG cap and a commercial BCI headset in a preliminary experiment. Most design specifications were met, and all the results were found to be similar to those of the commercial headset. Therefore, the suggested design method is a feasible alternative to traditional anthropometric design for BCI headsets and similar headgear.

## 3.2 INTRODUCTION

### 3.2.1 *Brain-computer interfacing*

Brain activity can be captured by a technique called electroencephalography (EEG), which detects voltage difference between certain points on the human cranium [125]. EEG measurement requires a number of electrodes to make electrical contact with the scalp on certain locations, specified by the international 10-20 system of electrode placement [23], see figure 36 (black circles). Traditionally, this placement is done either manually by an expert or, more commonly, using flexible electrode caps which stretch over the user's head and are fastened beneath the chin. In both cases, electrode placement starts by identifying four anatomical points: the nasion (Na), inion (I) and left and right preauricular points (respectively LPA and RPA) [23], see figure 37. All electrodes are then placed on relative distances between these points. First, a second set of reference points is determined by measuring the surface distance for the curve going from nasion to inion through the left preauricular curve. The first 10-20-points on this curve are placed at a 10% increment of the measured distance from the start and end points (nasion and inion). Intermediate points are placed at 20% increments of this distance. The procedure is then repeated on the other side of the head for the curve between nasion and inion going through the right preauricular point. Then, the points between nasion and inion on the curve on the plane that divides the head into a left and a right part -the midsagittal plane- are determined in a similar fashion to find the centerline reference points. Finally, all remaining 10-20-points are set by following the same procedure for each coronal curve from the lateral reference points through the centerline reference points. Electrodes are placed at a predetermined subset of these 10-20-points. Later on, alternative electrode placement systems were derived from the 10-20 system to improve the spatial resolution, namely the 10-10 system in which all electrodes are placed at 10% increments and the 10-5 system in which they are placed at 10% and 5% distances instead of 20% and 10% distances. The most commonly used electrodes are Ag/AgCl-electrodes, in combination with conductive gel to bridge the distance (and hair) between the electrode and the user's scalp [125].

EEG research focuses both on understanding human cognition and on applying EEG signals to affect the external world (brain-computer interfacing or BCI). Most of this research is done in medical or academic institutions [33]. While experiments in controlled environments have their advantages, there is also an urgent need to study the brain in real-world situations [126, 127]. Furthermore, there is a large group of potential applications outside of the research lab, such as control of prosthesis, communication without motor function, therapy and

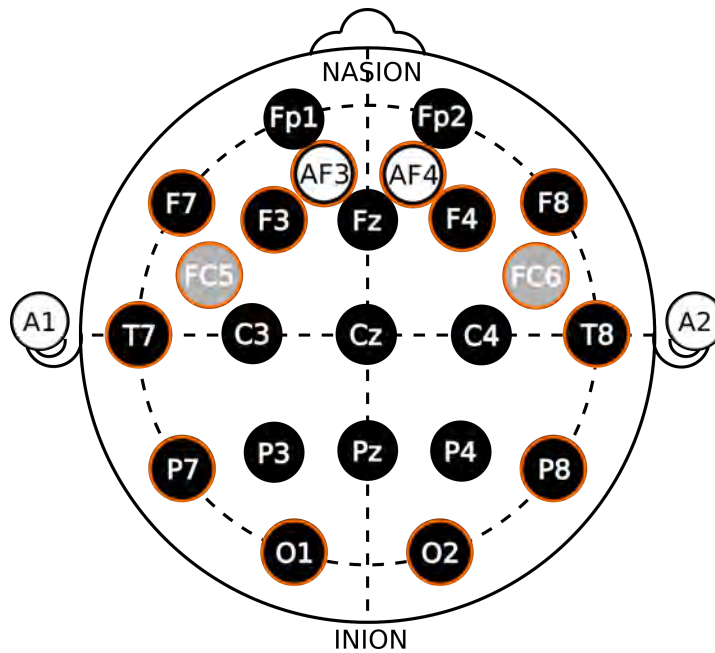


Figure 36: Electrode locations for the 10-20 system (black circles). The electrodes used throughout these work are circled in orange, including locations from the 10-10 (grey circles) and 10-5 (white circles) systems.

gaming [1, 2]. However, a number of problems arises when applying EEG outside of the laboratory. Experts are not always available, electrode caps are complex and time-consuming to put on, conductive gel requires users to wash their hair after each session. Devices that are easier to use and provide more accurate electrode placement would open up more real-world applications for BCI [1, 4, 26, 42].

### 3.2.2 BCI headsets

Several companies are targeting the consumer market with the development of low-cost commercial BCI headsets [2]. The most notable ones are the Emotiv Epoc (launched in 2009, see figure 38) and the Neurosky Mindwave (2007). While Neurosky offers a wide range of BCI-related software applications, Emotiv's Epoc has been the most popular device amongst BCI researchers and hobbyists [4]. One reason for this success is that the Epoc has 14 electrode channels, more than any other commercial BCI headset. Apart from that, the headset is wireless, uses saline electrodes instead of gel-based ones and offers access to the raw EEG signals.

Even though commercial headsets caused a spike in BCI-related research, real-world BCI applications are still rare [4]. Despite all of their advantages, these headsets often do not fit as well as EEG caps [26]. A bad fit causes electrodes to lose skin contact, shift during use and deviate from their target positions. A number of reasons for this

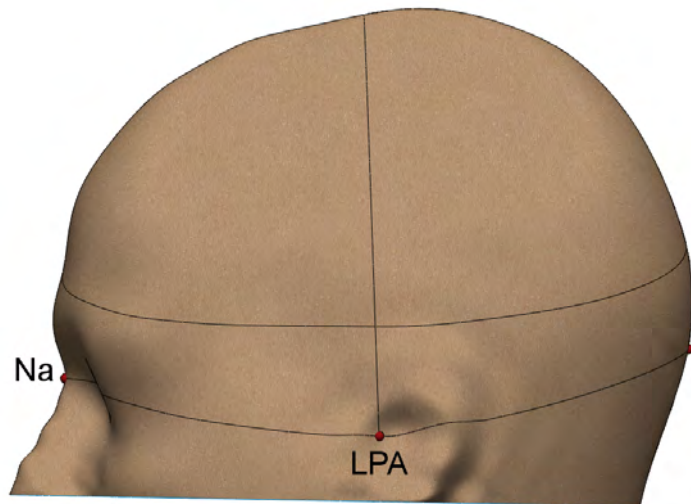


Figure 37: Reference points annotated on the average human head. RPA (not visible) is on the other side off the head, opposite LPA.

can be found in the history of the 10-20 system. First and foremost, human heads vary in size and shape. To date, the only EEG devices that can accommodate both size and shape variation are traditional EEG caps. The Epoc, for example, provides a good fit for different head shapes, but not for different head sizes [26]. Secondly, it was found that the 10-20 system can be used to place over 200 electrodes on the head, if -and only if- they were placed by an expert following a detailed placement procedure [23]. If the procedure is not followed exactly (as with commercial devices), electrode positions tend to vary more widely. This is especially true for the electrodes on the parasagittal and occipital regions of the head, such as P7-8, F3-4 and O1-2 [23, 128], see figure 36 (note: points P7-8 are referred to as T5-6 in [128], as was customary at the time. A modified nomenclature for these electrode positions has been introduced in 2006 [129]). Finally, some anatomical points on the head are difficult to locate by palpation, especially the inion [23]. The most easily identifiable anatomical positions are the nasion, the LPA and the RPA. However, none of the commercial devices use these reference points to mount the headset. Instead, the user is advised to place the reference electrodes on the mastoids, which are the bony areas behind the ears [130]. Because the mastoids have a surface area of several centimeters, it's impossible to precisely and reliably place the headset on the user's head. Electrode positions will thus vary between sessions.

Several papers call for more user-friendly EEG devices that better fit the variation in head shapes, sizes and anatomical points [26]. In order to improve the usability and accuracy, the headset should be designed in a way that brings the electrodes as close as possible to their ideal 10-20 positions and that ensures repeatability between measurement sessions.



Figure 38: Emotiv Epoc BCI headset.

### 3.2.3 3D anthropometry and ergonomics

Anthropometry is the field of science that deals with the morphological analysis of the human body [55]. Traditionally, anthropometrists used tools such as calipers and measuring tapes to take limited sets of measurements describing the body shape [131]. Ergonomics deals with the implementation of this knowledge in order to make better fitting products. In ergonomic product design, descriptive statistics (most commonly mean and standard deviation) are performed on a number of anthropometric measurements and a design equation is created to link these measurements to the shape and size of the product [132, 133]. For example, in the design of helmets, the head circumference is often used. A mannequin corresponding to the average circumference is made, and then linearly scaled up or down to correspond to different circumference values. The EN 960 standard prescribes a new design mannequin for every 10 mm increase or decrease in head shape [84].

Just as with electrode placement, for accurate measurement it is important that anthropometrists follow prescribed procedures [134]. When the measurements are performed by non-experts, the variation in measurements made by the same observer on the same subject (intra-observer) is in some cases even higher than the variation between those made by different observers (inter-observer) [54]. Though there are a number of procedures to quantify measurement errors, this is not done in all anthropometric or ergonomic studies [55]. Therefore, not all anthropometric tables correspond to each other, or to the actual body shapes, and products based on some of these tables will not fit the intended population very well.

Another disadvantage of traditional anthropometry is the assumption that several body dimensions vary uniformly, e.g. if the head

length increases, the head width is expected to also increase by the same amount. This is not always the case. For example, figure 39 shows the actual human head shape variation as derived from a 3D MRI scan database of a Western population [135]. It appears that head shape does not scale linearly with size: smaller heads are rounder, larger heads are more elongated. This indicates that products designed for different head sizes will also need to have different shapes.



Figure 39: Shape variation for Western heads.

In the last decade, new methods for registering body shapes have become available, the most important of which is 3D scanning [136]. Anthropometrists can now capture the complete shape in a manner of seconds. This has led to the development of 3D anthropometry, in which statistical shape analysis is performed on large collections of 3D scans. Shape modeling reveals valuable information on local and global shape variation and has been demonstrated to lead to improvements in product fit [137]. The benefits of 3D anthropometry have already been discussed for products such as helmets [138] and respirators [139, 140], though few studies verifying the fit of devices or products created using 3D anthropometry have been reported.

It is reasonable to presume that 3D anthropometry will become a valuable asset for the design of BCI headsets. In this paper, the impact of more ergonomic headset design on electrode positioning is discussed. The hypothesis is that 3D anthropometry can be used to create a BCI headset that meets all design requirements in terms of electrode placement, stability and repeatability. A one-size-fits-all BCI headset is created using a statistical shape model of the human scalp, and the electrode fit is verified with a 3D-printed prototype (section 3.3). Apart from the deviations of the electrode positions to the ideal 10-20 locations, the stability after controlled and spontaneous movement, and the repeatability (or test-retest reliability [141]) of electrode set-up are also verified. The same measurements are also performed on a commercial BCI headset for comparison (section 3.4). Finally, the findings are discussed in section 3.5 and concluded in section 3.6.

### 3.3 METHODS

The first part of this chapter, section 3.3.1, describes the design method for the prototype BCI headset. Section 3.3.2 contains the methods that were used to verify the prototype in terms of electrode positioning.

#### 3.3.1 *Prototype design*

The design specifications for the prototype were as follows: it should only be available in a single size (i.e. one-size-fits-all), it should cover the same electrode locations as Emotiv's Epoc (AF3, AF4, F7, F3, F4, F8, FC5, FC6, T7, T8, P7, P8, O1, O2), fit a Western population, remain as close as possible to their original location during movement (maximum displacement of 5 mm), have an average positioning error of maximum 25 mm (cord length between electrode position and 10-20 location, based on [26]) and should be easy to place on the head by non-experts.

The design was based on a statistical shape model of the human scalp containing 100 North-American individuals, described in a previous paper [135]. In order to determine the shape variation, principal component analysis (PCA) was performed on this dataset. PCA results in an ordered set of "directions" of variation, of which the first principal component (PC) will explain most of the variation, the second PC will explain the second largest part, etc. The resulting model consists of 9975 vertices, the position of which is represented by 99 principal components in total. In this case, the first PC was found to contain 71,21% of the variation. Three digital mannequins were created by taking the average head surface, the average head surface added with three standard deviations below the average PC weights and with three standard deviations above the average PC weights, representing the average head and the smallest and largest extremes respectively (see [135] for a detailed discussion). The mannequins were then imported in SolidWorks 2014 [122] as templates for the further headset design. The 10-20 system was constructed on the mannequins according to the procedure described in [23]. The heads were aligned according to the Frankfurt plane [84] so the local variation at the anatomical reference points Na, LPA and RPA was minimal. These points were chosen as reference since they are the easiest to identify by non-experts [23, 142]. Once the surfaces were aligned, the variation for the selected electrode positions could be visualized, as in figure 40.

The prototype frame was then designed around these distances and angles. The minimal configuration needed to cover all required points was a combination of two fixed horizontal rings (in transversal plane), connected with supporting struts. The headset's base rings were designed with an offset of 15 mm to the largest mannequin to provide

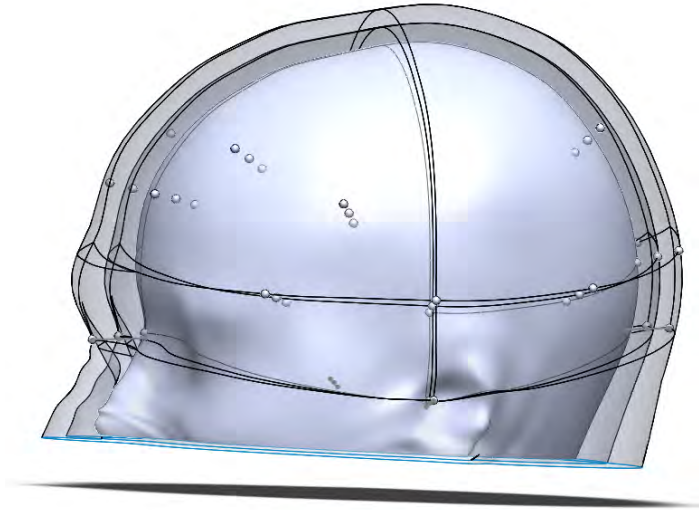


Figure 40: Electrode positions visualized on the smallest, average and largest design mannequin.

space for electrode parts and hair. Retractable cylindrical struts were created at the base of the headset in order to help the user identify the Na, LPA and RPA points and align the device properly. Sliding electrode mounts were then designed for each electrode according to the specific variation angle. Elastic bands (orthodontic MediMark 10 mm Heavy 4 oz. Elastics) were used in order to keep the electrodes in place on the head. Figure 41 shows the finished prototype, which will be referred to as the "Headset 2" in the remainder of this work.

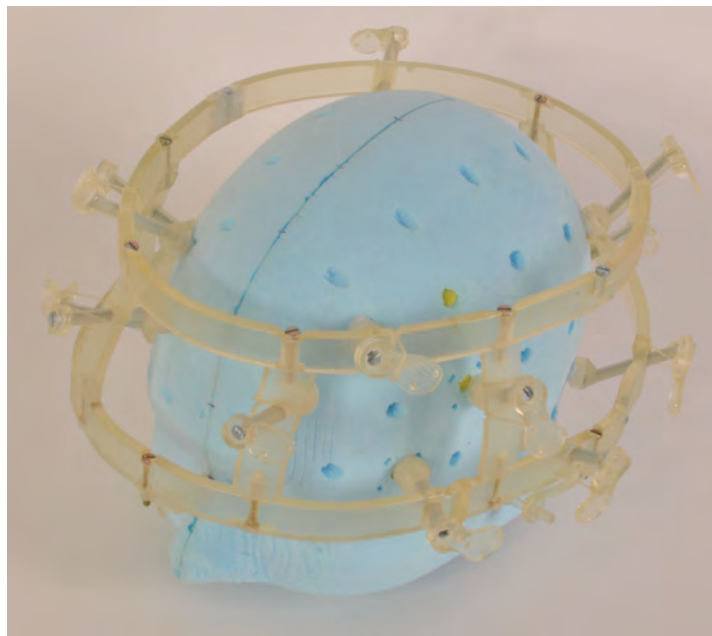


Figure 41: Prototype headset (headset 2) frame.

To place the headset on the user's head, first all of the electrodes should be retracted to the maximal position and fixated there. The headset is then placed on the user's head, aligning the reference struts to the anatomical landmarks described above. Then, the electrodes are released one by one until all of them make contact with the user's head. Finally, the reference struts can optionally be retracted. To remove the headset, the process is reversed.

### 3.3.2 *Experiment design*

A preliminary experiment to verify the design method was performed by 7 groups of graduate students (1st-year Masters in Product Development, University of Antwerp). The goal of the experiment was to investigate whether the design specifications could be met using the proposed method, and whether the electrode positioning, stability and repeatability of the prototype created using the 3D shape model were comparable to those of a commercial headset. This was tested by comparing the 3D locations for the fourteen electrode positions described in section 3.3.1 to those of a MedCat EEG cap (reference as "Cap" in the results) and by measuring electrode position deviation after movement and after repeated set-up. The same measurements were also performed on the Emotiv Epoc (referred to as "Headset 1"), which was chosen as a reference for commercial headsets. All 3D locations were digitized using a Microscribe MX digitizer connected to Rhinoceros 4 [143] and saved as text files for further processing.

#### 3.3.2.1 *Sample size*

The sample consisted of 13 students (6 male, 7 female), all of which were Caucasian and between the ages of 20-25. None of the subjects had head deformations or a history of head trauma. In each of the 7 groups performing the experiment, one person (designated as operator) was responsible for performing the 3D measurements. The measurements were repeated by 4 different operators for the 6 male subjects and by 3 different operators for the 7 female subjects.

#### 3.3.2.2 *Dependent and independent variables*

The independent variables are the EEG devices (Cap, Headset 1, Headset 2). Dependent variables are the locations of the electrodes after each stage in the experiment. From these, the positioning of the electrodes, stability of the headset and repeatability were calculated. The following conditions were tested:

1. FIT — distance of electrode's 3D locations to those of the ideal 10-20 positions

2. CM — deviation of the headset's electrodes from their original positions after controlled movement
3. SM — deviation of the headset's electrodes from their original positions after spontaneous movement
4. REP — average deviation of the headset's electrodes to the 10-20 positions after repeated set-up

The distances for the first three variables were calculated using the formula for euclidean distance between a reference 3D point  $\mathbf{v}$  (containing an  $x$ ,  $y$  and  $z$  coordinate) and a measurement 3D point  $\mathbf{v}'$ , as in equation 13. For example, in the case of FIT,  $\mathbf{v}$  would be the 3D position of an ideal 10-20 location as determined by the MedCat and  $\mathbf{v}'$  would be the 3D position of the same location for the headsets.

$$d(\mathbf{v}, \mathbf{v}') = \sqrt{(v_x - v'_x)^2 + (v_y - v'_y)^2 + (v_z - v'_z)^2} \quad (13)$$

In the case of REP, the arithmetic mean of the FIT distance between three subsequent headset set-ups was determined as in equation 14, with  $i$  being the number of the repetition and  $d_{\text{FIT},i}$  being the average distance between all pairs of corresponding points (electrode locations).

$$\text{REP} = \frac{1}{3} \sum_{i=1}^3 d_{\text{FIT},i} \quad (14)$$

### 3.3.2.3 *Equipment used*

The following equipment was used during the experiment:

- Microscribe MX digitizer
- Desktop computer running Windows XP SP3 and Rhinoceros 4
- Medcat caps 52, 54 and 58 cm (Cap)
- Emotiv's Epoc (Headset 1) (see figure 38)
- Prototype headset (Headset 2) (see figure 41)

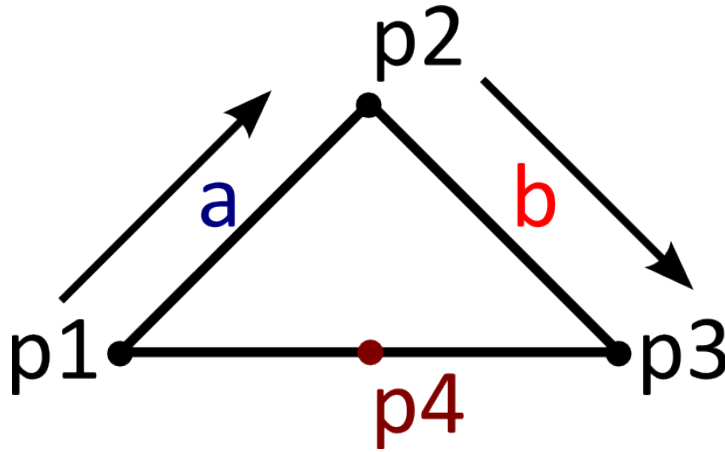
### 3.3.2.4 *Determining the electrode's 3D coordinates*

Placing the tip of the digitizer underneath the electrodes would cause undesirable shifts in the headset's position. Therefore, an alternative method was used to determine the electrode's coordinate positions. A 3D-printed plate was added parallel to the electrode contact surface at the end of the electrode mount, at a distance of 47.5 mm from the electrode. This plate contained three holes at fixed distance and on a

concentric alignment (see figure 42 (a)). Similarly, custom plates were printed for the Cap (at a distance of 5.5 mm) and for Headset 1 (at 15.5 mm).



(a)



(b)

Figure 42: Measuring plate at the end of Headset 2 (left), Cap (middle) and Headset 1 (right) electrode (a) and visualization showing the order in which the points were always measured (b).

The 14 points were measured in the order shown in figure 42 (b). On each electrode plate, three points were digitized by subsequently placing the digitizer tip in the holes in clockwise order, as in figure 42 (b).

The middle point between  $\mathbf{p}_1$  and  $\mathbf{p}_3$  was directly above the electrode. First, equation 15 was used to determine the coordinate for this point. Then, the cross product was used to determine the normal in the direction of the subject's head, as in equation 16. Finally, the midpoint  $\mathbf{p}_4$  was moved along this normal for a distance  $x$  specific to the headset (5.5 mm for the Cap, 15.5 mm for Headset 1, 47.5 mm for Headset 2) to find the electrode coordinate  $\mathbf{p}_e$ , see Equation 17.

$$\mathbf{p}_4 = \frac{1}{2} (\mathbf{p}_1 + \mathbf{p}_3) \quad (15)$$

$$\mathbf{n} = \frac{(\mathbf{p}_2 - \mathbf{p}_1) \times (\mathbf{p}_3 - \mathbf{p}_1)}{|(\mathbf{p}_2 - \mathbf{p}_1) \times (\mathbf{p}_3 - \mathbf{p}_1)|} \quad (16)$$

$$\mathbf{p}_e = \mathbf{p}_4 + (x * \mathbf{n}) \quad (17)$$

### 3.3.2.5 Experiment

The experiment was divided into two sessions, one for Headset 2 and one for Headset 1. At the start of each session, the subject was asked to take place in front of the custom set-up (see figure 43) and to bite down on a mouthpiece to ensure that their head was in the same position for each measurement.



Figure 43: Experiment setup. The test subject was seated on the red chair, biting down on the white mouth piece to stabilize their head. The box fixating the MicroScribe was positioned such that the experimenter could comfortably move the digitizer's arm around the person's head.

First, the Cap was placed on the user's head to serve as a reference for the ideal electrode positions. The fourteen relevant electrode locations on the cap were digitized using the MicroScribe. Then, Headset 1 was set up on the user's head, using the instructions in the electrode quickstart manual [130]: the reference electrodes were placed on the mastoids and the headset was positioned so that the frontal electrodes were approximately three fingers from the subject's eyebrow. When the device was properly in place, the electrode locations were again digitized (FIT). The subject was then asked to move the head 90 degrees to the left, then up, then down and finally to the right (using markers on the walls for reference). After this, the electrode positions were recorded (CM). The headset was then removed and remounted, and the electrode positions were again digitized. The subject was then asked to play "Just Dance" on the Nintendo Wii for three minutes,

in order to examine the stability of the headset during spontaneous movement (as in a real-world scenario). When the game was done, the electrode positions were digitized (SM). Finally, the headset was removed and remounted, and the positions were recorded for the last time (REP). In a second session of the experiment, the above procedure was followed using Headset 2, with the set-up instructions from section 3.3.1.

### 3.4 RESULTS

This section contains the results of the experiment. The distances between all electrodes were calculated using custom PHP- and Python-scripts, and statistics was done in R.

#### 3.4.1 Verification of design specifications

Table 13 shows the descriptive statistics for the deviation of Headset 2 electrode positions as compared to the Cap.

	Mean	St. dev.	Median	Min.	Max.
FIT	21.97	10.14	20.71	3.63	56.23
CM	8.47	4.85	7.57	0.99	30.93
SM	10.52	7.22	8.91	1.37	68.89
REP	11.28	6.11	9.87	2.06	47.88

Table 13: Descriptive statistics for Headset 2 measurements (in mm). FIT was compared to the Cap, REP was averaged over three headset set-ups for each test subject.

The deviation from the ideal 10-20 electrode positions was  $21.97 \pm 10.14$  mm, which is within the design specification of 25 mm. Surprisingly, the stability did not meet the specifications: the average electrode displacement after movement is larger than 5 mm in both cases ( $8.47 \pm 4.85$  mm and  $10.52 \pm 7.22$  mm). After placing the headset on user's heads on three separate occasions, the average electrode displacement was  $11.28 \pm 6.11$  mm.

#### 3.4.2 Comparison to commercial reference

Table 14 shows the same statistics for Headset 1. A Shapiro-Wilk test revealed that the data is not normally distributed, with p-value  $3.87e-33$  ( $<0.05$ ) for FIT,  $8.60e-26$  ( $<0.05$ ) for CM,  $1.87e-16$  ( $<0.05$ ) for SM and  $3.87e-33$  ( $<0.05$ ) for REP. Therefore, the Mann Whitney U-test was used to test for significant differences between the headsets. The distances were compared using the median because, like the Mann

Whitney U-test, it is non-parametric and thus not sensitive to outliers. Boxplots of the results for all dependent variables per headset are shown in Figure 44 (data shown is comprised of all observations for all electrode positions for all repetitions for each test subject).

	Mean	St. dev.	Median	Min.	Max.
FIT	26.10	15.02	23.37	3.32	91.04
CM	9.63	8.47	7.97	0.00	84.12
SM	13.37	11.88	9.32	1.09	71.69
REP	14.55	11.03	12.17	0.66	99.27

Table 14: Descriptive statistics for Headset 1 measurements (in mm). FIT was compared to the Cap, REP was averaged over three headset set-ups for each test subject.

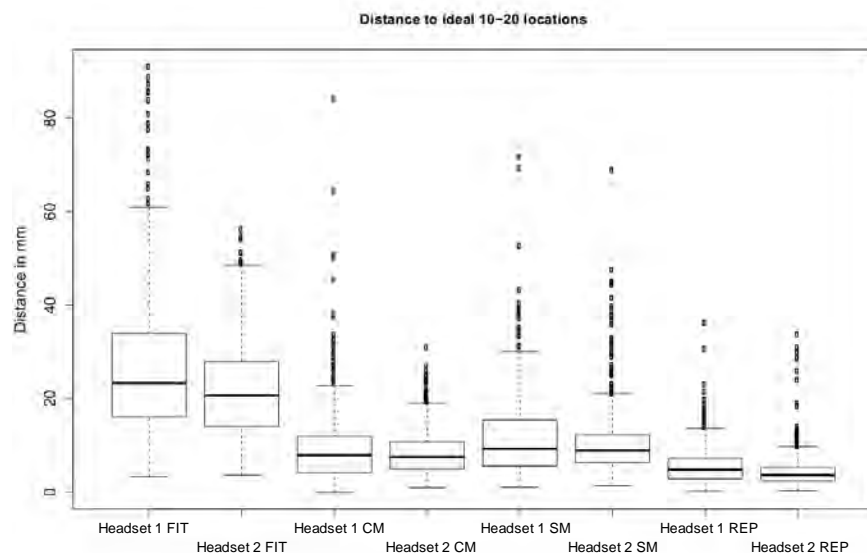


Figure 44: Box plots showing the distances between each headset and the Cap (FIT), the deviation in position after controlled movement (CM) and spontaneous movement (SM), and the average deviation of the electrodes to the 10-20 position after repeated set-up (REP).

For geometric fit of electrode positions there was a significant median difference of 2.67 mm,  $p$ -value  $9.39e-5$  ( $<0.05$ ). Controlled movement resulted in a non-significant difference of 0.40 mm,  $p$ -value 0.51 ( $>0.05$ ), spontaneous movement in a significant difference of 0.41 mm,  $p$ -value 0.01 ( $<0.05$ ). For repeatability there was also significant difference of 2.30 mm,  $p$ -value  $1.01e-16$  ( $<0.05$ ).

Stability was tested 4 times for 6 male subjects and 3 times for 7 female subjects, giving a total of 45 measurements for controlled

movement and 45 for spontaneous movement. Headset 1 fell off 2 out of 45 times for CM and 27 out of 45 times for SM. Headset 2 never fell off.

Finally, the median difference between individual electrode positions can be seen in Figure 45.

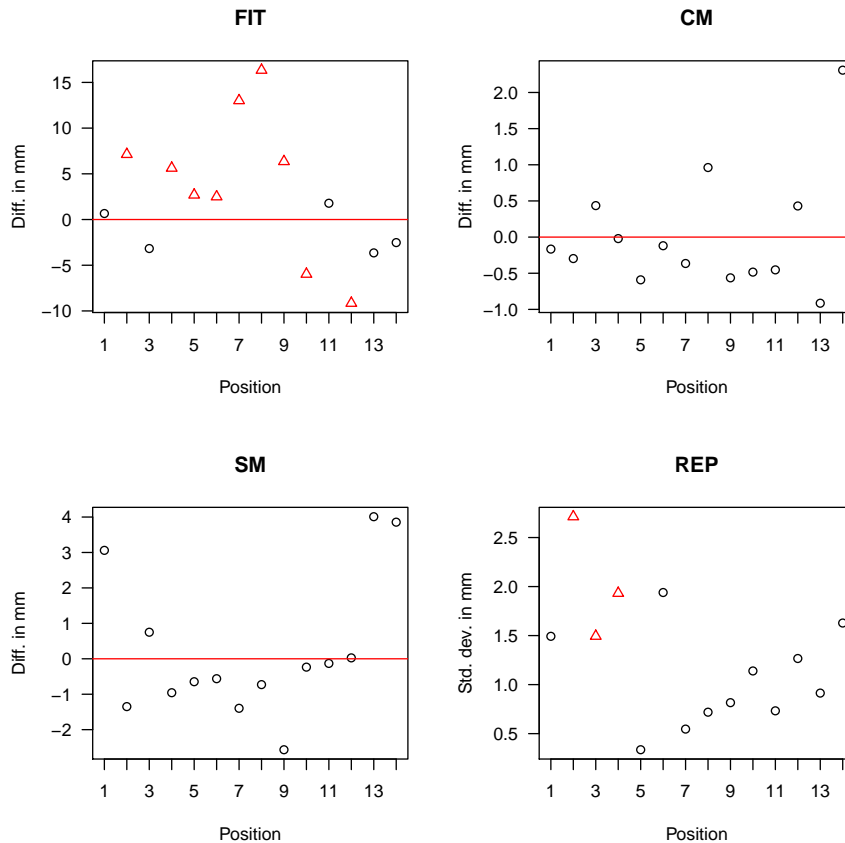


Figure 45: Effect size (median difference between Headset 1 and Headset 2) per electrode position as compared to 10-20 reference (FIT), before and after controlled movement (CM), before and after spontaneous movement (SM) and the average median difference after three repeated set-up measurements (REP). Positive values indicate a better fit for Headset 2, negative values are in favor Headset 1. Triangles (red) represent significant differences.

### 3.5 DISCUSSION

In this chapter, the results are discussed, starting with the implications of 3D anthropometry for the product design process in section 3.5.1. The following sections all deal with one of the tested aspects: electrode fit (section 3.5.3), stability (section 3.5.4) and repeatability (section 3.5.5). Limitations of the current study and suggestions for future work are found in 3.5.6.

### 3.5.1 3D anthropometry in product design

3D anthropometry was a considerable asset in the design process. By using the statistical shape model of the scalp, a number of time-consuming steps from traditional anthropometry could be omitted. For example, there was no need to limit the fit to a single measurement such as circumference, or to create a design equation in order to link this measurement to a CAD product (as in [132]). Nor was there a need to interpolate the remaining head shape once an appropriate number of mannequins for these measurements were created (as in [84]). Instead, three representative digital mannequins could be created in a matter of seconds using the shape model, and then imported into SolidWorks for immediate CAD design.

Furthermore, 3D anthropometry offers more flexibility in the creation of mannequins. Though the first PC was chosen in this work because it represented the largest part of the variation (section 3.3.1), shape models contain sufficient information to allow for many other parametrizations. For example, a number of principal components could be combined to cover even more of the shape variation. Alternatively, more intuitive parameters such as circumference or head length could be used in combination with the shape model, as discussed in [135]. This will be explored in future work.

In addition to one-size-fits-all design, a number of other design strategies can be considered, e.g. performing clustering analysis on the shape model to create non-linear sizing systems [133].

There are a lot of opportunities for 3D anthropometry in product design, and these should be explored in further research. Once a number of optimal methods has been established, 3D anthropometry will be invaluable for the design of all products that need to physically fit the human body.

### 3.5.2 Choice of variables

To the best of the authors' knowledge, the only variable that has been quantified in previous research is the fit to the 10-20 system, albeit in slightly different ways (e.g. Hairston et. al. used cord length instead of euclidean distance [26]). In this work, a number of new variables have been introduced in order to objectively quantify the stability (CM and SM) and repeatability (REP). Because there was no data available for comparison, these variables were compared to commonly used EEG positioning tolerances (e.g. electrodes within 1-2 cm diameter of the ideal 10-20 locations, as well as to the same measurements for Headset 1. However, since CM, SM and REP are all based on the measure of geometric fit to 10-20 location, they are expected to be valid for future verifications of the ergonomics of EEG and BCI headsets.

### 3.5.3 *Fit to 10-20 electrode positions*

The results relating to geometric fit of the headset were well within the design specifications and are similar to other commercial BCI headsets [26]. Compared to Headset 1, there's even a slight improvement in electrode positioning.

When considering the individual electrode positions, there's a notably high difference in geometric fit for the electrodes at the occipital region of the head (O1 and O2). Interestingly, Headset 1 offers a better geometric fit for locations T8 and F4. It's unclear why this is the case. Since these are the most variable electrode positions, a more detailed study on how to realize an optimal fit for these locations would result in insights with a large impact on the ergonomics of BCI devices.

Whether or not this will result in improved functionality is an open question. In-house experience indicates that because of the low spatial resolution of EEG, electrode locations can vary by 1 or 2 cm without notable effects on the EEG signal. However, to the author's knowledge this has not yet been verified. More research is required to determine exactly how critical the electrode positions are for the signal quality.

Even so, if the location for electrode position O1 in one paper deviates from the O1 position in another paper by 3 cm, can they be considered to compare the same EEG signals? Improved electrode positioning is important for the replication and comparison of experiments. Using 3D anthropometry for design will result in EEG equipment that follows the 10-20 standard and its derivatives more precisely.

### 3.5.4 *Stability*

Neither controlled (CM) nor spontaneous movement (SM) values met the design specifications. It is possible that the specification of 5 mm was too strict and that some displacement is inevitable after movement, although a stronger fixation method should also be considered.

The resulting values are close to those of Headset 1, and no significant differences could be found for individual electrode positions. While there is an overall significant difference for spontaneous movement, it is very small. It was observed that Headset 2 never fell off the user's head, which supports the specifications that it should be easy to use. However, this may be partly due to the fact that the prototype did not yet include electronics and was thus relatively light-weight.

In any case, because the results for stability were still within the general practice for EEG (<15 mm), and since they were comparable to those of the commercial reference, these results should not form an objection for the use of the proposed method.

### 3.5.5 *Repeatability*

Repeatability is important for several reasons. Firstly, a good inter-session fit is crucial in scientific research: more reliable electrode positioning will reduce inter-observer variability as a source of signal variability. Secondly, if the same electrode positions are consistently covered between sessions, the user might not need to recalibrate the BCI device each time it is used, resulting in a better user experience. Finally, repeatability reduces the complexity of the headset. If the electrodes always cover the same locations on the user's head, there is less need for electrode adjustment based on impedance measurements. There's also no longer a need for experts to position the electrodes; the headset can be mounted by the user's family members or caretakers.

While the average electrode displacement after repeated set-up was slightly higher than expected, the prototype shows similar results to the reference headset for most electrode locations, and even a slight improvement in general. This confirms the validity of the proposed method and is within general practice (see section 3.5.4, *Stability*), though further research should be conducted in order to find how better repeatability can be achieved.

### 3.5.6 *Limitations of current study*

The largest limitation of the current work is the small sample size and high number of outliers in the data. Therefore, no strong conclusions can be drawn from the quantitative data. However, while the sample may not be representative for the general population, the average head circumference of the test subjects was found to be similar to the values reported in other studies, e.g. the MRI dataset used to create the shape model (North American sample, 20-40y) [71] and the DINED dataset (Dutch sample, 20-30y) [75]:  $566.9 \pm 18.0$  mm compared to  $564.9 \pm 25.7$  mm and  $562.0 \pm 25.0$  mm, respectively. Still, the described experiment should be repeated with a representative sample in order to obtain conclusive results.

A second limitation regards the prototype design: Headset 2 was created primarily to verify the electrode positioning of BCI headgear based on 3D anthropometric data. Functionality, usability, aesthetics and user comfort were considered out of scope for this work. However, for a BCI headset to be truly ergonomic, all these aspects will need to be incorporated in the design process.

Even so, the results do indicate that using the proposed design method results in BCI headsets that adhere to current industry standards with regards to electrode positioning and repeatability, while at

the same time offering more efficiency, flexibility in region or points of interest, and clear visual feedback to the product developer.

### 3.6 CONCLUSION

3D anthropometric data was used in the design process of a BCI headset. A one-size-fits-all BCI headset frame was based on a statistical shape model of the human scalp and 3D printed. In order to verify the ergonomics of the device, the electrode positions of the printed prototype headset were compared to those of a medical-grade EEG cap, electrode positions were compared before and after movement, and repeatability of the headset set-up was measured.

All of the target specifications were met, with the exception of those related to stability (average displacement after movement lower than 5 mm). The electrode positions deviated from the ideal 10-20 locations by  $21.97 \pm 10.44$  mm on average. The electrodes had shifted by  $8.47 \pm 4.85$  mm after controlled movement and by  $10.52 \pm 7.22$  mm after spontaneous movement. Between-session deviation was  $11.28 \pm 6.11$  on average. These values are all within the deviations accepted in EEG measurement and were found to be similar to those of a commercial reference device.

The results demonstrate that 3D anthropometry is a feasible tool for the design of ergonomic BCI headsets. Alternatively, the proposed method can also be applied to improve the ergonomics of other head-based products such as glasses, helmets and respirators.



## PRODUCT SIZING WITH 3D ANTHROPOMETRY AND K-MEDOIDS CLUSTERING

---

Daniël Lacko<sup>a,b,c</sup>, Jochen Vleugels<sup>a</sup>, Toon Huysmans<sup>b</sup>, Guido De Bruyne<sup>a</sup>,  
Marc M. Van Hulle<sup>c</sup>, Jan Sijbers<sup>b</sup>, Stijn Verwulgen<sup>a</sup>.

<sup>a</sup> *Department of Product Development, Faculty of Design Sciences,  
University of Antwerp, Antwerp, Belgium*

<sup>b</sup> *iMinds-Vision Lab, University of Antwerp, Antwerp, Belgium*

<sup>c</sup> *Laboratorium voor Neuro- en Psychofysiologie, KU Leuven, Leuven,  
Belgium*

Original research article under review for publication in Journal of  
Computer-Aided Design in 2017.

### 4.1 ABSTRACT

Aside from anthropometric data tables, 3D shape models of the human body are becoming increasingly common and call for new product sizing methods based on 3D anthropometry. Though some shape model-based methods exist, most of them focus on mathematical clustering and do not discuss the usability of the clustering results for product design. In this paper, a new shape-model based clustering method for product sizing is presented that takes into account both shape information and usability for designers. The new method, called constrained k-medoids clustering, is applied on a shape model of 100 human heads. It is compared to a partitioning around medoid (PAM) clustering of anthropometric measurements of the same 100 heads (i.e., feature-based), as well as to PAM clustering of the shape model (i.e., shape based). Several metrics were used to evaluate the quality of the clusters, including the Ray-Turi index, the size-weighted variance and the average within-cluster point-to-point distances. Results show that both shape-based and constrained clustering perform better than feature-based clustering, with an average size-weighted variance (SWV) of  $0.22 \pm 0.07$  and  $0.23 \pm 0.03$  as compared to  $0.29 \pm 0.05$ , respectively. The average point-to-point distances in shape-based and constrained k-medoids were found to be similar to those of feature-based k-medoids, indicating that using 3D-anthropometry for product sizing will not have a negative impact on designer workload and/or a higher cost to implement more sizes. The results suggest that for head-based products, which require accurate shape and size

fit, sizing systems should be created using either shape-based or constrained k-medoids, with the latter being slightly less accurate but more intuitive for further design and verification.

## 4.2 INTRODUCTION

Ideally, products such as clothing or headgear should fit the shape of the human body, because in many cases badly fitting products will cause discomfort or even pain [45, 49]. The best product fit can be achieved by having clothing or apparel tailored to the individual's shape. However, custom-tailored products are expensive. On the other hand, while mass-production might be cheaper, it makes it less straight-forward to create well-fitting products. Instead of having precise measurements of the customer, clothing and wearables companies have to infer measurement data from small samples of their intended markets. In addition, globalization has resulted in the need to fit wearables to increasingly large and ethnically diverse populations. For these reasons, a number of product sizes is developed to fit several subgroups of the targeted customer population. The required number of product sizes and dimensions is determined by a sizing system based on anthropometric body measurements on a population sample. This section gives an overview of a number of methods for creating sizing systems based on traditional anthropometry and 3D anthropometry.

### 4.2.1 *Product sizing based on anthropometric features*

Traditionally, sizing systems are created on the basis of one or two measurements that the designers deem most relevant. The product dimensions for each product size are based on the percentage of the population that has predetermined measurement values, e.g. for a product with three sizes the 5th, 50th and 95th percentile (respectively P5, P50, P95) are commonly used [45, 46, 132]. While this method has been the industry standard for quite some time, it does not take into account the correlation between various body measurements.

To overcome this problem, multivariate statistics are used to determine the relevance of and correlation between anthropometric measurements. In multivariate sizing, principal component analysis (PCA) is performed on an anthropometric data table. PCA is a method that finds the structure of the variation in the anthropometric data by defining a new coordinate system with its axis in the directions of data variance [144]. It can be used to discover which measurements contribute most to the shape variation [133] (for a detailed description on how this is done, please see section 4.3.2).

Once the most important measurements have been determined, their percentile values are used to create physical or digital manikins. The required number of product sizes depends on the total percent-

age of the population covered by all sizes, also called the accommodation rate. Once the required number of sizes is known, products are modeled according to the manikins for each size and a design equation is determined in order to assign anthropometric measurements to different product sizes [46, 132]. Even with multivariate sizing, however, this often results in an incorrect fit [133, 145].

#### 4.2.2 *Product sizing based on 3D anthropometry*

Over the past decade, there has been a growing set of 3D shape data collected either via medical imaging or by 3D scanners of various kinds. Because 3D data contains a complete representation of the human shape, it is a more versatile source of information than traditional anthropometric data tables, provided that the collected 3D shapes are represented in the same coordinate system and consist of corresponding points. A collection of 3D shape surfaces with corresponding orientation and points is called a shape model [107]. Apart from the fact that anthropometric measurements can still be performed on shape models digitally, a statistical analysis of shape models results in a complete and accurate representation of the local and global shape variation [145, 146].

Various research groups have suggested methods to incorporate 3D anthropometry in product sizing. For example, Wuhler et al. performed anthropometric measurements on a shape model of the human head in order to support the design of glasses or helmets [147]. They achieved this by representing each head surface as a single point in a multi-dimensional space determined by two or three relevant feature dimensions. They then found the best possible way to cover most individuals in this feature space by a predetermined number of "boxes", the area or volume of which is defined by predetermined tolerances for each dimension. Manikins were created by taking the mathematical average of all head surfaces within each box. The idea was based on an optimization method for the production of electronic VLSI-chips [148, 149] and resulted in manikins with a realistic appearance, though no verification was provided that this results in better fitting product sizes.

Luximon et al. created a shape model of the human foot from 3D scans of 70 males [133]. They performed PCA on the shape model to find the structure of variation in shape space instead of in feature (measurements) space, as in traditional multivariate sizing. By calculating the correlation coefficient between the anthropometric measurements and the principal components, they were able to define which measurements mostly influenced shape variation. By assum-

ing a linear relationship between these two measurements and the first two PCs, they predicted new foot shapes using anthropometric measurements as parameters. To evaluate, they compared prediction errors resulting from the method using PC-correlated measurements with prediction errors from shape prediction with PC scores, as well as with traditional anthropometric measurements. They found that PC-prediction has the lowest prediction errors, but that prediction using correlated measurements still outperforms traditional measurements. This observation is similar to [135], which can be regarded as an extension of the correlation method, applied to the human head.

Niu et al. present a method in which the corresponding 3D surfaces are divided into uniform patches (or blocks) and are represented by vectors describing the average and standard deviation of the inter-subject distances within each patch [150, 151]. They refer to these vectors as block-distance based vectors and create a sizing system by performing k-means clustering on block distances. k-Means is an algorithm that divides data into k groups of surfaces with similar shape, based on the distance between each surface and the group means. In [152], the authors compare the results of k-means clustering on 1D measurements, on a set of principal components of 1D measurements and on block-distance based vectors. Their results show that k-means based on principal components or on block-distances based vectors results in clusters with less internal variation than k-means performed on anthropometric features. Since the differences between PC based and block-vector based k-means were small, block-distance based vectors were preferred as they yield a feasible input to product sizing.

While the methods discussed above have the potential to render mass-production design more effective by automating the creation of sizing systems, none of them utilize the full 3D shape information contained in the shape model. Instead, sizing is based either on traditional anthropometry or by simplified parameters which inevitably leave out part of the shape information, and the shape models are effectively only used at the beginning of the sizing process. Furthermore, while a number of design applications are suggested, including product sizing, it is not specified how these mathematical clustering methods should be implemented by product designers. As discussed in [135], statistical analysis on shape models results in a set of statistical parameters (e.g. high-dimensional vectors of principal components and principal component scores) that are not intuitive for designers, leading to a slow adoption of 3D anthropometry for product development. As long as the end-users are not considered in development and discussion of new shape modeling and clustering methods [145, 146], the use of these methods in design will be limited to the-

oretical applications. Alongside the development of new clustering methods, it should be made clear how designers should interact with shape models [146].

Recently, Baek and Lee were the first to perform clustering based on 3D shapes and to consider the representation and interaction required by product developers [153]. In their paper, they focused on updating the anthropometric design process for shoe design. They created a statistical shape model of the human foot, based on a database of 350 3D scans, and then performed hierarchical clustering to group these 3D scans into 8 similarly shaped clusters. An average geometric foot shape for the entire dataset was determined as a reference, and average shapes per cluster served as manikins, along with a color map of how the manikins differed from the clusters. From the statistical model, they derived the anthropometric features that are most important for the shape variation. They then virtually measured these features for each cluster and set up new sizing tables for each group. They proposed that shoe makers use these measurements, as well as the cluster manikins, to create new virtual shoe lasts for each group. Intuitively, their approach should perform much better than traditional anthropometric clustering based on foot length only. However, they did not provide a comparison between their 3D-based clustering method and foot length-clustering. They also suggested that apart from eight clusters, two, three or four would be possible as well, but did not elaborate on how a shoe maker or designer should make this choice. Furthermore, while their statistical analysis, virtual measurements and 3D manikins provide valuable insights into the shape variation of the human foot, using only geometric averages as CAD-manikins for each cluster will exclude many individuals which shapes that are more extreme within this group [45]. Finally, their proposed solution is a return to anthropometric sizing tables, where new customer would need to be measured for seven different foot dimensions. This increases complexity for the user compared to memorizing only one measurement (foot length) and using that as a reference for buying new shoes.

In this paper, a new method based on k-medoids clustering on (corresponding) 3D coordinates of all points in a shape model of the human scalp [135] is suggested. Because clustering is performed on all 3D points instead of on intermediate parameters, the resulting clusters more accurately represent morphological differences in the underlying population. Furthermore, a novel version of the k-medoids algorithm is provided, where clustering is still based on morphological differences between scalp surfaces, but is also constrained by one or more anthropometric features, in order to make product sizing more intuitive to designers and potentially also to end-users. Both

methods are verified by comparing the within- and between-group variation of the resulting clusters to those of k-medoids clustering based on traditional anthropometric features, the hypothesis being that k-medoids clustering will perform better than traditional anthropometric clustering. Finally, in addition to comparing the clustering methods, a workflow for the application of the clustering method for product sizing is discussed, including a method to select the optimal number of product sizes.

## 4.3 METHODS

In this section, the examined clustering algorithms and evaluation methods are described. The sample used for clustering consisted of 100 scalp surfaces and is briefly described in section 4.3.1. The independent variables for the experiment were the clustering methods and number of clusters, dependent variables were the metrics used to assess the obtained clusters. The existing methods that were used as a reference are described in sections 4.3.2 to 4.3.4, the new clustering methods (constrained clustering) is presented in 4.3.5. The metrics used to compare these methods were Ray-Turi index and size-weighted variance, outlined in section 4.3.6, and the point-to-point distances within each cluster, described in section 4.3.7.

### 4.3.1 Data acquisition

The analysis below was performed on a data set of 100 MRI images of the human scalp, which were used in previous work of the authors to develop a statistical shape model [135]. The shape model consists of an equal amount of males and females, between 20 and 40 years old. The following anthropometric measurements were used as features: head length ( $hL$ ), face width ( $fW$ ), bitracion width ( $bW$ ), ear height ( $eH$ ), horizontal position of the ear ( $hE$ ), vertical position of the ear ( $vE$ ), projected ear height ( $pE$ ), circumference ( $cF$ ), arc length ( $aL$ ) and arc width ( $aW$ ).

### 4.3.2 Statistical analysis of shape variation

In a preprocessing step, each of the 100 head surfaces obtained from the MRI scans is converted into a point set of 10 000 points that are approximately uniformly distributed over the head and are at corresponding locations. Such a corresponding point set representation is obtained using a three-step, group-wise correspondence optimisation procedure [107, 135]. First, a one-to-one flattening of each surface to a common square planar region is calculated. This brings the surfaces into an initial correspondence. Second, the correspondence is

improved by applying a non-rigid transformation to each of the flattenings, in a multi-resolution fashion using B-spline grids. The Minimum Description Length criterion, favouring compact shape models, is used as the optimisation objective and it is optimised with the LBFGS-algorithm. In the final step, the correspondence is used to calculate the average head shape and a set of 10 000 points is uniformly distributed over this average head. The corresponding locations in the common planar square domain are used to sample each of the 100 surfaces, finally resulting in a 100 corresponding point sets.

After processing, each head surface can be represented by a vector of 3D coordinates  $\dot{\mathbf{x}}_i = [\mathbf{v}_{i,1}, \dots, \mathbf{v}_{i,n_p}] = [x_{i,1}, y_{i,1}, z_{i,1}, \dots, x_{i,n_p}, y_{i,n_p}, z_{i,n_p}]$  with  $n_p$  the number of vertices (in this case,  $n_p = 10000$ ) and combined in an  $3n_p \times n_s$  shape matrix  $\mathbf{X} = [\dot{\mathbf{x}}_1^T, \dots, \dot{\mathbf{x}}_{n_s}^T]$  with the  $3n_p$  coordinates in rows (as variables) and  $n_s$  individual head surfaces in columns (as observations, in this case  $n_s = 100$ ). In order to study the variability in shape, PCA was performed on shape matrix  $\mathbf{X}$  using singular-value decomposition (SVD), as described in [107]. A short summary of the technique is given below; readers are referred to the original work for further details. First,  $\mathbf{X}$  is zero-centered: the mean head shape is calculated coordinate-wise as in equation 18 and subtracted from the columns of  $\mathbf{X}$  to form matrix  $\mathbf{X}_z$  in equation 19:

$$\bar{\mathbf{x}} = \frac{1}{n_s} \sum_{i=1}^{n_s} \dot{\mathbf{x}}_i \quad (18)$$

$$\mathbf{X}_z = [\dot{\mathbf{x}}_1^T - \bar{\mathbf{x}}^T, \dots, \dot{\mathbf{x}}_{n_s}^T - \bar{\mathbf{x}}^T] \quad (19)$$

The SVD of this zero-centered landmark matrix is defined as:

$$\frac{1}{\sqrt{n_s - 1}} \mathbf{X}_z = \mathbf{P} \mathbf{S} \mathbf{Q}^T \quad (20)$$

with  $\mathbf{P}$  a  $3n_p \times 3n_p$  orthonormal matrix containing the left singular vectors as its columns, which describe the principal component vectors or shape modes.  $\mathbf{S}$  is a  $3n_p \times n_s$  matrix with singular values in descending order, which are the standard deviations for the corresponding shape modes (i.e. the squares of these are the variances contained in each shape mode). Finally,  $\mathbf{Q}$  is an  $n_s \times n_s$  orthonormal matrix with the right singular vectors as its columns. Note that  $\mathbf{X}_z$  is divided by  $\sqrt{n_s - 1}$  to calculate the covariance PCA, as explained

in [144]. However, it is computationally more efficient to factorize the  $n_s \times n_s$  covariance matrix  $\mathbf{C} = \mathbf{X}_z^T \mathbf{X}_z$  as follows:

$$\mathbf{C} = \mathbf{Q}\mathbf{S}^2\mathbf{Q}^T \quad (21)$$

$\mathbf{Q}$  and  $\mathbf{S}$  can then be used to determine the first  $m$  columns of  $\mathbf{P}$ , i.e. the  $m$  shape modes for this shape model:

$$\mathbf{P}_m = \frac{1}{\sqrt{n_s - 1}} \mathbf{X}_z \mathbf{Q} \mathbf{S}_m^{-1} \quad (22)$$

$\mathbf{P}$  is then used to project the points in  $\mathbf{X}_z$  on the shape modes, resulting in an  $n_m \times n_s$ -matrix of shape mode scores (also called weights), represented in equation 23:

$$\mathbf{B} = \mathbf{P}^T \mathbf{X}_z \quad (23)$$

The principal components of  $\mathbf{X}$  capture all shape variation already contained in the individual shape vectors (3D coordinates of a large number of points on the scalp surfaces), which is much more accurate than if PCA were to be performed on an anthropometric measurement table and are also referred to as shape modes. The first shape mode (PC1) represents the largest shape variation, the second shape mode (PC2) the next largest variation (but does not contain any of the variation contained in PC1) and so on [144]. PCA is often used for dimensional reduction or data compressing. The scalp shapes can be represented and parametrized by the shape mode scores  $\mathbf{B}$ , with 99 scores for each head instead of 30 000 points coordinates. New shapes  $\mathbf{x}'$  can also be constructed as a linear combination of principal component vectors (matrix  $\mathbf{P}$  by setting new scores (score vector  $\mathbf{b}'$ , as in equation 24:

$$\mathbf{x}' = \bar{\mathbf{x}} + \mathbf{P}\mathbf{b}' = \mathbf{P}\mathbf{M}\mathbf{f}^T \quad (24)$$

Since  $\mathbf{X}$  was zero-centered to perform the PCA, the result is added to the mean shape coordinates  $\bar{\mathbf{x}}$ . Because the shape modes are difficult to interpret, a mapping  $\mathbf{M}$  can also be calculated between the shape mode scores and a  $n_f \times n_s$  matrix of anthropometric features  $\mathbf{F}$ ,

with  $n_f$  the number of features (in this work  $n_f = 10$ ) by multiplying the scores by the pseudoinverse of the features (described in [135]), as in equation 25:

$$\mathbf{M} = \mathbf{BF}^+ \quad (25)$$

This results in an intuitive parametrization that can be used to predict new head shapes accurately, as shown in equation 26, and is discussed in detail in a previous publication [135].

$$\mathbf{x}' = \bar{\mathbf{x}} + \mathbf{PMf}^T \quad (26)$$

When PCA is used for dimensionality reduction, the elements on the main diagonal of  $\mathbf{S}^2$  are added until a desired percentage of total variance is reached, and all remaining shape modes are discarded [144]. While there is a number of methods to determine which principal components are most relevant to the shape variation [144], a generally accepted method is to select those components that explain a cumulative percentage of the population [132, 133, 154–156]. A threshold between 70% and 90% is sufficient for most applications [157]. The percentage of variance explained by each shape mode was calculated by dividing each element of the diagonal of  $\mathbf{S}^2$  [133] by the total variance, which is the sum of all diagonal elements  $\lambda_i$  of  $\mathbf{S}^2$ , with  $i = 1, \dots, n_s$ .

To determine which measurements are the most relevant for shape variation, the correlation of each anthropometric measurement with the shape modes was determined. This was done by finding the Pearson's correlation coefficient  $\rho$  between the features (or measurements) in  $\mathbf{F}$  and the scores in  $\mathbf{B}$  for those shape modes that add up to explain 70% of shape variation. The correlation between pc score  $B_i$  and feature  $F_j$  can be found as in equation 27:

$$\rho_{B_i, F_j} = \frac{\text{cov}(B_i, F_j)}{\sigma_{B_i} \sigma_{F_j}} \quad \forall i \in 1, \dots, n_m, j \in 1, \dots, n_f \quad (27)$$

#### 4.3.3 Dissimilarity between 3D shapes

As discussed in the introduction, clustering is the process of grouping data into clusters that share similar characteristics. The dissimilarity

of two individuals is determined by the average difference between their characteristics, and is used to determine which cluster an individual belongs to. In clustering based on traditional anthropometry, the characteristics are anthropometric measurements and the dissimilarity between two individuals is determined by taking the average distance between their measurements.

In shape model based clustering, the Euclidean distance between each point coordinate on each individual head surface can be used instead. The average of the Euclidean distances between all corresponding points of two individual heads determines their dissimilarity, as in equation 28, resulting in a symmetric  $n_s \times n_s$ -matrix  $\mathbf{D}$  with main diagonal 0 and the difference between individual  $l$  and  $j$  at index  $(l, j)$  and  $(j, l)$ :

$$\mathbf{D}_{j,l} = \frac{1}{n_p} \sum_{i=1}^{n_p} d(\mathbf{v}_{j,i}, \mathbf{l}, \mathbf{j}) = \frac{1}{n_p} \sum_{i=1}^{n_p} \sqrt{(x_{j,i} - x_{l,i})^2 + (y_{j,i} - y_{l,i})^2 + (z_{j,i} - z_{l,i})^2} \quad (28)$$

#### 4.3.4 Mathematical clustering of 3D shape model using k-medoids

k-Medoids is a variant of k-means clustering that involves the distance to the cluster medoids instead of cluster means [158]. The medoid of a cluster is the individual in that cluster that is closest to the mathematical mean shape. The most commonly used k-medoids method is partitioning around medoids, as described in [158] and implemented as in algorithm 1, similar to the implementation presented in [159].

The only required input for algorithm 1 is the desired number of clusters, the desired number of trials and a  $n_s \times n_s$  dissimilarity matrix  $\mathbf{D}$ . Since  $\mathbf{D}$  can be precomputed for any dataset, the same algorithm can be used for clustering by difference in anthropometric features and clustering by geometric differences. The row and column indices of  $\mathbf{D}$  correspond to the scalp surfaces represented in the columns of  $\mathbf{X}$ . A random set of  $k$  indices is selected from  $\mathbf{D}$  for each of the  $k$  clusters, and the remaining  $n_s - k$  surfaces are assigned to a cluster based on which medoid they are the most similar with, i.e. the minimum dissimilarity according to  $\mathbf{D}$ . This is done by making a copy of the rows from  $\mathbf{D}$  at the medoid indices,  $\mathbf{D}'$  (line 8). In  $\mathbf{D}'$ , the rows then correspond to the currently selected cluster medoids and the columns correspond to the differences between the medoids and the other surfaces in  $\mathbf{X}$ . Therefore, in line 11, the indices of the  $l$  array (length  $n_s$ ) correspond to the indices of the columns in  $\mathbf{D}$ ,  $\mathbf{D}'$ ,

and  $\mathbf{X}$ . Because the rows of  $\mathbf{D}'$  corresponds to the  $k$  clusters, its row indices can be used to label which cluster each surface belongs to. In line 12, after the closest medoid for a certain surface found, the entire column is marked as traversed (after all, there's no need to check whether that surface is closer to another cluster medoid). Once all the entries in  $\mathbf{D}'$  are traversed, the currently used medoid indices are stored (line 14), and new medoid indices are selected by considering the dissimilarity of surfaces within clusters: the surface with a minimum total dissimilarity to all other surfaces in the cluster is chosen as a new medoid (lines 15-25). The cluster medoid reassignment is repeated until the cluster medoids converge, meaning that the surfaces in each cluster are indeed the most similar to that cluster's medoid and that the clustering is optimal (lines 7-26). Finally, the cost of this clustering is determined by adding the sums of the dissimilarities of each cluster medoid to the other surfaces within that cluster (lines 27-30). To find an optimal clustering, this entire process is repeated  $n$  times. If the cost of a clustering iteration is lower than the previous lowest cost, that iteration's medoid indices and labels are saved (lines 31-35). The algorithm then returns the final medoid indices, the cluster labels for each surface and the total cost of clustering around these medoids at line 37.

---

**Algorithm 1** k-medoids clustering - part 1
 

---

**Input:**  
 $k$  - number of clusters (scalar)  
 $\mathbf{D}$  - precomputed  $n_s \times n_s$  dissimilarity matrix (multidimensional array)  
 $n$  - number of trials (scalar)

**Output:**  
 $\mathbf{m}$  - medoid indices (array)  
 $\mathbf{l}$  -  $n_s$  vector containing cluster labels (array)  
 $c$  - total clustering cost (scalar)

```

1:  $\mathbf{m} :=$  empty array of size  $k$ 
2:  $\mathbf{l} :=$  empty array of size  $n_s$ 
3: for  $i := 0; i < n; i ++$  do {for a specified number of trials}
4:    $\mathbf{m} :=$   $k$  random indices from  $\mathbf{D}$ 
5:    $\mathbf{m}' :=$  empty array of size 0 {list of saved medoid indices}
6:   while  $\mathbf{m} \notin \mathbf{m}'$  do
7:      $\mathbf{D}' := \mathbf{D}_{\mathbf{m},:}$  {copy full rows with indices  $\mathbf{m}$  from  $\mathbf{D}$ }
8:     while all values in  $\mathbf{D}' \neq \infty$  do { $\infty$  marks traversed entries}
9:       get index (row, col) for minimum value in  $\mathbf{D}'$ 
10:       $\mathbf{l}_{\text{col}} :=$  row {set label for surface with index col}
11:       $\mathbf{D}'_{:, \text{col}} := \infty$  {mark entire column col of  $\mathbf{D}'$  as traversed}
12:    end while

```

---

**Algorithm 1** k-medoids clustering - part 2

---

```

13:   append  $\mathbf{m}$  to  $\mathbf{m}'$ 
14:   for  $j := 0; j < k; j++$  do {for all clusters}
15:      $\mathbf{jIndices} :=$  all indices of  $l_{ind}$  for which  $l_{ind} = j$ 
16:      $minDis := \infty$  {minimum dissimilarity for this cluster}
17:     for  $o := 0; o < \text{len}(\mathbf{jIndices}); o++$  do {for all surfaces in
      this cluster}
18:        $tempDis := \sum \mathbf{D}_{:,o}$  {dissimilarity of surface  $m$ }
19:       if  $tempDis < minDis$  then
20:          $minDis := tempDis$ 
21:          $\mathbf{m}_j := o$  {surface  $m$  is new cluster medoid}
22:       end if
23:     end for
24:   end for
25: end while
26:  $c' := 0$  {cost of this clustering trial}
27: for  $j := 0; j < k; j++$  do {for all clusters}
28:    $c' := c' + \sum \mathbf{D}_{:,m_j}$  {add within-cluster dissimilarity to current
      cost}
29: end for
30: if  $c' < c$  then
31:    $\mathbf{m} := \mathbf{m}'$ 
32:    $\mathbf{l} := \mathbf{l}'$ 
33:    $c := c'$ 
34: end if
35: end for
36: return  $\mathbf{m}, \mathbf{l}, c$ 

```

---

This algorithm was applied to both the anthropometric features (dissimilarity based on difference between measurements) and the geometric shape (dissimilarity based on Euclidean distance between coordinate points). The former is referred to as "feature-based clustering", the latter as "shape-based clustering". In both cases,  $n$  was set to 100 iterations, as in [159].  $k$  was varied from 2 to 10 clusters, since a single product size for an entire population requires a different design approach ("one-size-fits-all" design), and few head products exist in more than 10 sizes.

#### 4.3.5 Constrained clustering

Finally, the k-medoids based algorithm was slightly modified by constraining the clustering in the most important feature dimensions (as determined by the PC-feature correlation in section 4.3.2). This modification makes the clustering method more applicable to product design by linking it to commonly used anthropometric measurements,

and is described in algorithm 2.

The main difference with algorithm 1 is that in this case, a matrix  $\mathbf{F}$  containing features to constrain the clustering is also required as input.  $\mathbf{F}$  in this case has a number of features in its rows (e.g. head length and circumference) and the scalp surfaces corresponding to the columns of  $\mathbf{X}$ ,  $\mathbf{D}$  and  $\mathbf{B}$  in its columns. The clustering is again based on the dissimilarity between the medoids and the other surfaces. However, in this case the minimum and maximum feature boundaries of each cluster are also determined dynamically as each cluster grows. Before assigning any surface to the cluster with the closest nearest medoid at line 42, first a check is made to see if assigning the surface to this cluster would result the cluster to overlap in all feature dimensions with any other cluster (lines 28-38), i.e. to follow the previous example: if the maximum head length of one cluster is larger than the minimum head length of another, there is overlap in the head length dimension. If all features overlap with any of the other clusters, the surface is not assigned to the cluster (line 40) but is instead grouped with the next closest medoid - again provided that this does not cause all features to overlap. As long as there is at least one feature dimension for which the clusters can be clearly separated, the overlap test passes and the surface can safely be assigned to the current cluster. Just as before, the algorithm is performed 100 times for 2 to 10 clusters, and the medoid indices, cluster labels and cost of the clustering with the lowest possible cost is returned.

---

**Algorithm 2** constrained k-medoids clustering - part 1
 

---

**Input:**

$k$  - number of clusters (scalar)  
 $\mathbf{D}$  - precomputed  $n_s \times n_s$  dissimilarity matrix (multidimensional array)  
 $n$  - number of trials (scalar)  
 $\mathbf{F}$  -  $n_f \times n_s$  matrix with features in rows and scalps in columns (multidimensional array)

**Output:**

$\mathbf{m}$  - medoid indices (array)  
 $\mathbf{l}$  -  $n_s$  vector containing cluster labels (array)  
 $c$  - total clustering cost (scalar)

- 1:  $\mathbf{m} :=$  empty array of size  $k$
- 2:  $\mathbf{l} :=$  empty array of size  $n_s$
- 3:  $c := \infty$
- 4: **for**  $i := 0; i < n; i ++$  **do** {for a specified number of trials}
- 5:    $\mathbf{m} :=$   $k$  random indices from  $\mathbf{D}$
- 6:    $\mathbf{m}' :=$  empty array of size 0 {list of saved medoid indices}
- 7:    $\mathbf{minBoundaries} :=$  empty multidimensional array of size  $n_f \times k$
- 8:    $\mathbf{maxBoundaries} :=$  empty multidimensional array of size  $n_f \times k$

---

**Algorithm 2** constrained k-medoids clustering - part 2

---

```

9:   while  $\mathbf{m} \notin \mathbf{m}'$  do
10:      $\mathbf{D}' := \mathbf{D}_{\mathbf{m},:}$  {copy full rows with indices  $\mathbf{m}$  from  $\mathbf{D}$ }
11:     for  $j := 0; j < k; j++$  do {for all clusters}
12:        $\mathbf{minBoundaries}_{:,j} := \mathbf{F}_{:, \mu_j}$ 
13:        $\mathbf{maxBoundaries}_{:,j} := \mathbf{F}_{:, \mu_j}$ 
14:     end for
15:     while all values in  $\mathbf{D}' \neq \infty$  do { $\infty$  marks traversed entries}
16:       get index (row, col) for minimum value in  $\mathbf{D}'$ 
17:        $\mathbf{minBoundaries}' := \mathbf{minBoundaries}$ 
18:        $\mathbf{maxBoundaries}' := \mathbf{maxBoundaries}$ 
19:       for  $o := 0; o < n_f; o++$  do {for all features}
20:         if  $F_{o,col} < \mathbf{minBoundaries}_{o,row}$  then {if feature for this
surface is smaller than corresponding feature for medoid}
21:            $\mathbf{minBoundaries}'_{o,row} := F_{o,col}$ 
22:         end if
23:         if  $F_{o,col} > \mathbf{maxBoundaries}_{o,row}$  then {if feature for this
surface is larger than corresponding feature for medoid}
24:            $\mathbf{maxBoundaries}'_{o,row} := F_{o,col}$ 
25:         end if
26:       end for
27:       overlap := false
28:       for  $j := 0; j < k; j++$  do {for all clusters}
29:         if  $j = \text{row}$  then
30:           continue {skip comparing features of current cluster
with itself}
31:         else
32:           if (all features in  $\mathbf{maxBoundaries}'_{:,j} >$  all features in
 $\mathbf{minBoundaries}'_{:,i}$ ) OR
33: (all features in  $\mathbf{minBoundaries}'_{:,j} <$  all features in
 $\mathbf{maxBoundaries}'_{:,i}$ ) then
34:             overlap := true
35:             break {exit loop}
36:           end if
37:         end if
38:       end for
39:       if overlap = true then
40:          $\mathbf{D}'_{row,col} := \infty$ 
41:       else
42:          $l_{col} := \text{row}$  {set label for surface with index col}
43:          $\mathbf{D}'_{:,col} := \infty$  {mark entire column col of  $\mathbf{D}'$  as traversed}
44:          $\mathbf{minBoundaries} := \mathbf{minBoundaries}'$ 
45:          $\mathbf{maxBoundaries} := \mathbf{maxBoundaries}'$ 
46:       end if
47:     end while

```

---

---

**Algorithm 2** constrained k-medoids clustering - part 3

---

```

48:   append  $\mathbf{m}$  to  $\mathbf{m}'$ 
49:   for  $j := 0; j < k; j++$  do {for all clusters}
50:      $\mathbf{jIndices} :=$  all indices of  $l_{ind}$  for which  $l_{ind} = j$ 
51:      $minDis := \infty$  {minimum dissimilarity for this cluster}
52:     for  $o := 0; o < len(\mathbf{jIndices}); o++$  do {for all surfaces in
      this cluster}
53:        $tempDis := \sum \mathbf{D}_{:,o}$  {dissimilarity of surface  $m$ }
54:       if  $tempDis < minDis$  then
55:          $minDis := tempDis$ 
56:          $\mathbf{m}_j := o$  {surface  $m$  is new cluster medoid}
57:       end if
58:     end for
59:   end for
60: end while
61:  $c' := 0$  {cost of this clustering trial}
62: for  $j := 0; j < k; j++$  do {for all clusters}
63:    $c' := c' + \sum \mathbf{D}_{:,m_j}$  {add within-cluster dissimilarity to current
      cost}
64: end for
65: if  $c' < c$  then
66:    $\mathbf{m} := \mathbf{m}'$ 
67:    $\mathbf{l} := \mathbf{l}'$ 
68:    $c := c'$ 
69: end if
70: end for
71: return  $\mathbf{m}, \mathbf{l}, c$ 

```

---

Note that adding constraints to the clustering will not be as optimal as unconstrained clustering, and will result in clusters (product sizes) with higher within-cluster shape variability. Depending on the number and nature of the constraining features, this will have an effect on the runtime on the clustering algorithm and -as there is more shape variation to take into account- will make it more difficult for the designer to create a product size that fits each cluster. However, if the clusters can be distinguished by a distinct set of anthropometric features, this enables the creation of a sizing table to assign any individual to the correct cluster (i.e. product size) without performing a 3D scan or trial-and-error fitting of several sizes. Therefore, the benefits to the user of the products might be higher than the inconvenience of more geometrically heterogeneous clusters. For further discussion on this, see section 4.5.6.

#### 4.3.6 Evaluating clustering quality using cluster validity indices

A number of metrics exist to evaluate the quality of k-means or k-medoids clustering. These metrics, referred to as cluster validity indices, are generally defined in terms of intra- and inter-cluster variance. For example, the Ray-Turi index is the ratio of the squared distances between all points in a cluster and their barycenter (usually the mean) to the minimum of the squared distances between all barycenters [160]. As such, it is a relative measure of dissimilarity.

For the application to 3D clustering methods, the medoids were used as barycenters and the squared Euclidean distances between the 3D-coordinates of each individual shape were used as a distance metric (see section 4.3.3). Niu et al., however, observed that the Ray-Turi index has a sensitivity problem and propose a modified version where the numerator is the average instead of the minimum inter-cluster distance [151]. In this work, their suggestion is adopted and the modified Ray-Turi index, which will be referred to as CVI (cluster validity index), is calculated as in equation 29, with  $k$  the number of clusters,  $n_s^c$  the number of surfaces in cluster  $c$  and  $m^c$  the medoid for cluster  $c$ :

$$\begin{aligned} \text{intra} &= \frac{1}{N} \sum_{c=1}^k \sum_{i=1}^{n_s^c} \|\dot{\mathbf{x}}_i^c - \mathbf{m}^c\|^2 \\ \text{inter} &= \frac{2}{k(k-1)} \sum_{c=1}^{k-1} \sum_{c'=c+1}^k \|\mathbf{m}^c - \mathbf{m}^{c'}\|^2 \\ \text{CVI} &= \frac{\text{intra}}{\text{inter}} \end{aligned} \quad (29)$$

In addition, the size-weighted variance (SWV) was calculated as a measure of absolute dissimilarity with equation 30:

$$\text{SWV} = \frac{1}{n_s} \left( \sum_{c=1}^k n_s^c \times \frac{1}{n_p} \sum_{i=1}^{n_p} \text{Var}(\dot{\mathbf{x}}_i^c) \right) \quad (30)$$

The reason for selecting the Ray-Turi index and SWV as metrics is twofold. Firstly, while most cluster metrics have been used primarily for image processing purposes, these metrics were used in previous research regarding clustering for product design [151]. Secondly, a number of relative and absolute clustering metrics from [161] were calculated alongside the CVI and SWV and were found to give similar results for the clustering algorithms in this work. Because the minor differences in performance or precision were not relevant for

distinguishing between clustering methods and because a full comparison between metrics was considered out of scope, other metrics were not included in the present study.

#### 4.3.7 *Product-related clustering metrics*

When using mathematical clustering for product development, each cluster represents a group in the population that required a separate product size. While cluster validity indices provide a good overall measure of clustering quality, they are not directly usable in product design or sizing systems, since they represent geometric shape variation in a manner that is not clearly applicable to subject-product distances. Therefore, this section introduces a number of product-related metrics. Each of these metrics has some general rules of thumb, but their specific relevance and thresholds will vary on a product-to-product basis. In order to provide a tangible example, a prototype EEG (electroencephalography) headset that is currently under development at the University of Antwerp will be used, shown in figure 46. EEG is the measurement of electrical activity in the brain, either by electrodes implanted in the brain or electrodes on the scalp. One major challenge in designing EEG headsets such as the Epoc+ by Emotiv [34], is getting the electrodes in the correct position and maintaining contact with the skin throughout measurement. For the UAntwerp prototype, the goal is to create a headset in a number of product sizes without any adjustable or movable parts, thereby eliminating positioning errors by the user as much as possible. While the device is still under development at the time of writing, the following product-related metrics have been considered.

- **Number of clusters.** The number of product sizes is generally a trade-off between cost and complexity: the fewer sizes are used, the faster and cheaper the product can be produced. However, with each product size accommodating a larger set of shapes, the within-cluster variability becomes larger, which makes it more difficult to design a fitting product.

For example, the first version of the EEG headset was printed in three sizes due to budget and time constraints. Initial tests revealed that while the positioning and stability of the device were good and the overall fit was acceptable, two frontal electrodes didn't make contact with the head of a number of head subjects in all three clusters. This indicates that there is one or more head geometry types (e.g. elongated heads) which are now spread over the other clusters. In this case, increasing the number of clusters would result in an extra product size specifically suited for people with this head type.



Figure 46: One product size for a prototype EEG headset currently under development at UAntwerp.

- Population percentage covered by each cluster and by all clusters combined.** The accommodation rate or population covered by a set of product sizes should be as large as possible. Furthermore, each cluster should ideally contain equivalent portions of the population, because it is economically undesirable to design for outliers and to produce a specific product size for an extremely small portion of the population. In practice, designers will often opt to design for a specific part of the population, such as those people between the 5th and the 95th percentile. However, the feature-based, shape-based and constrained clustering algorithms described above assign each surface in the dataset to a cluster and will thus result in a total accommodation rate of 100%, theoretically providing a solution for all members of a population. When comparing this kind of clustering methods, only the proportion of the population represented by each cluster should be compared, and methods that provide few clusters containing outliers will be favoured. (Of course, these methods can always be adapted so as to only accommodate a certain population percentage.)

To use the example of the EEG headset again, it might be that increasing the number of clusters reveals that the extra head type discussed above only represents a very small percentage of the populations, e.g. the accommodation rates for the four clusters are 50%, 20%, 25%, and %5 (the latter being the new head type). Instead of developing and producing a separate cluster,

the designers could choose to find another solution, such as using extra padding or a more flexible material. Alternatively, they could decide not to take this part of the population into account at all.

- **Point-to-point distances for each cluster.** The point-to-point distance is defined as the Euclidean distance between corresponding points of two surfaces in the dataset. To determine and visualize point-to-point distances within clusters, the minimum and maximum cluster envelopes are created by calculating the standard deviation of each point in a cluster in the normal direction, then moving the medoid point in the normal direction by three times that standard deviation. The normal direction at each vertex point in this case is the normalized average of the surface normals of the three faces that contain the vertex [162]. This results in (aesthetically unrealistic) head shapes that show the minimum and maximum location of each point within the cluster and thus the physical boundaries for products designed for that size.

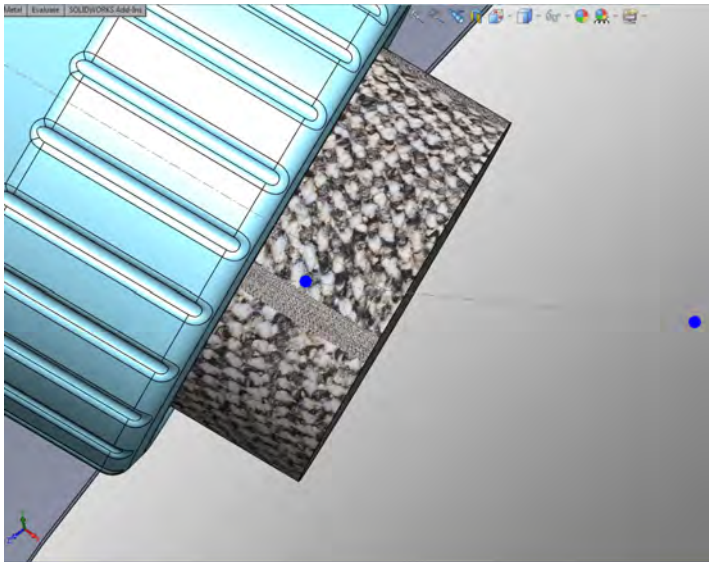


Figure 47: Detailed view of electrode holder and compressed sponge of the prototype EEG headset. Minimum and maximum surface points for the cluster are shown as blue stars.

Choosing a clustering with appropriate point-to-point distances depends heavily on the desired flexibility or adjustability of the product, as well as on the contact points of the product with the user's head. In completely fixed products, the desired point-to-point distances will depend on the maximum allowable errors in the product shape. On the other hand, in flexible or adjustable products the optimal point-to-point distance is determined by the degree of product flexibility/adjustability. If the

allowable range of point-to-point distances is sufficiently large, a good clustering can decrease the required flexibility or even eliminate the need for flexibility altogether, although in the latter case a larger range of product sizes needs to be designed and manufactured.

In the case of the EEG headset, the most important contact points are between the electrodes and the user's scalp. Each electrode has a removable and compressible sponge in front of it, that is soaked in a saline solution before use in order to ensure good electrical contact. A detailed view of the CAD design with the sponge in compresses state and the maximum and minimum surface points in the cluster is visualized in figure 47. The sponges are 10 mm thick and can be compressed to 1 mm. This means that for this prototype, each product size can accommodate 9 mm of variation within its respective cluster. Thus, when selecting clustering methods or determining the number of clusters, the within-cluster point-to-point variations should be no more than 9 mm.

As became obvious from the discussion above, even for a single product, the choice of clustering metrics (relevance and threshold values) requires design experience, a good understanding of the target market and familiarity with the user. Therefore, it is difficult (if not impossible) to provide a general set of guidelines. However, when the target product is known, these metrics offer are a good solution to compare clustering methods and guide product sizing.

#### 4.4 RESULTS

In this section, first, the results of the comparison between feature-based, shape-based and constrained clustering are presented in section 4.4.1. Next, constrained clustering is explored in more detail, with section 4.4.2 showing example headforms constructed from the resulting clusters and showing within-cluster point-to-point differences when the number of clusters is varied. Section 4.4.3 shows which features should be selected as clustering constraints, based on their individual contribution to the scalp shape variation. Finally, section 4.4.4 shows the effect of varying the number of constraints on the composition and shape variation of the clusters.

##### 4.4.1 *Comparison of clustering methods using cluster validity indices*

Table 15 shows a summary of the results for the three clustering methods. The average CVI was  $0.29 \pm 0.05$  for feature-based clustering,  $0.22 \pm 0.07$  for shape-based clustering and  $0.23 \pm 0.03$  for constrained

clustering. The average SWV was  $70999 \pm 11931$ ,  $61616 \pm 16750$  and  $66311 \pm 3475$ , respectively, and the average point-to-point distances were  $8.93 \pm 1.88$  mm,  $8.33 \pm 2.30$  mm and  $8.43 \pm 0.89$  mm, respectively. As expected, 100% of the population is covered by each of the clustering methods.

method	# clusters	comb. % pop.	CVI	SWV	mean avg pt-pt (mm)
feature-based	3	100 %	0.40	86335	10.89
	5	100 %	0.23	69118	8.90
	7	100 %	0.28	63742	7.96
shape-based	3	100 %	0.30	79779	10.73
	5	100 %	0.22	59106	8.47
	7	100 %	0.18	53229	7.11
constrained	3	100 %	0.31	78979	10.58
	5	100 %	0.23	63151	8.67
	7	100 %	0.16	59782	7.50

Table 15: Summary of clustering results for three different methods and three different numbers of clusters.

In figure 48, the clustering results for the three methods are visualized in 2D for  $k = 3$  and using circumference and arc length as constraints. Note that in all three methods, all clusters are mutually disjoint and cover the entire space of models, meaning that an individual can never belong to two or more product sizes at the same time. However, when using sizing tables (visualized by the black boxes in figure 48), there is more ambiguity as to which cluster an individual should belong. Using constrained clustering, with features from the sizing table as constraints, mitigates this problem and clearly separates all three clusters in at least one feature dimension.

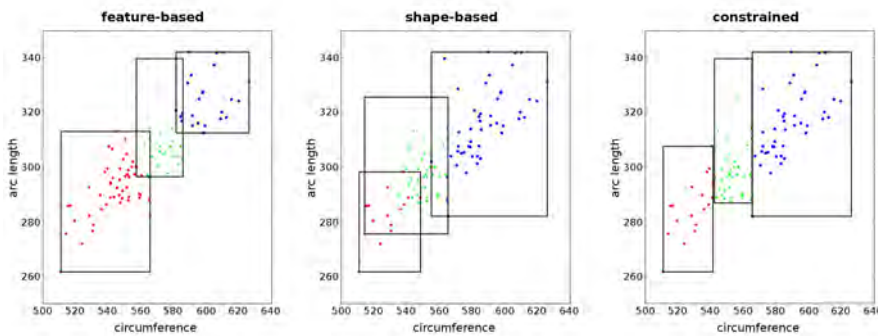


Figure 48: Clustering results in 2D for the three different clustering methods.

Figure 49 shows the response of the cluster validity indices for an increasing number of clusters, as well as for the three different clustering methods. While this figure confirms the results from table 15,

it is also clear that feature-based clustering has a less stable progression as the number of clusters is increased. Although the CVI should not necessarily be perfectly linear at small intervals of clusters, the CVI value between two adjacent data points (numbers of clusters) should not differ too much and a higher number of clusters should usually show a lower CVI score (due to lower intra-cluster and higher inter-cluster distances). Figure 49 (a) shows that CVI fluctuates less in shape-based or constrained clustering (with the exception of the peak at 8 clusters for constrained-clustering), suggesting that the latter two methods are more robust.

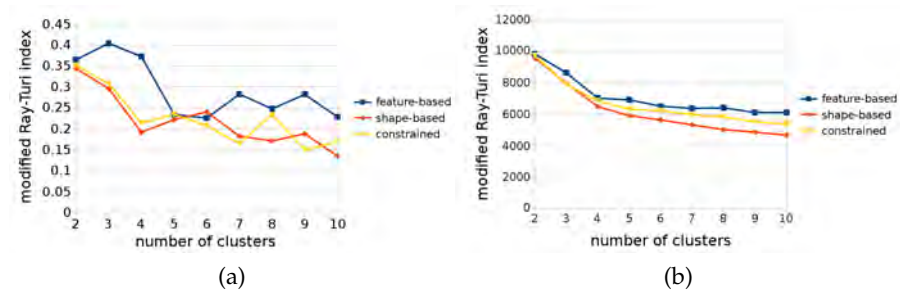


Figure 49: Ray-Turi cluster validity index (a) and size-weighted variance (b) for the three different clustering methods using different numbers of clusters.

#### 4.4.2 Point-to-point distances and minimum-maximum envelopes in *k*-medoids constrained clustering

Table 16 shows the average of the minimum, maximum and average point-point distances for different numbers of clusters in constrained clustering using the circumference.

# clusters	cluster	% pop.	avg pt-pt	std pt-pt	min pt-pt	max pt-pt	cF min.	cF max.
2	1	47 %	12.85	3.70	5.18	31.14	557	626
	2	53 %	13.09	3.62	6.71	36.15	511	566
3	1	24 %	10.52	2.91	4.51	30.97	581	626
	2	26 %	9.13	2.88	3.61	21.71	557	586
	3	50 %	13.01	3.49	6.71	34.78	511	566
4	1	20 %	10.13	3.07	3.52	31.07	589	626
	2	13 %	8.98	3.00	2.48	25.62	511	539
	3	40 %	10.22	3.49	4.31	24.75	538	566
	4	27 %	8.59	2.89	3.26	21.67	563	586
5	1	10 %	7.68	2.69	2.85	18.77	598	626
	2	15 %	8.87	3.20	2.99	26.17	581	599
	3	39 %	10.12	3.53	4.31	24.65	538	566
	4	13 %	8.98	3.00	2.48	25.62	511	539
	5	23 %	8.85	2.96	3.03	20.85	557	585
6	1	10 %	7.68	2.69	2.85	18.77	598	626
	2	17 %	7.86	2.49	2.66	18.95	529	547
	3	9 %	7.69	3.14	1.52	25.73	511	531
	4	23 %	8.85	2.96	3.03	20.85	557	585
	5	26 %	8.90	3.10	3.84	24.48	547	566
	6	15 %	8.87	3.20	2.99	26.17	581	599
7	1	16 %	8.93	3.20	2.98	26.19	581	599
	2	12 %	8.37	3.06	2.48	25.64	511	536
	3	9 %	7.44	3.20	2.00	19.10	538	551
	4	16 %	7.42	2.94	2.10	24.57	547	565
	5	16 %	8.53	2.72	3.64	25.03	539	566
	6	22 %	8.34	2.87	3.03	20.84	563	585
	7	9 %	6.68	2.21	2.08	18.77	605	626
8	1	18 %	9.62	3.26	3.07	26.99	581	612
	2	16 %	7.95	3.05	2.64	24.54	547	565
	3	9 %	7.69	3.14	1.52	25.73	511	531
	4	7 %	7.12	2.20	1.49	18.75	590	626
	5	9 %	6.74	2.24	1.52	19.26	545	572
	6	14 %	7.58	2.41	2.66	18.60	529	547
	7	15 %	7.22	2.65	2.52	20.84	571	585
	8	12 %	7.64	2.84	2.43	25.41	547	566
9	1	11 %	5.86	2.24	1.31	16.68	579	598
	2	8 %	8.54	3.39	1.57	28.07	572	606
	3	19 %	7.99	2.99	3.17	24.54	547	566
	4	9 %	7.05	2.63	1.67	17.94	557	572
	5	8 %	7.11	3.34	0.70	17.62	538	551
	6	8 %	6.61	2.22	2.45	18.86	599	626
	7	16 %	8.12	2.59	2.90	20.32	529	552
	8	9 %	7.69	3.14	1.52	25.73	511	531
	9	12 %	6.17	2.32	2.31	16.23	571	585
10	1	7 %	7.46	2.77	1.58	18.59	598	626
	2	9 %	6.35	2.20	1.90	19.75	529	547
	3	14 %	7.90	3.05	2.44	24.55	547	557
	4	12 %	7.85	2.66	1.98	20.28	535	552
	5	15 %	7.22	2.65	2.52	20.84	571	585
	6	4 %	5.01	2.35	0.12	17.67	590	610
	7	14 %	8.74	3.22	2.99	26.23	581	599
	8	9 %	7.69	3.14	1.52	25.73	511	531
	9	8 %	5.79	1.95	1.20	17.23	557	572
	10	8 %	5.26	2.13	1.33	20.96	559	566

Table 16: Population percentages, point-to-point differences in mm, and measurements for each cluster in constrained clustering (by circumference). Note: clusters are not sorted according to size in this table.

The medoids for three clusters are shown in figure 50. The minimum and maximum envelopes for three clusters are shown in figure 51.

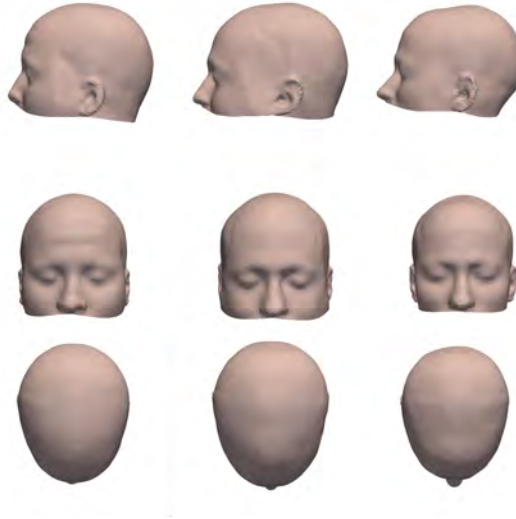


Figure 50: Side, front and top view of medoid surfaces for three clusters, using constrained clustering with circumference as constraint.

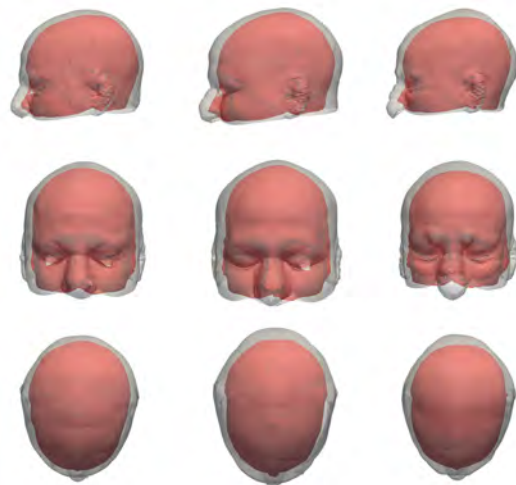


Figure 51: Side, front and top view of minimum (red) and maximum (white, transparent) envelopes for three clusters, using constrained clustering with circumference as constraint.

#### 4.4.3 *Selecting features for sizing and constraints*

Table 17 shows the squared eigenvalues of the first ten principal components of the shape model. The first principal component already

explains 71 % of shape variation, so the only features that need to be considered are those that are strongly correlated with this PC.

PC 1	PC 2	PC 3	PC 4	PC 5	PC 6	PC 7	PC 8	PC 9	PC 10
0.71	0.09	0.04	0.02	0.02	0.01	0.01	0.01	0.01	0.01

Table 17: Percentage of shape variation explained by each shape-space principal component.

Table 18 shows Pearson’s correlation coefficients between the anthropometric measurements and the first 10 principal components.

Feature	hL	fW	bW	eH	hE	vE	pE	cF	aL	aW
PC 1	0.87	0.57	0.83	0.40	0.68	0.75	0.42	0.97	0.80	0.74
PC 2	0.43	0.22	0.39	0.08	0.42	0.20	0.08	0.12	0.12	0.34
PC 3	0.06	0.17	0.15	0.05	0.01	0.43	0.02	0.03	0.30	0.33
PC 4	0.05	0.21	0.01	0.01	0.17	0.02	0.02	0	0.19	0.17
PC 5	0.0	0.08	0.06	0.30	0.21	0.20	0.31	0.11	0.05	0.13
PC 6	0.04	0.20	0.09	0.09	0.06	0.09	0.08	0.02	-2.53	0.13
PC 7	0	0.16	0	0.05	0.26	0.08	0.05	0.01	0.02	0.01
PC 8	0.03	0.04	0.07	0.10	0.05	0.13	0.11	0	0.01	0.06
PC 9	0.01	0.06	0.08	0.09	0.08	0.06	0.09	0.01	0.01	0
PC 10	0.01	0.01	0	0.15	0.02	0.07	0.15	0.01	0.06	0.03

Table 18: Pearson correlation coefficients between principal component scores and anthropometric measurements. (0 is no correlation, 1 indicates strong positive correlation, and -1 indicates strong negative correlation.)

The most important features for variation seem to be circumference, head length and arc length, all of which have a correlation of >0.75% on the first principal component.

#### 4.4.4 Varying the number of constraints in constrained clustering

The effects of varying the number of constraints can be seen in table 19 for a clustering with three clusters. There seems to be no difference for within-cluster accommodation rates when more features are added, suggesting that only one distinguishing dimension is required.

## 4.5 DISCUSSION

The aim of this article was to compare the application of several mathematical clustering methods to product sizing. While the methods and results sections focus mostly on the clustering algorithms, this section aims to define a clustering method that is maximally useful

constraint	# clusters	cluster	% pop.	avg pt-pt	std pt-pt	min pt-pt	max pt-pt
cF	3	1	18 %	9.69	2.95	3.77	31.10
	3	2	38 %	9.71	3.09	4.24	24.41
	3	3	44 %	12.35	3.19	5.79	31.11
cF + hL	3	1	18 %	9.69	2.95	3.77	31.10
	3	2	38 %	9.71	3.09	4.24	24.41
	3	3	44 %	12.35	3.19	5.79	31.11
cF + hL + bW	3	1	18 %	9.69	2.95	3.77	31.10
	3	2	38 %	9.71	3.09	4.24	24.41
	3	3	44 %	12.35	3.19	5.79	31.11

constraint	cF min.	cF max.	hL min.	hL max.	bW min.	bW max.
cF	511	541	n.a.	n.a.	n.a.	n.a.
	542	565	n.a.	n.a.	n.a.	n.a.
	566	626	n.a.	n.a.	n.a.	n.a.
cF + hL	511	541	169	194	n.a.	n.a.
	542	565	183	202	n.a.	n.a.
	565	626	193	222	n.a.	n.a.
cF + hL + bW	511	541	169	194	131	149
	542	565	183	202	136	153
	565	626	193	222	141	167

Table 19: Point-to-point distances in mm and measurements ranges in mm for constrained clustering in three clusters using circumference, a combination of circumference and head length, and a combination of circumference, head length, bitragion width.

for designers. Chapter 4.5.2 discusses the results of the comparison, and chapters 4.5.3 to 4.5.6 describes how the proposed metrics and results should be incorporated into product design and development.

#### 4.5.1 The effect of the statistical shape modeling characteristics

Several properties of the statistical shape model used for shape-based or constrained clustering might have an effect on the results. Firstly, because shape-based clustering is completely based on geometric differences between the surfaces, the sampling method and resolution for the original input scans are extremely important. In this work, the surfaces were sampled from MRI images with a resolution of  $1 \times 1 \times 1$  mm, using a uniform grid based on the triangle area distortion when the original surfaces are projected into a planar rectangle, as discussed in [107]. Each surface in the dataset is represented by 10000 points and all further statistical analysis is based on these points. Increasing the resolution to 100000 points did not have a large effect on previous statistical analyses with this shape model, so the current resolution was deemed sufficient for the clustering of human scalp shapes. However, for more complex shapes with many large surface angles or high local shape variation, it would be more appropriate to use higher resolutions, and to experiment with different

sampling methods.

Secondly, using more principal components might result in different clustering results for constrained clustering, since it would require a different set of anthropometric features. For example, if a threshold of 80% explained variation was chosen (see section 4.3.2), PC2 would have to be included in constrained clustering. From table 18, the most important feature for PC2 is head length. Therefore, circumference and head length would have to be used as constraints. However, from table 19, it appears that adding head length does not affect the clustering results in this case. This is due to the fact that the circumference provides a clear separation between clusters each time, as is further discussed in section 4.5.4. For more complex body shapes where the shape variation is spread out over more principal components, more PCs and more features might be required. Note that this has no further implications for the purely shape-based clustering, as the underlying shape model contains all principal components.

Finally, principal component analysis is a linear method, which assumes the underlying data to be Gaussian distributed. In this work, a comparison of different dimensionality reduction methods for the underlying model were considered out of scope. Following general practice ([153, 155]) and for the sake of simplicity, other dimensionality reduction methods were not considered. However, non-linear methods might provide significantly different clustering results, especially for more complex shapes.

However, the statistical shape model in this work suffices to compare clustering methods for the scalp shape and to demonstrate the product sizing workflow, which is the main topic of this work.

#### 4.5.2 *Performance of clustering methods*

From table 15 and figure 49, it appears that shape-based clustering performs better than the other two methods in terms of cluster validity indices, although the difference between shape-based and constrained clustering is small. As expected, feature-based clustering scores worse than the other two methods for all metrics. This is because there is much more information to base the clustering on: instead of a limited set of measurements the clustering can take into account the dissimilarity between tens of thousands of points, i.e. the full geometric shape of the head. Since the implementation of both methods is equally simple, if a statistical shape model is available and close product fit is important for functionality or comfort, designers should always use shape-based or constrained clustering.

A surprising result is that the average point-to-point distances between clustering methods do not differ significantly. This could be explained by the observation that the spacing between the minimum and maximum envelopes does not change a lot between clustering methods. In shape-based clustering, however, the point-to-point differences can be explained due to shape and size differences in a cluster, whereas in feature-based clustering the overall size is the most important factor (shape changes only for a small set of features).

The population percentages are also similar for the different clustering methods. The current method of evaluating the accommodation rate is therefore not suitable to distinguish between cluster methods. Even so, population percentages could be relevant for product design and should be reevaluated in future studies.

#### 4.5.3 *Interpretation of cluster metrics*

The cluster metrics chosen to evaluate the clustering methods were the Ray-Turi index (CVI) and the size-weighted variances (SWV). As mentioned in [152], the former is a good relative measure of the shape variability in each cluster, while the latter is a good absolute measure for the overall variability resulting from the clustering method. This can clearly be seen in figure 49, where SWV shows a gradual -almost linear- progression, whereas CVI shows more local fluctuations. As such, SWV is better suited to compare clustering methods to each other, whereas CVI is a good measure to determine the clustering quality for changes in the number of clusters.

The point-to-point differences show an expected decrease as the number of clusters increases and the clusters become smaller. Since there is hardly any difference between clustering methods, it is better not to use them for clustering comparison.

However, knowing the point-to-point differences can help designers to select the optimal number of product sizes, as discussed in section 4.5.5. Furthermore, dividing the point-to-point distances by the standard deviation within a cluster, or by the number of members, might be a more suitable measure of clustering quality because it would give less weight to cluster with less individuals or with higher inter-cluster variability. Another way to perform a more product-based cluster evaluation might be to only select a predefined region of interest or points of interest when calculating point-to-point differences. Alternatively, using only the dissimilarity between these points might provide a more product-specific clustering result, at the expense of losing overall accuracy. These options should be explored in future

research.

#### 4.5.4 *Selecting features for sizing and constraints*

In this paper, circumference, arc length and head length were chosen as most significant features because they have the highest loading on the first principal component, see section 4.4.3. However, arc length and head length are highly correlated. Furthermore, head length is more difficult to measure than arc length. Therefore, in real-life scenarios it might be more efficient to choose a different measurement. The next best feature is the vertical position of the ear, but since this is even more difficult to measure than the head length, it will not result in a good sizing system. When using three constraining features, arc width would be the next best choice, with a 63% loading on PC1.

Based on the results in table 19, using multiple constraining features should be avoided when using a small number of clusters, as in this case it has no effect on the clustering, but complicates product sizing. Furthermore, the most intuitive sizing tables are those with only one feature, e.g. as for shoe sizes. However, multiple constraints are likely to have a bigger impact for higher numbers of clusters, or when sufficiently distinctive constraint can not be found, e.g. when multiple features have the same loading on the relevant principal components. Further research into the effect of using different numbers of clusters is required to verify this.

#### 4.5.5 *Selecting the optimal number of sizes and creating representative manikins*

In theory, it would be possible to automatically select the optimal number of clusters. However, several cluster metric algorithms tend to get stuck at the extremes of the cluster ranges, which in most cases is not desirable for product development. For example, the Ray-Turi index will generally favor a small number of clusters, because in this case the inter-cluster distances are large while the intra-cluster distances are small, resulting in a small Ray-Turi index [160]. On the other hand, the average point-to-point distances in a cluster will continue to decrease as the number of clusters grows. Ray and Turi advised to circumvent this problem by not considering anything below four clusters. Though this might be feasible for their intended application (color clustering in 2D images), there are many products that are limited to three sizes (e.g. small, medium, large). Thus, the Ray-Turi index will not be ideal for fully automated product sizing.

In practice, a product designer will usually need to set some boundaries for the right number of sizes. A combination of the point-to-point distance plot and the CVI plot can be used for this purpose. The designer should first set the upper boundary for the number of sizes, depending on the manufacturing constraints (i.e., the maximal number of sizes that is economically feasible). Then, they set the lower limit by looking at the point-to-point distances. As discussed in section 4.5.3, point-to-point distances will decrease as the number of clusters increases. The designer should determine the maximum admissible point-to-point distance based on material properties and prior experience (i.e., if the material is flexible, larger within-cluster point-to-point differences can be accommodated). The maximum point-to-point distance will determine the minimum possible number of product sizes. Finally, the optimal number of product clusters is the one with the minimum CVI within this range. A visualization of this method is shown in figure 52.

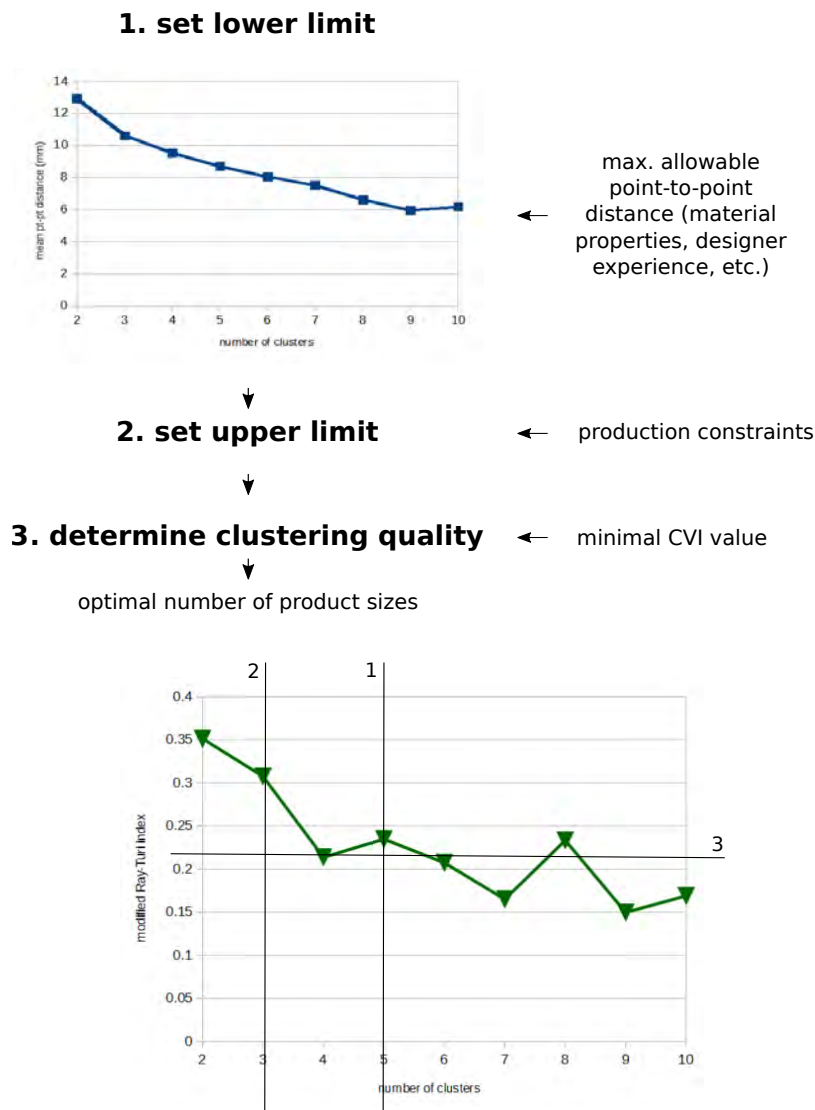


Figure 52: Workflow for product sizing using clustering based on 3D anthropometry. The presented workflow can be used with shape-based clustering and -after anthropometric feature constraints have been selected- with constrained clustering.

Once the optimal number of product sizes is determined, a number of representative head forms can be created by using 3D information from the statistical shape model. For example, the minimum and maximum envelopes shown in figure 51, section 4.4.2, can be used as manikins: the contact points of the product should fit within these two envelopes. Alternatively, the shape model can also be used to predict realistic minimum and maximum shapes within a cluster by using the constraining feature (in this case, circumference) as a parameter (see [135]). Minimum and maximum shapes for three clusters are shown in figure 53. Another option is to use the average or medoid head forms as manikins and use markers such as colors or arrows to show the required offset at that point. For example, figure 54 shows the average head forms for three clusters with a color map indicating the offset.

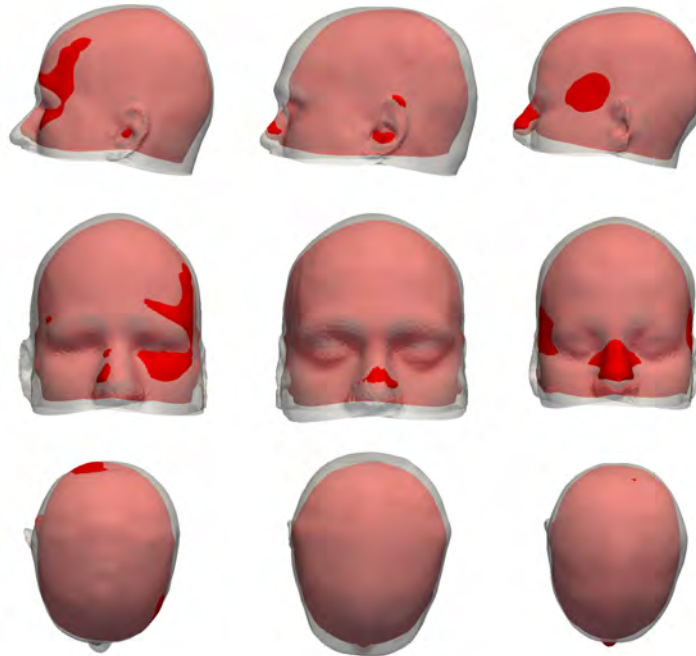


Figure 53: Side, front and top view of minimum (red) and maximum (white, transparent) shape for three clusters, using constrained clustering with circumference as constraint.

Various visualization options exist within 3D anthropometry, and the choice heavily depends on the type of product and the preferences of each designer. Therefore, the best solution might be to develop a tool that gives designers the flexibility to select their own visualization options. Further research is needed in order to find out which kind of manikins are preferred, if any, as well as the specifications of the required software interfaces.

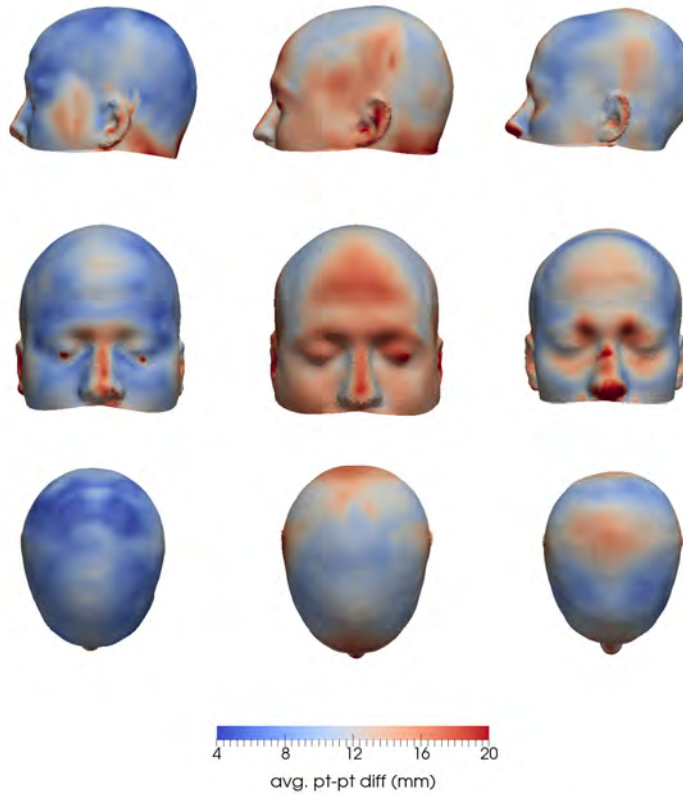


Figure 54: Side, front and top view of medoid shapes for three clusters, using constrained clustering with circumference as constraint, with color map indicating the average point-point distances.

#### 4.5.6 *Creating intuitive sizing tables*

Using constrained k-medoids clustering results in groups that have a very different shape and can be clearly separated for one or a number of measurements. From section 4.4, it is evident that constrained clustering performs only slightly worse than pure shape-based clustering. The biggest advantage is that once the product has been created in different sizes, new individuals can easily be assigned to their product size by taking a small number of measurements. Because the cluster mannequin represents the underlying shapes better than in traditional sizing systems, it is expected that no fitting is required, which is especially advantageous for products distributed through online shopping.

In fact, table 19 indicates that for most types of headgear, only the circumference is required: each cluster has exclusive ranges for the circumference while there is some overlap in the other measurements. The other measurements have no impact on the clustering methods. Therefore, a very simple size table can be made to assign a product

size to a new individual. See figure 55 for an example.

product size	circumference (mm)
A	511 - 541
B	542 - 565
C	566 - 626

Table 20: Sizing table for three product sizes using constrained clustering based on head circumference.

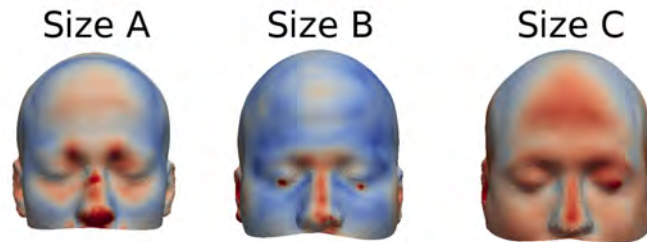


Figure 55: Size manikins for sizing table 20 (cluster medoids with colors showing the point-point distances).

An advantage of using a one-dimensional size table is that this is faster and more intuitive, because people are used to finding fitting clothing items based on single measurements, e.g. hats (head circumference) or shoes (foot length). The only reason not to use constrained clustering is when the accuracy of the clustering is more important than the usability of the method. This might occur with the design of products containing biosensors, such as the EEG headset discussed in section 4.3.7, but this needs to be evaluated case by case.

#### 4.5.7 The disadvantages of shape-based clustering

As has been demonstrated in the previous sections, clustering based on 3D shape surfaces instead of anthropometric data table has a great potential to deliver better fitting products and to optimize a range of product sizes. However, shape-based clustering also has a number of disadvantages when it comes to feature-based clustering. While 3D scanners are becoming cheaper and statistical shape modeling is becoming more widespread, the financial cost and the time investment in creating a 3D shape database are still significant and requires several trade offs. For example, if the entire body is 3D-scanned, the local resolution of various body parts will be low, resulting in less representative shape models. If, instead, a specific body part of interest is scanned, the 3D model will be better, but the entire process will have to be repeated for each body part and will thus be much more expensive. Furthermore, the number of individuals that should

be included in the dataset in order to properly represent the underlying population is not clear. There are models with less than 100 and models with more than 1000 individuals, but as of yet there is no industry standard to ensure representative models. Finally, in contrast to feature-based clustering (and traditional anthropometry), there are currently few publicly available 3D datasets and their suitability for product design has not yet been established.

Therefore, 3D anthropometry and shape-based clustering are not necessarily appropriate for each type of product. Currently, for most commercial products, it would still be advisable to use traditional anthropometry in combination with previous experience and/or fitting experiments with population samples. However, products which require a correct fit to multiple points of the human body and which are now mostly provided through high cost customized solutions, would benefit from using 3D anthropometry. For this type of products, shape-based clustering will provide new opportunities for mass-customization which will benefit all parties involved: users, designers and manufacturers.

#### 4.5.8 *Future work*

While this work indicates that shape-based and constrained clustering are feasible methods for product sizing, the verification was purely theoretical. Further steps are required before the proposed workflow can be implemented in product design. Apart from repeating the described analyses using different data sets and parameters, a number of practical aspects should be resolved:

- The parameters of the underlying shape model should be varied, such as the sampling method, resolution, and non-linear dimensionality reduction methods (see section 4.5.1). The effect of this on the clustering should be evaluated.
- The optimal input parameters for the clustering algorithms should be determined: the number of trials, the range of clusters, and the dissimilarity metric.
- User research should be performed with designers in order to discover whether the proposed clustering method is indeed sufficiently intuitive, and whether the clustering metrics are sufficiently informative. If necessary, the methods should be compared again using a different set of metrics.
- The clustering for the prototype EEG headsets described in section 4.3.7 should be repeated with a larger allowable number

of product sizes, and the effect of this on product fit should be evaluated.

- The clustering method described in this article should be used to create a set of prototypes for other products requiring a close fit to the human head (i.e. sports helmets). The physical fit of these prototypes should be verified on a representative sample of the intended population.
- The usability of the workflow presented in section 4.5.5 should be verified. For example, by giving a set of ergonomic product specifications for a relatively simple product (e.g. a hat or earphones) to two groups of experienced designers, with one group using traditional anthropometry (or feature-based clustering) and the other using 3D anthropometry (either shape-based or constrained clustering) and comparing the two methods in terms of time, effectiveness, learning curve ease of use.

#### 4.6 CONCLUSION

In this paper, a method is presented to incorporate 3D anthropometric data in product sizing by applying k-medoids clustering on a statistical shape model of the human head. When compared to traditional sizing based on the head circumference, k-medoids clustering resulted in superior clusters based on both the Ray-Turi index and size-weighted variance. In order to make the method more easily applicable in product design, the k-medoids algorithm was modified by adding the constraint that clusters should not overlap in one or more key dimensions. This constrained clustering was found to perform almost as good as traditional feature-based clustering, with an average CVI of  $0.23 \pm 0.03$  compared to  $0.29 \pm 0.05$ . While shape-based k-medoids clustering was slightly better, constrained clustering supports the creation of sizing tables and is more intuitive to use.

Furthermore, a method was presented to select the optimal number of product sizes, given manufacturing constraints, within-cluster point-to-point distances and the Ray-Turi cluster validity index as a measure of sizing quality. An example of creating sizing tables and digital manikins from constrained clustering was also provided.

The results show that shape-based and constrained clustering are feasible methods for creating sizing systems, and that they are preferable to traditional feature-based sizing for head products requiring an accurate fit, e.g. EEG equipment. It is expected that constrained clustering based on 3D anthropometry will result in better fitting and more comfortable headgear.

Part III

DISCUSSION



## DISCUSSION

---

In this section, the answers to the three research questions are discussed. The chapter is then concluded with a section on suggestions for further research.

### 5.1 SUMMARIZED ANSWERS TO THE RESEARCH QUESTIONS

#### 5.1.1 *How well can the global and local shape variation of the human scalp be quantified in a statistical shape model?*

In chapter 2, it was shown that the 3D shape of the human scalp can be adequately captured using statistical shape modeling with an input dataset of at least 90 MRI scans. Individual shape predictions using this model resulted in average prediction errors of  $0.64 \pm 0.12$  mm. Since this is well below the spatial resolution of the input surfaces (1 mm in all dimensions), the model could be said to represent the underlying shapes properly. Local shape variation can be visualized on a statistical shape model by projecting a color map on the average scalp shape, as has been demonstrated in chapter 2, or by showing various points of interest in 3D space, as was done in chapter 3 and discussed in chapter 4. Various distance metrics can be used to quantify the variation in this case, including euclidean distances or Frobenius norms. Global variation can be visualized by varying the principal component weights as in chapter 2, by showing the minimum and maximum envelopes within a population, or by moving all points of the average head surface in their normal direction by a specified number of standard deviations of their point-to-point distances, as in chapter 3, and then visualizing the resulting 3D surfaces. It can be quantified by averaging the distance metrics used for local variation and by studying the correlations between principal component weights, anthropometric measurements or even semantic parameters. By mapping a set of anthropometric measurements of each scalp to its principal component weights, the local and global variation can also be quantified using intuitive parameters that designers are already familiar with.

#### 5.1.2 *Does the use of shape models have an impact on the geometric fit, stability and repeatability of EEG sensors in BCI-equipment?*

In chapter 3, a one-size-fits-all BCI headset was created using the anthropometric shape model from chapter 2. The impact of 3D an-

thropometry on the geometric fit of the EEG sensors was determined by comparing the 3D locations of the EEG sensors of the prototype headset with those of a commercially available BCI device, using a standardized EEG cap as reference. It was shown that the prototype's electrode positions by  $21 \pm 10.44$  mm, which is accepted in EEG practice and closer than the sensor positions of the commercial device. Stability of EEG sensors was tested by measuring the electrode displacement after movement, which was no more than  $10.52 \pm 7.22$  mm on average. Furthermore, the prototype headset remained fixated on the user's head during movement, while the commercial device often fell off. In terms of repeatability, the average electrode displacement after mounting the headset three times was  $11.28 \pm 6.11$  mm, again within the accepted distance and slightly better than that of the commercial device. While more extensive experiments will need to be performed in order to definitively quantify the difference in EEG sensor positioning, it is clear that 3D anthropometry has a positive impact on sensor placement and stability.

### 5.1.3 *How can 3D anthropometry be implemented in product sizing to create better fitting headgear?*

Chapter 4 compared a number of methods to cluster anthropometric data into groups for product sizing. Clustering based on the 3D shape model was shown to be more effective at separating the scalp shapes into groups than clustering based on traditional anthropometric features. The best performance was offered by performing k-medoids clustering on the 3D surfaces of the scalps, using the euclidean distances between the 3D coordinates of those surfaces as a measure of dissimilarity. A variation of k-medoids which also takes into account the possible overlap in anthropometric features, named constrained clustering, also resulted in better groups than traditional feature-based clustering, and supports the creation of sizing tables to assign correct product sizes to individuals. In chapter 4, a workflow was also presented to select the optimal number of product sizes based on the performance of the chosen clustering method and on a number of product-specific metrics such as point-to-point distances and population coverage. Therefore, performing k-medoids clustering or constrained clustering on a 3D anthropometric model (i.e. a statistical shape model) results in more representative clusters, meaning clusters with lower intra-cluster shape variation and higher inter-cluster variation, than traditional clustering. By using the subset of the statistical shape model that belongs to a cluster as a digital manikin for that cluster, a headgear can be designed in a similar manner as the BCI headset from chapter 3. Since using 3D anthropometry resulted in a better fitting one-size-fits-all headset, using the same techniques on clusters of the statistical shape model is likely to result

in better fitting BCI headsets in specific, as well as fitting headgear in general.

## 5.2 SHAPE VARIATION OF THE HUMAN SCALP

The first research question to answer was how to quantify the shape variation of the human scalp. It was shown in chapter 1 that traditional anthropometry does not suffice to study the shape variation at specific locations on the human head, and that a new method was required. In chapter 2, a new representation for the human scalp was introduced: a statistical shape model showing the overall shape variation and the variation for specific regions, i.e. electrode contact locations.

Before making any claims about the morphology of the scalp (for this population), the results from chapter 2 should be verified. In order to truly evaluate whether the measurements are realistic for the measured population, ISO 20685 recommends that the measurements should be repeated by an experienced anthropometrist [163]. The measurement error between the measurements reported in chapter 2 and the anthropometrist's measurements should then be compared, and if the difference is below certain thresholds (detailed in the norm), the measurements can be said to be correct. However, this would require a significant amount of time and (for physical measurements) access to the individuals of which the MRI scans were taken, and thus was considered out of scope for this work.

Instead, the measurements are compared against various other anthropometric studies. The earliest study used for comparison is the anthropometric survey of U.S. army personnel by Gordon et al. [164], with a total sample of 3982 participants (1774 male, 2208 female), ages 17-51. Next, the anthropometric head-and-face study of U.S. respirator users by Zhuang et al. [165] was used, who report using a stratified sample of a total of 3997 voluntary participants, ages 18-66. While the reported tables are separated into male and female, it is unclear how many members of each gender were included in the study. The DINED data [75] was also considered, although in this case only the ages of the sample are certain: 20-30 years. The only sample size available on the website refers to anthropometric measurements performed on Dutch students in 1985 and 1986, whereas the sample that was used for comparison is labeled as "Dutch adults, dined2004". Finally, the DINBELG website [166] was also considered. Although the author of DINBELG reports a sample of 150 000 Belgian people aged 18-65, it seems that only body height was measured. All other measurements reported in the DINBELG tables were extrapolated based on the correlation between the DINED 2003 measurements.

A direct comparison between these studies was more difficult than expected, not only because of the uncertainty about the samples and the ethnic and geographic difference between the sampled populations, but also due to the difference in measurement techniques, instruments and anatomical landmarks (in the few cases that these are unambiguously reported). Nevertheless, tables 21, 22, and 23 show the comparison between the mean (and standard deviation), minimum, and maximum of anthropometric measurement values reported in chapter 2 and those found in the studies mentioned above. Note that only those measurements were chosen that appear in all studies.

study	head length				bitragion width				circumference			
Study	head length				bitragion width				circumference			
	mean	st. dev.	min	max	mean	st. dev.	min	max	mean	st. dev.	min	max
Lacko et al. 2013	198.50	10.60	168.60	221.50	147.70	8.00	130.70	166.60	564.90	25.70	511.00	626.10
DINED (20-30y)	194.00	11.00	168.00	220.00	148.00	8.00	129.00	167.00	562.00	25.00	504.00	620.00
DINBELG (18-65y)	188.00	8.10	169.00	207.00	145.00	6.20	131.00	159.00	569.00	23.00	515.00	623.00
Mean diff.	7.50	1.00	0.10	8.00	1.20	0.90	0.70	3.60	-0.60	1.70	1.50	4.60

Table 21: Comparison between anthropometric measurements from chapter 2 and previous studies for mixed population. All values are in mm.

study	head length				bitragion width				circumference			
	mean	st. dev.	min	max	mean	st. dev.	min	max	mean	st. dev.	min	max
Lacko et al. 2013	191.10	7.40	168.60	206.10	142.10	5.20	130.70	152.00	545.90	16.10	511.00	585.60
Zhuang et. al. 2005 (18-66y)	187.50	7.20	152.00	215.00	146.80	5.60	129.00	165.00	554.90	17.80	475.00	654.00
Gordon et. al. 1989	186.70	5.80	158.00	211.00	145.60	5.20	126.00	167.00	546.50	14.30	500.00	611.00
DINED (20-30y)	189.00	8.00	170.00	208.00	144.00	5.00	132.00	156.00	550.00	17.00	510.00	590.00
DINBELG (18-65y)	184.00	6.60	169.00	199.00	142.00	5.00	130.00	154.00	553.00	16.00	516.00	590.00
Mean diff.	4.30	0.50	6.40	-2.20	-2.50	0.00	1.40	-8.50	-5.20	-0.20	10.80	-25.70

Table 22: Comparison between anthropometric measurements from chapter 2 and previous studies for female population. All values are in mm.

study	head length				bitragion width				circumference			
Study	head length				bitragion width				circumference			
	mean	st. dev.	min	max	mean	st. dev.	min	max	mean	st. dev.	min	max
Lacko et al. 2013	205.80	7.90	189.20	221.50	153.30	6.30	139.80	166.60	584.00	18.30	550.60	626.10
Zhuang et. al. 2005 (18-66y)	197.30	7.40	174.00	225.00	153.00	6.00	135.00	179.00	575.70	17.10	520.00	639.00
Gordon et. al. 1989	196.80	6.90	173.00	220.00	153.60	5.30	128.00	173.00	570.90	15.50	514.00	627.00
DINED (20-30y)	199.00	7.00	183.00	215.00	152.00	6.00	138.00	166.00	573.00	18.00	531.00	615.00
DINBELG (18-65y)	193.00	6.80	177.00	209.00	149.00	5.50	136.00	162.00	584.00	18.00	542.00	626.00
Mean diff.	9.30	0.90	12.50	4.30	1.40	0.60	5.60	-3.40	8.10	1.20	23.90	-0.60

Table 23: Comparison between anthropometric measurements from chapter 2 and previous studies for male population. All values are in mm.

The small absolute differences between the average, minimum and maximum values suggest that the measurements performed in this work and the measurements from previous studies are very similar. For the bitragion width and circumference, the average difference is never above 0.5 cm, and it is still below 1 cm for head length. The reason for the larger difference in head length might be twofold. Firstly, different reference points might have been chosen. While the databases from Gordon et al. and from Zhuang et al. seem to use the

same reference points (glabella and ophisthokranion) as this work, it is unclear which anatomical locations were used in the DINED and DINBELG studies. Secondly, even if the same reference points were chosen theoretically, these points might have been identified differently because the anatomical points at the occipital region of the head are difficult to identify by palpation or on sight (see sections 1.1.2 and chapter 3). The reference points for the other two measurements are not as difficult to locate.

study	head length		bitragion width		circumference	
	t	p-value	t	p-value	t	p-value
DINED (20-30y) mixed	4.21	0.00	-0.39	<i>0.69</i>	1.13	<i>0.26</i>
DINBELG (18-65y) mixed	9.85	0.00	3.32	0.00	-1.58	<i>0.12</i>
Zhuang et. al. 2005 (18-66y) M	7.59	0.00	0.30	<i>0.77</i>	3.17	0.00
Gordon et. al. 1989 M	8.04	0.00	-0.37	<i>0.71</i>	5.00	0.00
DINED (20-30y) M	6.08	0.00	1.40	<i>0.17</i>	4.20	0.00
DINBELG (18-65y) M	11.42	0.00	4.73	0.00	-0.01	<i>1.00</i>
Zhuang et. al. 2005 (18-66y) F	3.45	0.00	-6.37	0.00	-3.92	0.00
Gordon et. al. 1989 F	4.21	0.00	-4.74	0.00	-0.28	<i>0.78</i>
DINED (20-30y) F	2.03	<i>0.05</i>	-2.58	0.01	-1.80	<i>0.08</i>
DINBELG (18-65y) F	6.77	0.00	0.13	<i>0.90</i>	-3.10	0.00

Table 24: One sample t-test of difference between head measurements in sample from Lacko et al. 2013 [135] and those reported in various other studies.

A one-sample t-test was used to compare the means reported in the anthropometric studies with the sample from chapter 2, the null hypothesis being that the reported means come from the same sample. At a significance level of 0.05, for p-values  $>0.025$  the null hypothesis cannot be rejected and thus the means can be considered to not be significantly different. The p-value threshold of 0.025 was chosen because the means can be either significantly smaller or larger, meaning an area of 0.025 at either end of the distribution, or 0.05 in total. The results are shown in table 24. P-values  $>0.025$  are shown in italics. Surprisingly, most of the head length differences and half of the bitragion width and circumference differences were found to be significantly different from the sample from chapter 2. While the populations of DINED and DINBELG are indeed different from the North American sample used in chapter 2, the samples from Gordon et al. and Zhuang et al. were drawn from the same population. Since no pattern can be discerned in table 24, it is not clear why this is not the case. In other words, while the absolute measurement values between the examined studies are similar, most of them seem to come from a different population than the one in chapter 2.

Apart from the one-dimensional measurements, the three-dimensional shape was also discussed in chapter 2: figure 24 shows the first five shape modes of the head, meaning the directions of variation in descending order. The first five principal components were found to account for 88.2% of the variation. PC<sub>1</sub> corresponds to the size or volume of the head, PC<sub>2</sub> to the elongation of the head, PC<sub>3</sub> to the shape and height of the head. PC<sub>4</sub> and PC<sub>5</sub> are much less clear to interpret. Similar studies have been performed by Roger Ball in 2011 [50] on a population of 600 Western and 600 Chinese heads, and by Liu et. al. in 2015 [167] on a dataset of 350 Chinese heads. Their definitions of the shape modes are similar to that from chapter 2. Ball concludes that PC<sub>1</sub> corresponds to the overall size or volume of the head, PC<sub>2</sub> to the height and "change from oval to round", PC<sub>3</sub> to the proportion of the face to head and the height of the cranium, PC<sub>4</sub> to the depth of the head and PC<sub>5</sub> to the jaw area and the shape of the cranium. For Liu, PC<sub>1</sub> represents the overall size, PC<sub>2</sub> the width and flatness of the head, PC<sub>3</sub> the shape of the face (long and narrow versus short and wide), PC<sub>4</sub> the protrusion of lower face and forehead and PC<sub>5</sub> the shape change of the head and face width. A comparison of the first shape mode for the three studies can be seen in figure 56. The reason for their clearer interpretations of PC<sub>4</sub> and PC<sub>5</sub> is probably due to the fact that their shape model included the lower part of the face. Even so, it is remarkable how even with different populations, the shape of the head seems to vary in the same way: the most variation is always in the volume or size.

According to the results reported in chapter 2, volume is also a determining factor between male and female populations, as well as the shape of the eyebrow ridge, which is more prominent in males. In mixed populations (including the one from [145]), smaller heads (according to PC<sub>1</sub>) seem to show a number of Asian features, such as slightly tilted eyes and rounder heads. Larger heads show rather African facial traits such as wide noses and large eyebrow ridges. When designing head products, going from smaller to larger heads, contact points on the sides of the head will only need to move linearly from the inside to the outside of the head. Contact and fixation points on the frontal or parietal regions of the head will need to be moved in a lateral and posterior-anterior direction and will provide a greater challenge to the designer.

Considering the mapping between anthropometric measurements and shape modes, the measurements that most influence shape prediction are circumference, head length and bitragion width (or head breadth). If only a limited set of measurements can be considered for design, these three should be included. Ear height seems to have the least influence on head shape, although this could also be explained by the fact that the ear was not well represented in this shape model,

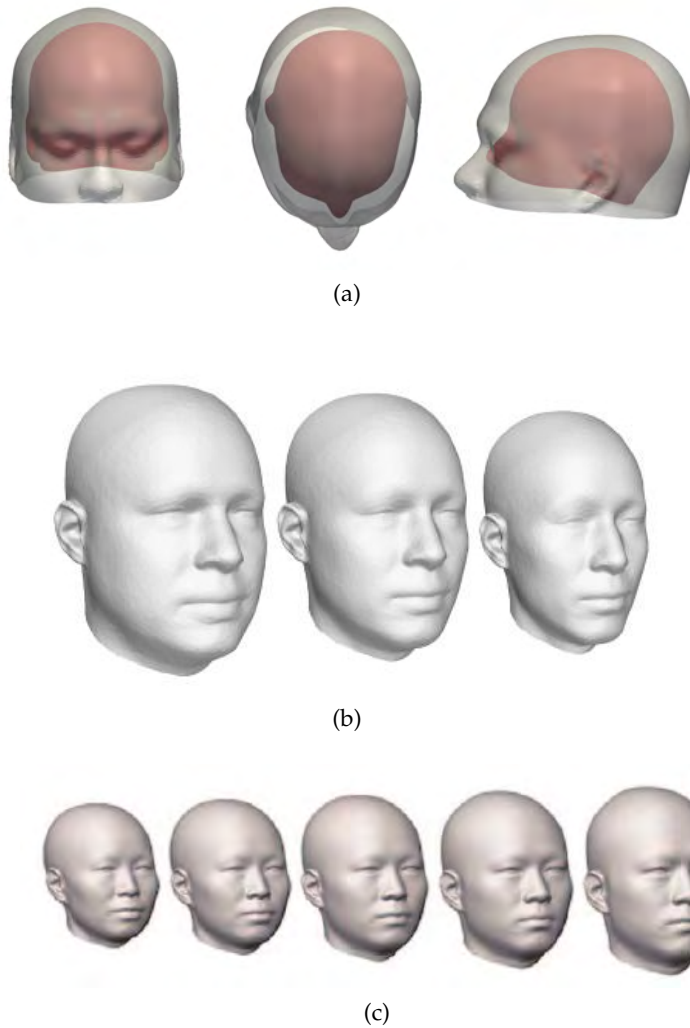


Figure 56: Comparison of first shape mode (variation according to first principal component) of this work (a) with the shape models of Ball [50] (b) and Liu et al. [167] (c).

i.e. due to image artefacts caused by supportive struts that were used for head stabilization in the MRI scan.

It is unclear to which extent the shape model from chapter 2 is appropriate for Belgian or Dutch populations. While the sample statistically appears to be from a different population, this might mean that the North American and West European populations have significantly different head shapes, or it might be that different ethnic groups were included in the samples (e.g. African-American, Caucasian, ...). Unfortunately, since it is unknown which ethnicities were present in the shape model from chapter 2 (and it a manual classification based on the head surfaces was ineffective), or in which proportion, it was impossible to determine the effect of ethnicity on shape variation. Not much literature was found on the shape vari-

ation within and between different ethnicities, apart from the work of Roger Ball [50], which showed that Chinese and Caucasian heads do have sufficiently different head shapes to require specific anthropometric models and methods. Most other work on morphological differences in head shape between ethnicities is focused on the facial area, e.g. [168, 169], in which significant differences are reported. Other factors that might explain the discrepancies in anthropometric measurements are age ranges included in the samples or BMI, although the scalp shape does not change much after the age of thirty [170] and obesity seems to have only have a minimal effect on it [171] (if any, since the differences reported in [171] are measured in percentages of other body dimensions which are also subject to change with rising fat mass).

In any case, the initial results related to product fit for BCI headsets designed using the model from paper 2 are promising. Both the quantitative results from chapter 3 and the preliminary evaluation in section 5.4 indicate that the model is indeed useful for Belgian males and females between 20 and 30 years old. Even if this was not true, since the modes of variation between samples from different populations are very similar, the methods and techniques presented in this dissertation are relevant to statistical shape models from any population. The only requirement is that an appropriate shape model is created as input for the methods. Due to the increasing amount of 3D body images and scans that are currently available, this should not pose much difficulty, and as soon as one shape model has been verified to correctly represent a target population, it can be reused for any application within that region of the world.

### 5.3 THE USE OF 3D ANTHROPOMETRY IN THE PRODUCT DESIGN PROCESS

Figure 57 shows the product design process according to Roozenburg and Eekels [172]. (Note that they make a distinction between the product development and product design process, where product development contains additional phases that precede and follow the design phase, including brainstorming and ideation as well as distribution and sales.) Although alternative models exist, this model and its derivatives are taught at multiple universities, including the University of Antwerp (Product Development) and the Technical University of Delft (Industrial Design).

According to this model, product design is an iterative process in which the designer cycles through analysis, synthesis, simulation and evaluation phases until a predefined set of specifications has been achieved. The second research question of this doctorate was how 3D anthropometry should be included in product design. In sev-

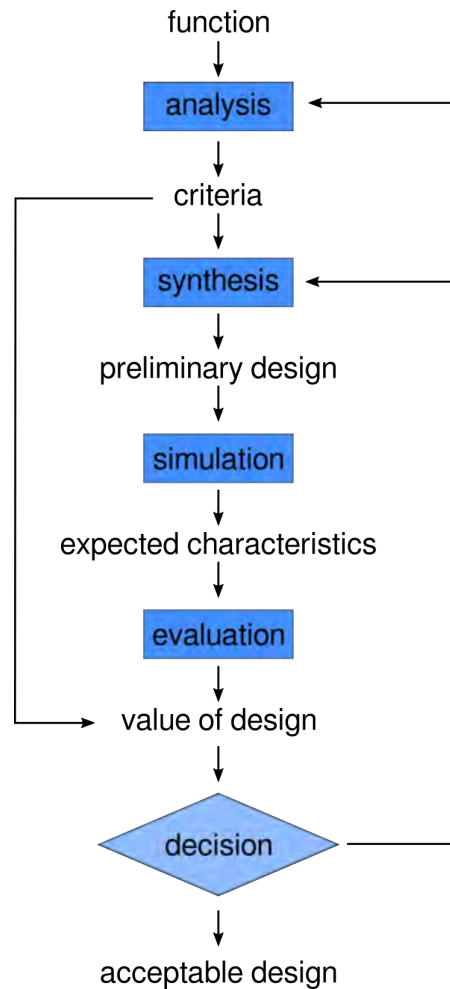


Figure 57: Basic product design process according to Roozenburg and Eekels [172]

eral of the previous chapters, applications have already been demonstrated and discussed separately. Furthermore, in the past few years 3D shape models have been used in a number of student assignments and master theses at Product Development [58, 173, 174]. In the next few paragraphs, these experiences are summarized and are considered from the perspective of Roozenburg and Eekels' model.

A first application of shape models in the Analysis phase was demonstrated in chapter 3, where a first step in the design of a one-size-fits-all BCI headset was to find out whether one-size-fits-all was actually possible or whether there was too much variation in head shape. For this purpose, the shape variation for four reference points was visualized (figure 58) and measured. Based on these measurements and on the spread of the variation (showing that the variation was mostly linear), one-size-fits-all design was deemed to be a feasible solution. In effect, 3D anthropometry can be used to analyze and visualize head variation for the entire head, for various

sub-populations (as in figure 31 in chapter 2) or for specific contact points.

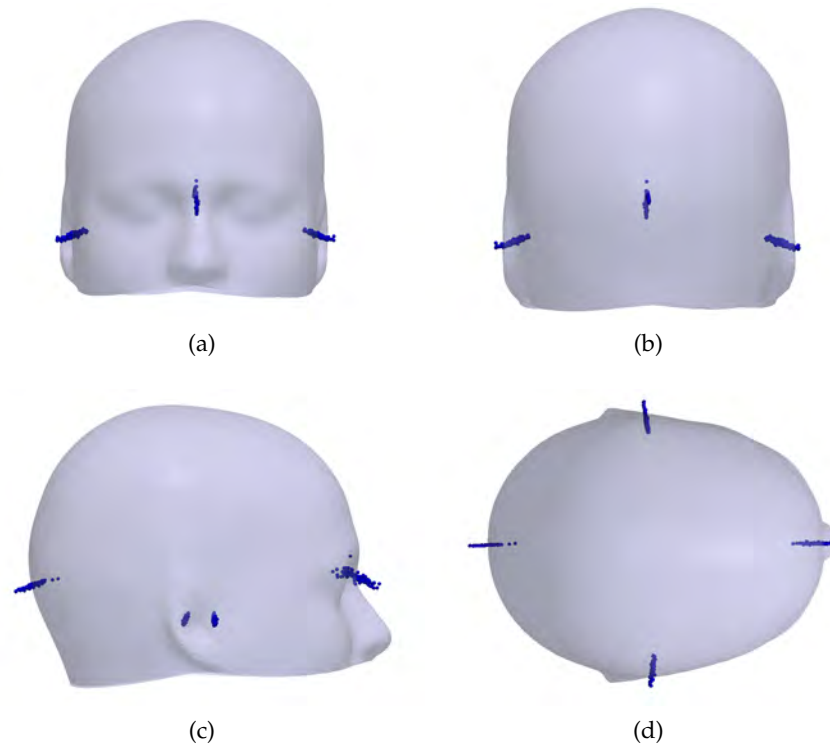


Figure 58: Shape variation of reference points visualized.

On the other hand, one thing that became clear when working with students is that the accuracy in local shape variation for the BCI headset is not necessarily an asset for all kinds of products. In a number of master theses, it was considered to be too complex for the student's purposes. Usually, this was the case for products such as helmets or glasses, which do not contain biosensors and do not require a specific placement of contact points. In these cases, the student (or their supervisor) decided that a traditional approach to ergonomic design, such as the ones described in sections 1.3.4.2 and 1.3.4.3, was more appropriate. Even so, it often occurred that the desired anthropometric measurements were either not available in literature, or were only available for other population than the student's target population. When this happened, the shape model of the scalp was used to perform the anthropometric measurements digitally. Instead of organizing and performing a measurement session, a shape model was used to predict surfaces for certain shape percentiles (e.g. 5th, 50th and 95th percentile according to the first principal component). Since the shape model generates accurate and realistic predictions of the full shape (as shown in chapter 2), any measurement on these percentile predictions can be assumed to correspond to the value that would be obtained by taking that percentile of a set of 1D measurement values.

Measurements can be taken in CAD-software or in custom software, as shown in figure 59.

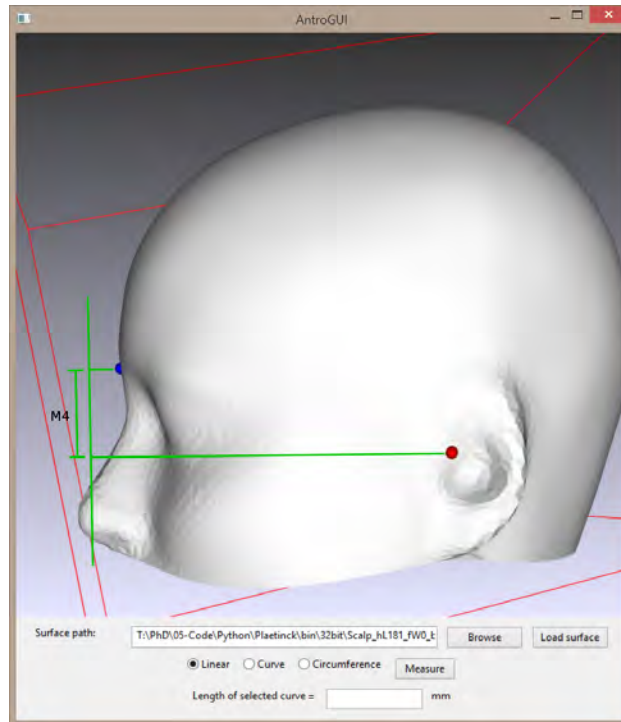


Figure 59: Screenshot of new anthropometric measurement performed on representative manikin (average head) derived from shape model. (custom software)

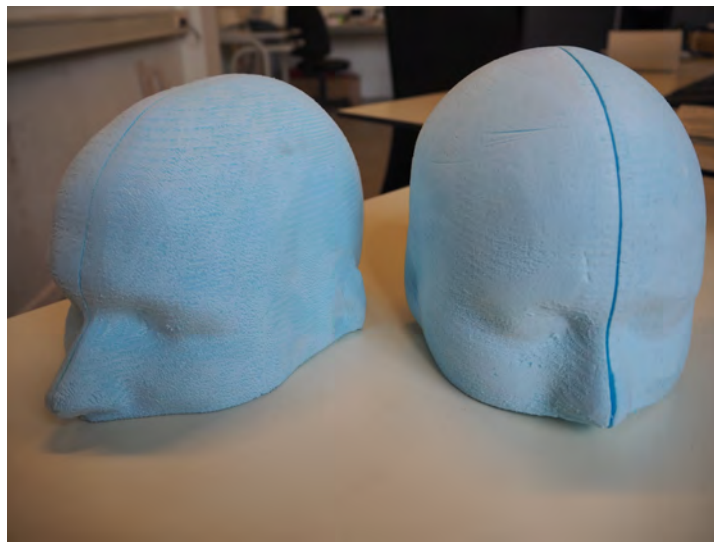
In the Synthesis phase, 3D shape models can be used as digital or physical design templates or manikins. For example, in chapter 3 the 1st, 50th and 99th percentiles of shape variation along the first principal component were used to determine the total displacement distance and angle for each of the contact points (also referred to as points-of-interest or POI further on). In this way, the designer knows precisely how much customization or flexibility will be required in his or her product. It might also occur that, based on these value, a different design approach is chosen (e.g. creating multiple sizes) because the differences are too great.

Furthermore, physical manikins of representative shapes can be a valuable tool during brainstorming and ideation, see figure 60 for some examples. In the annual Workshop Week of 2015, a group of students at Product Development were given three foam manikins representing the P1, P50 and P99 headforms and asked to generate concepts for commercial BCI headsets. While brainstorming and ideation usually results in drawings and sketches, the students working with the physical manikins started considering size and shape differences early on and were quick to create cardboard prototypes to test their (preliminary) concept's viability as soon as possible. On

the basis of the physical manikins, several concepts could be rejected much sooner than in a traditional design process, where problems with fit would only become apparent during prototype evaluation. Some sketches of the final concepts can be seen in figure 61.



(a)



(b)

Figure 60: Examples of physical manikins based on shape models: 3D-printed average head shape with color map showing variation (a) and manikins in blue foam (b).

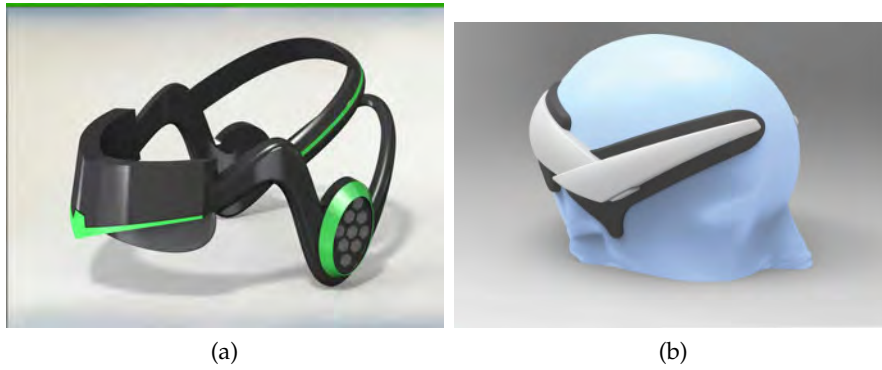


Figure 61: Two quickdesign sketches based on ideation and concept generation workshop with physical shape model templates.

Apart from creating realistic 3D manikins, Simulation is probably the most intuitive application of 3D anthropometry. Many contemporary papers on shape models suggest a combination of shape modeling with finite element modeling in order to simulate the physiological effects of the designed product on the human body. Some applications already exist, such as Siemens Jack and Jill, in which human models from different populations can be generated and their interaction with the product can be simulated. On a more localized scale, shape models of the underlying structures of the human head could be used to accurately predict skin and bone thicknesses in order to simulate user comfort or safety, e.g. in sports helmets, although this will be no trivial task. Furthermore, a CAD model of the product could be compared against a large number of random head shape predictions for a target population. Since the product contact points on these predictions correspond to the points on other shape model representations that might have been used in the Synthesis phase to create 3D models of the product (e.g. average headform), the distance between or intersection of the validation head surfaces and the contact points of the CAD-model of the product could be determined and visualized in CAD software.

Finally, the results from the Simulation phase (e.g. number of intersections between product and skin surfaces) can be used to either accept the design or continue to the next iteration of the design process. In the Evaluation phase, the shape models could be used to provide suggestions for this decision, based on numerical analysis of these parameters.

#### 5.4 CASE STUDY: SIMPLIFIED DESIGN PROCESS FOR BCI HEADSET IN THREE SIZES

In chapters 3 and 4, two methods were introduced to create BCI headgear using 3D shape models: one for designing a one-size-fits-all

headset, and one for creating a headset in a number of different sizes. In order to demonstrate the place and the value of 3D anthropometry in the product design process, the latter method was applied to create a BCI headset in three different sizes. A simplified product design process was followed, in which the only design criterion was that the headset should have 14 electrodes that make contact with the user's head, as in chapter 3. A number of important portions of the design process have been left out of this discussion. Furthermore, only one iteration of the design process is shown.

#### 5.4.1 *Analysis phase*

A first step in the analysis process was to analyze the overall shape of the head. A preliminary analysis of the shape models, as in chapter 2, showed that the most global variation is in the head volume or size (first principal component) and that the circumference is a good measurement to use for the sizing process and the size chart. Secondly, figure 31 in chapter 2 shows that the difference between male and female heads is only 5 mm on the largest part of the head and that most of the variation is localized in the face (especially the eyebrow ridge), while the scalp (i.e. parietal) region only shows small morphological differences. Thus, the same shape model could be used for both male and female heads, and there was no need for a separate product line for males and females; at least not for this population.

Next, the process presented in chapter 4 was used to determine how many product sizes should be created. In this example, electric contact between the user's scalp and the electrode is made with sponges soaked in a saline solution. The sponges are about 10 mm long and can be compressed to 1 mm, which gives 9 mm of flexibility. Furthermore, the prototypes were to be 3D printed, and the photopolymer used in most 3D printers is not completely rigid. Therefore, a combined within cluster average point-to-point distance of 12 mm was deemed acceptable for this specific application. To determine the average point-to-point distances, the tables and graphs from chapter 4 can be used, as well as custom software that performs the clustering and generates template models (e.g. the average or medoid for each size) as in figure 62. As can be seen in figure 63, three clusters would be a minimum under these constraints. Ideally, according to the method described in chapter 4 and visualized in figure 52, four clusters should be used (lowest cluster validity index within the selected range of sizes). However, due to time and budget constraints, three clusters were used for this first iteration.

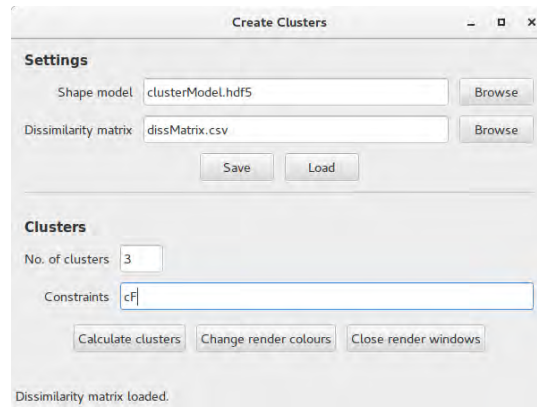


Figure 62: Example GUI program for creating any number of clusters given a shape model in HDF5-format, a dissimilarity matrix (dissimilarity between the shapes in the shape model) and optional constraints.

Measurement	Cluster A	Cluster B	Cluster C
head length	182.8 - 201.6	192.8 - 221.5	168.6 - 193.8
bitrignon width	135.6 - 153.5	141.0 - 166.6	130.7 - 149.4
circumference	542.3 - 565.3	565.6 - 626.1	511.0 - 541.4
arc width	313.1 - 374.4	327.5 - 388.8	298.3 - 353.7

Table 25: Sizing table according to four anthropometric measurements. All values are in mm.

#### 5.4.2 Synthesis phase

The feature-constrained clustering discussed in chapter 4 was used in order to create three clusters of the human head, as in figure 64. Four anthropometric measurements were chosen as constraints: circumference, bitrignon width, head length and arc width. (In fact, as discussed in chapter 4, only the circumference would have sufficed. However, this work was done in parallel with the publication of that paper. The detailed comparison of clustering methods and analysis of the results was not yet available at that point.) Finally, a sizing table based on the circumference, head length, bitrignon width, and arc width was then determined (see table 25), to be used to assign new individual to their representative clusters.

The next step was to determine the variation (distance and angle) for each of the electrode locations. To achieve this, the desired 10-20 locations were marked on the average head shape, after which a construction line was drawn in the normal direction for each of those points. Minimum and maximum envelopes were then created for each of the clusters, as in figure 51 in chapter 4. The intersection

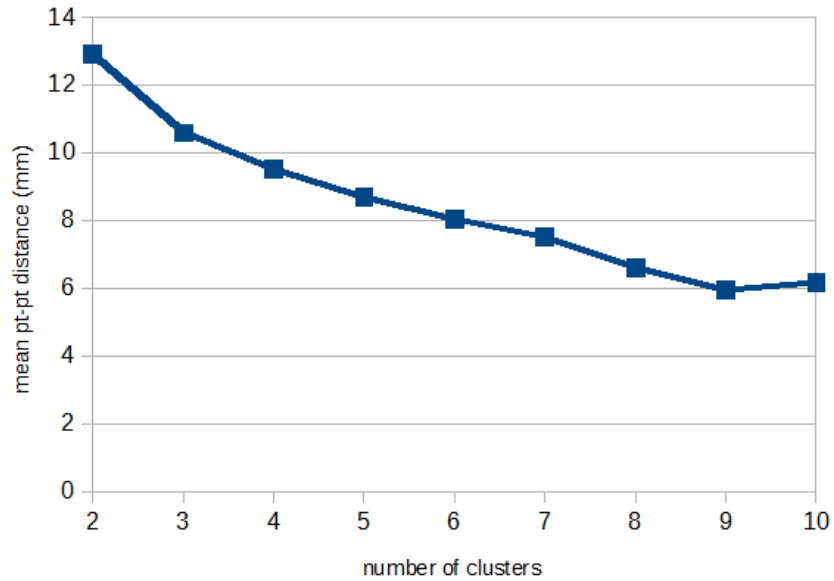


Figure 63: Graph showing the average point-to-point distances for clusters after constrained clustering.

between the envelopes and the 10-20 construction lines marked for each cluster, representing the absolute minimum and maximum distance that would have to be accommodated for in this population, see figure 65. Note: because the envelopes do not represent realistic head surfaces, using these to determine the variation angle for the 10-20 locations would not be representative for the studied population. Since the results in chapter 3 revealed that the distribution of points was mostly linear, the normal direction of the average head was deemed to be more appropriate.

In SolidWorks, the electrodes were then placed at 80% of the minimum-maximum envelope distance for each point. Electrodes were drawn with the sponge in compressed state, see figure 66. The rationale for choosing 80% was that the absolute maximum point might be an outlier and that the flexibility of the photopolymer would ensure that the electrode did not cause discomfort in this kind of extreme cases. The rest of the distance between maximum to minimum envelope was to be covered by the flexibility of the sponge. Finally, the electrodes were oriented so the plane at the contact points was parallel to the average head surface. Another option would be to place them perpendicular to the 10-20 construction lines, but the normals of individual vertices might not represent the direction of the complete surface covered by the sponge, and electrodes oriented in this manner might cause discomfort.

After all electrodes were drawn, the remainder of the headset was designed. The minimum and maximum envelope surfaces were used as a template to ensure that the rest of the product would have the



Figure 64: Top view of three clusters of the head, clustered using constrained clustering with circumference, bitracion width, head length and arc width as constraint.

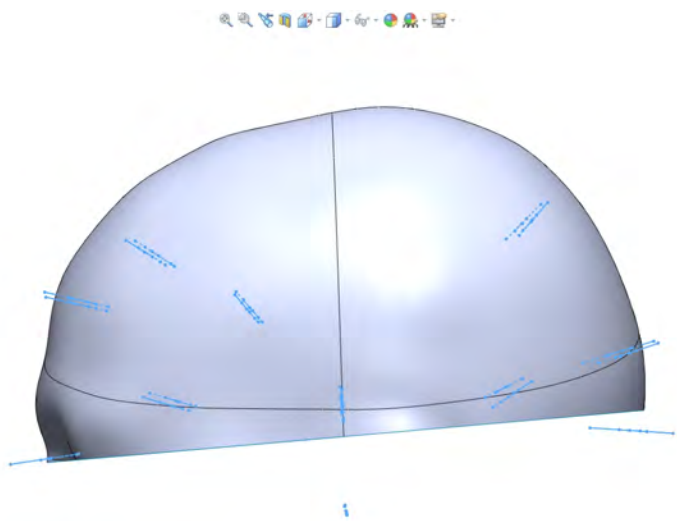


Figure 65: Construction lines showing minimum and maximum electrode locations for each product size (i.e. cluster).

correct shape and would not make contact with the user's head, see figure 67. The final prototypes are shown in figure 68. One thing that was immediately apparent is how different the shape of the three headsets is. Using traditional anthropometry, this exercise would have resulted in three headsets of different sizes but with the exact same shape (e.g. small, medium, large). From the 3D models in figure 64, it's clear that this would have result in a bad fit for at least two of the population clusters. Instead, the shape model-based designs provide more difference in shape than in size, corresponding to the findings in section 5.2 - the smallest headset is rounder where as the larger is more elongated.

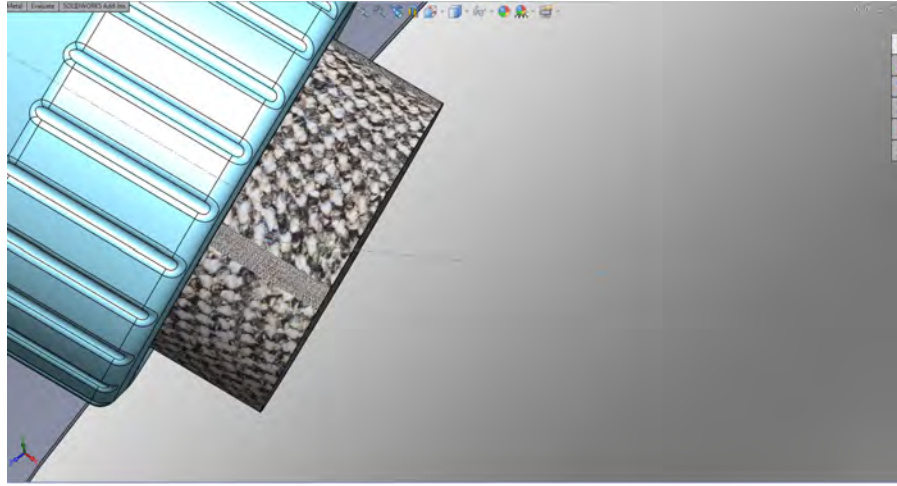


Figure 66: Example of electrode design with minimum and maximum 10-20 point location.

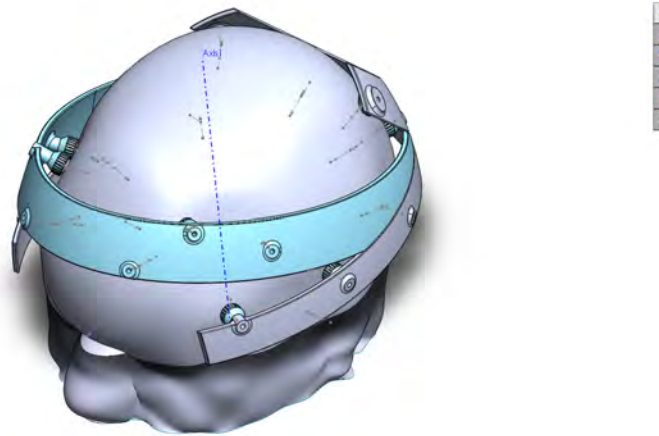
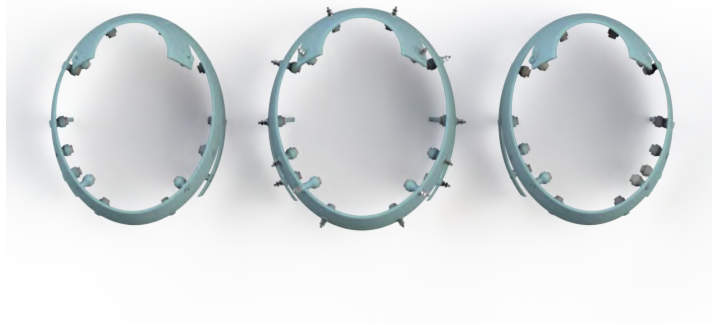


Figure 67: Prototype headset designed with maximum envelope of cluster B as manikin.

#### 5.4.3 *Simulation phase*

In the simulation phase, 3D-printed prototypes of the three headset sizes were fit onto the heads of 49 test subjects. The fit of the three headset sizes was verified digitally and physically. For the physical verification, the 3D locations of the 14 electrode points (i.e. product contact points) were measured using a Microscribe MX, as in chapter 3. In this case, an EEG-cap derived from the MedCat caps was put on each subject's head, and the Microscribe pointer was moved through the holes corresponding to the electrode locations until it made contact with the skin. The 3D surface of each subject's head was predicted (or simulated) using the method discussed in chapter 2. The measured 3D coordinates were then aligned to the predicted skin surfaces using iterative closest points (ICP) and compared in



(a)



(b)

Figure 68: Final design of BCI headset prototypes in three sizes.

order to quantify the accuracy of the prediction, see figure 69. The average prediction error was found to be  $-0.86 \pm 0.6$  mm, with the negative sign indicating that the measured point coordinates in general are located on the inside of the predicted head surface. Next, the 3D coordinates of the electrode points for each subject were compared to the electrode locations used to create the CAD models for the three headset sizes. The headset size for which these distances were the smallest was deemed to be the best fit, and these distances were used for further analysis.

For the physical simulation of fit, each participant was asked to qualitatively evaluate the fit of their assigned product size (according to the sizing table) and to indicate a better fitting product size, if applicable (see figure 70). Most participants found the headset to be comfortable, although for two students with smaller heads, no product size fit comfortably. Most subjects also noted that the electrodes at the front of the head, 10-20 locations AF<sub>3</sub> and AF<sub>4</sub>, didn't make contact with their head, even for the best fitting product size.

Finally, various methods of assigning product sizes to individuals were tested. Initially, assignment was done on the basis of the siz-

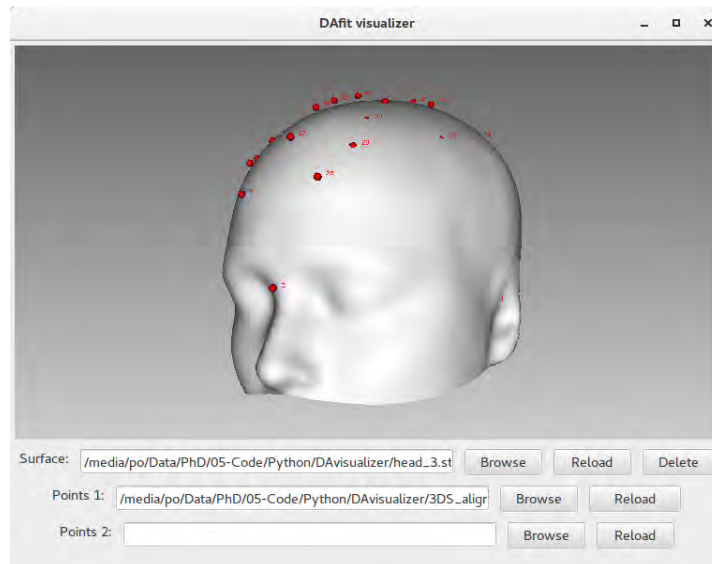


Figure 69: Example of measured 3D coordinates of electrode locations overlaid on predicted head surface. (custom software)

ing table, using the participant's head circumference, head length, bitracion width and arc width. Furthermore, the predicted head surface for each individual was compared to the representative (digital) manikins of the product sizes (i.e. cluster medoids, as described in chapter 4) and the product size for the manikin with the smallest average difference to the predicted head was selected. This will be referred to as assignment by shape. In a similar manner, the distance between the 14 product contact points of the CAD models and the predicted head surface was compared, called assignment by points of interest. Compared to the best fitting size as selected by the physical prototypes, assignment by sizing table only managed to correctly assign sizes for 14% of the subjects. With assignment by shape, 27% of the subjects were assigned a correct headset, which was still much lower than expected. Assignment by points of interest (POI), on the other hand, did manage to assign the correct size in 64% of the cases. The reason for the poor performance of assignment using sizing tables might be explained by the fact that inappropriate constraints were chosen for this amount of clusters (see section 4.4.3). In a next iteration of the design process, using circumference as first (or only) constraint might result in better sizing tables.

#### 5.4.4 Evaluation phase

From the subjective physical verification, it appears that the chosen clusters do not fit the population very well, with at least two of the frontal electrodes hardly ever making contact with the skull.

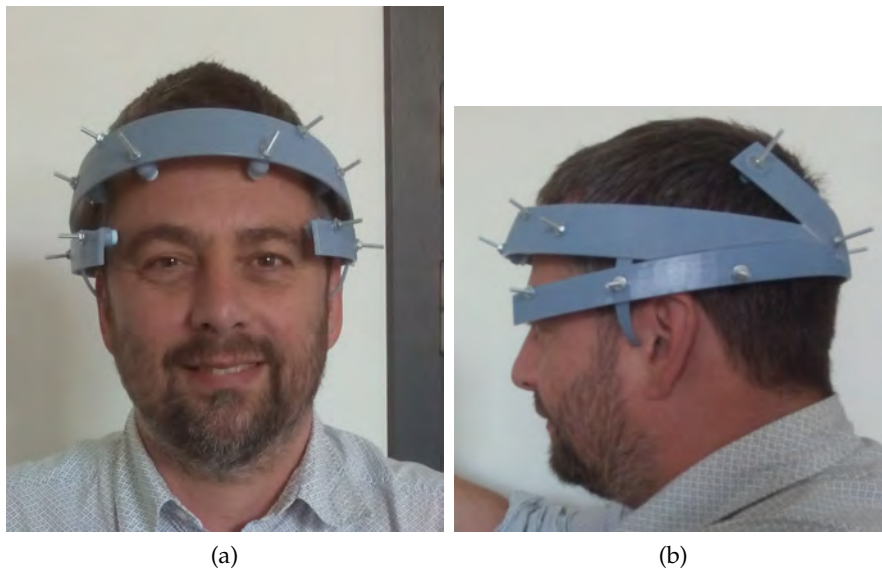


Figure 70: One of the test subjects wearing the prototype for product size B. Published with permission of the subject.

This might be due to several reasons. Firstly, as mentioned in section 5.4.1, a higher number of product sizes would offer better clustering. As shown in chapter 4, the clustering quality improves when using four clusters (shown by the lower cluster validity index), but decreases again at five clusters. It might be that there is a specific head shape with higher surface at the location of the AF3 and AF4 electrodes, but that this very local variation has caused the clustering algorithm to prioritize other shape variations and spread subjects with these types of heads over the three current clusters, biasing the design for each cluster. Allowing one additional cluster might have resulted in these head types being grouped in a separate cluster.

Another possibility is that the electrode sponge flexibility (estimated at 9 mm) was misjudged or that the sponges had lost part of their flexibility due to reuse. Using a different type of sponges or changing the sponges between subjects might have helped in this case. Alternatively, a lower average point-to-point distance should have been chosen, which would have again resulted in the requirement to have four clusters.

A third possibility is that in the synthesis phase, placing the electrodes at 80% of the distance between minimum and maximum envelopes was still too high. Since no subjects reported discomfort from electrodes exerting too much pressure or the headset being too rigid, a lower distance might have been better suited, e.g. 60% or even 50%.

Furthermore, the sizing table was not effective in assigning the correct product size to individuals. Instead, comparing the product's contact points with the predictions of the user's head shape (based on anthropometric measurements) resulted in the best product size assignment.

Based on these results, it would be advisable to do a next design iteration, using either a different clustering method that performs the clustering based on the product's contact points instead of on the full surfaces, using a higher number of clusters, or adjusting the design so the problematic electrodes are more likely to make contact, e.g. by using different materials with more flexibility (or another solution to allow some variation in electrode positioning).

Finally, as mentioned in section 5.2, the scalp shape model might not be representative for a Belgian population. A shape model based on a Belgian sample might result in far better initial clusters, less design iterations and of course a better fitting overall design.

## 5.5 EVALUATION OF PROTOTYPE BCI HEADSETS ACCORDING TO ESSENTIAL DESIGN REQUIREMENTS

In table 26, the two BCI headset prototypes developed in the course of this work, referred to as the POpoc 1 and the POpoc 2, are evaluated according to the design criteria for consumer-grade BCI headgear defined in section 1.2.3. Because these devices were not intended as fully functional BCI headsets, a number of design requirements could not be verified. Even so, evaluation the prototypes against the design requirements should give an indication of whether 3D anthropometry is the right method to design BCI headgear.

For each prototype, the table shows a "Y" (yes) if the requirement was met, "N" (no) if it was not, and "n.a." (not applicable) if it was considered out of scope or not verified. If the requirement was met, references are included to the sections, tables or figures where it was verified.

For electrode positioning (req. 1), both prototypes were with electrode locations according to the 10-20 system. POpoc 1 was found to fit those locations with an adequate positioning accuracy, and while the physical verification for POpoc 2 was only done subjectively, a physical verification of the electrode positions on the predicted surfaces used as the basis for POpoc 2 confirmed that the predicted contact points were very close to the correct electrode positions.

POpoc 1 could not be self-applied by the user because of the elaborate manner in which the electrodes need to be adjusted before applying the headset (req. 4). However, if the adjustment method is optimized in a redesign, the reference struts should make it very easy for the user to place the headset on correctly. In POpoc 2, test subjects had no problems mounting the applying the product sizes themselves.

However, POpoc 2 did require a brief instruction on how to apply the headset, since the design currently allows to place it on the head backwards (req. 5.1). This is not the case for POpoc 1, which does not

fit comfortably if it is put on backwards, and for in which the Na, LPA and RPA reference points can be used for guidance.

POpoc 1 displayed better repeatability than a commercial BCI headset (req. 5.2), and while the electrode positions did deviate slightly after repeated set-up, electrode displacement was not more than currently accepted within EEG practice.

None of the test subjects reported (or showed marks of) any discomfort while wearing either prototype headset (req. 6.1), although further research is required to verify whether this holds true for prolonged use (e.g. an hour) as well.

Finally, POpoc 1 often exceeded the required sensor set-up time (req. 7.2), again due to the necessary electrode adjustments before set-up. However, test subjects were able to apply or take off POpoc 2 in a manner of seconds.

This preliminary evaluation indicates that using statistical shape models is a promising design technique for BCI headset: for those requirements that were considered during the design of BCI headsets. Table 26 shows that, for those requirements that were considered, at least one of both prototype headset passes. With further refinement of the design methods and optimization of the prototypes, it should be possible to meet the remaining requirements.

ID	POpoc 1	POpoc 2	Reference
1	Y	Y	sections 3.4.1, 3.4.2, and 3.5.3, table 13, figure 45
2.1	n.a.	n.a.	
2.2	n.a.	n.a.	
2.3	n.a.	n.a.	
3	n.a.	n.a.	
4	N	Y	section 5.4.3
5.1	Y	N	section 3.3.1
5.2	Y	n.a.	sections 3.4.1, 3.4.2, and 3.5.5, table 13
5.3	n.a.	n.a.	
5.4	n.a.	n.a.	
6.1	Y	Y	section 5.4.3
6.2	n.a.	n.a.	
6.3	n.a.	n.a.	
7.1	n.a.	n.a.	
7.2	N	Y	section 5.4.3
7.3	n.a.	n.a.	

Table 26: Evaluation of POpoc 1 and POpoc 2 prototype headsets.

## 5.6 EXPECTED IMPACT OF SHAPE MODELS ON THE DESIGN OF BCI HEADGEAR

The examples in chapter 3 and section 5.4 indicate that the use of shape models has three major implications for BCI headsets: an improved electrode fit, better stability or robustness during movement and a higher repeatability.

- Improved fit of electrodes will likely result in lower electrode impedance and thus higher signal quality [43, 44, 175]. Combined with new types of electrodes that don't require conductive gel or saline solution (i.e. [41, 176]), better fitting electrodes will also improve user comfort. A better knowledge of shape variation at 10-20 systems will also allow for more optimal placement of electrodes, possibly minimizing the required number of electrodes and allowing for custom electrode channel selection per headset or application. This results in higher convenience, higher user comfort, and maybe most importantly: more pleasing aesthetics, which will in turn affect user acceptance of the new technology [4, 42, 127]. Furthermore, there are indications that custom electrode channel selection could also increase EEG performance [25, 177].
- A better understanding of the human head shape variation will result in better headset stability during movement, because designers will be able to not only position electrodes more precisely, but also to study how and where to place contact points that fixate the product on the user's head. The ability to move around freely while wearing a BCI headset will positively influence the convenience and especially the mobility of EEG devices [42, 178]. New electrode design practices might also lead to a reduction of motion artifacts, which would again increase EEG performance [178].
- The largest benefit from higher repeatability will be a lower need for calibration and a shorter set-up time, which was found to be an important factor in BCI headset usage, both in our own work (section 1.2.1) and in previous literature [26, 42, 127, 179].

In turn, these three factors could have a significant impact on the field of brain-computer interfacing. First and foremost, a more user-friendly and better fitting BCI headset could cause a resurgence of BCI research, similar to the one observed around the 2012 when the Epop was introduced [4]. If better electrode fit indeed improves the performance of EEG electrodes, dry electrodes might finally become recognized as feasible alternatives to gel-based ones, making it easier to recruit participants for studies and greatly reducing the duration of experiments. Higher repeatability indicates that BCI researchers

would be able to use such a headset to quickly prototype, test and demonstrate new BCI algorithms, speeding up the development of new paradigms and applications. Due to the higher stability, BCI applications could be tested in real-world scenarios, improving the usability and the shortening of their time to market.

Aside from academic research, more convenient and better looking BCI headsets would increase the public awareness and technology acceptance. Combined with a higher number of applications that were verified in dynamic environments, this would inevitably lead to the long expected use of BCI headsets for games and other home applications [4, 26, 180]. Furthermore, if the user requirements set forth by Nijboer in [42] were met and applications for alternative communication and control could be tested with real patients more often, people suffering from conditions such as ALS or MS -who have been the supposed target users for 'mindspeller' applications for decades- might finally benefit from BCI technology.

To summarize, the expected effects of 3D anthropometry on the design of BCI headgear are a higher user comfort, lower calibration and set-up time, higher convenience, better looks, increased mobility, increased signal quality (at least compared to current commercial devices), resulting in an increased amount of BCI research and thus a higher number of potential BCI applications. However, because researchers tend to overestimate how soon BCI technology will be ready for home use [4], it's important to realize that the first benefits from more user-friendly BCI headsets will be seen in research. The integration of BCI as a new human-machine interface in everyday life is a commendable goal, but researchers should be careful about communicating these expectations to the outside works, so as to not create an unrealistic view of BCI in the eyes of the general public, which could push people away from the technology out of fear for 'mind reading', as well as disappoint early adopters when current applications find their way to their homes.

## 5.7 SUGGESTIONS FOR FUTURE RESEARCH

Suggestions for research in statistical shape modeling and 3D anthropometry:

- A head (scalp) shape model from CT or MRI scans of a Belgian or Dutch sample should be created and verified by comparing its predicted shape surfaces to the physical head shapes of the individuals included in the sample.
- Head shape models should be created for various ethnicities and regions. Using the techniques described in section 2.5.3,

these models should be compared in order to determine which ethnicities or regions require separate shape models. For example, it would be interesting to know whether a single European head or scalp shape model would suffice for product design across Europe, or whether separate shape models should be created for individual regions or even countries.

- The influence of different hair types on the product fit should be quantified. Even in people with short hair, the shape model might not offer the best fit because a (flattened) layer of hair would alter the actual contact point of the product. If it's found that hair has a significant impact on the product fit, this impact should be measured and hair types should be included as parameters for the shape model.
- Shape models of the internal structures of the cranium should be created. By combining the external shape model with shape models of the internal bone layers and brain, it would be possible to study the correlation between external features and internal structures, resulting in three-dimensional information on the variation of skin and skull thickness on each point of the cranium. This could be combined with finite element modeling in order to simulate user comfort or to perform impact simulations (e.g. for helmets).

Suggestions for research in product development and industrial design:

- The sizing system prototypes should be remade according to the insights and results from section 5.4, which was still under development when the first design iteration was performed. The method used for simulation and evaluation in chapters 3 and 4 should be adapted to an experiment protocol and a scientific study should be performed to verify the effectivity of the constrained clustering method.
- The 3D anthropometric methods described in this work should be verified by comparing a design process based on traditional anthropometry with one based on 3D anthropometry. This should preferably be done with two groups of multiple designers, with one group using the traditional method and one group using the new methods, so as to avoid biased results due to designer skill levels. Both methods should be compared for efficiency and effectivity in meeting a set of predetermined design specifications.
- The methods described in this work should be implemented into software interfaces that can be used by designers. A first version of such an interface in the form of a SolidWorks plugin

has been developed during the CADANS project [181], but this interface should be tested and expanded to other platforms.

- Other applications of parametric shape models should be considered. For example, 3D anthropometry might benefit the design of prosthetics, the cost and effectivity of pressure masks to prevent scarring after severe burns and many others.

Suggestions for research in brain-computer interfacing:

- Further experiments should be performed with the one-size-fits-all prototype. Since the study in chapter 3 was performed as a pilot study with students, a more extensive experiment should be organized. The prototype should be adapted to include the weight of the electronic components (e.g. the OpenBCI board and electrodes) and battery in order to fairly compare stability to commercial devices. It should also be compared with multiple commercial headsets instead of just the Epoc.
- The expected improvements described in section 5.6 should be tested. Electronics should be incorporated into the one-size-fits-all prototype to test whether better electrode positioning has a significant impact on signal-to-noise-ratio and electric impedance.
- The existence and effect of motion artifacts should be compared between traditional EEG caps, current commercial devices and prototypes based on 3D anthropometry.
- It would also be interesting to see whether the higher repeatability might decrease the need for calibration and thus improve the convenience of using the headsets.



Part IV

CONCLUSION



## CONCLUSION

---

3D anthropometry offers a major potential to help designers understand the shape variation of the human body. Ever since the first research papers about statistical shape models were published, researchers have pointed out their possibilities to assist in designing products with a better fit. However, no standardized methods exist for 3D anthropometry. Even for traditional anthropometry, most designers depend on intuition and experience in to make products fit their users, rather than relying on the vast set of anthropometric data that is currently available. Data is only considered after the product is introduced on the market, at which point further changes to product fit are driven by sales figures. While it might work in some cases, this approach is highly dependent on the skills of individual designers. In companies that employ designers without much experience, or companies that wish to create new products with which their designers do not have any experience, it can take years to get the fit quite right. Apart from the unnecessary production costs that inevitably result from this experimental way of working, unsatisfied users might switch to competing products in the meantime. Or even worse, some users might not even find comfortable products that properly fit. A new, evidence-based approach would benefit everyone involved in the design of products that need to fit closely to the body.

In this thesis, instead of focusing on general and abstract methods, the use of 3D anthropometry in product design and development was studied through the application on a specific type of products that would greatly benefit from a closer contact with the user's skin, but in which design is often an afterthought: headgear for brain-computer interfacing or BCI. While the initial goal was to explore all aspects of BCI headset design (including electronics and software) and to formulate an integrated method to create fully functional, user-friendly BCI headsets, it quickly became clear that the lack of accurate anthropometric data on the shape variation of the human head, as well as a lack of standardized methods for using the data that was available, was a major limiting factor in BCI headgear design. Curiously, despite many claims on the potentials of this technology to change the lives of users by offering new possibilities for communications, well-being and entertainment, said user is hardly ever considered during the research or implementation. Considering these observations, the scope of the doctorate was at the same time limited to only those aspects of BCI that relate to usability and user comfort, as well as broadened to

the application of 3D anthropometry in product design.

First, a statistical shape model of the human head was created in order to study the size and shape variation of the scalp. The largest variation of the scalp shape was found to be in the overall size or volume of the head, which is also the most important distinguishing difference between male and female head shapes, along with the shape of the eyebrow ridge. Apart from studying the ability of this model to accurately predict and represent head shapes, the statistical parameters were also mapped to traditional anthropometric measurements (features), which are more intuitive to use in product design. The more features that were used, the better the shape prediction and the narrower the distribution of errors across the scalp. The head circumference was found to be the best single parameter for shape prediction and manipulation, although a combination of head length, bitracion width (head breadth), circumference and arch width (bitracion coronal arc) is a good compromise between ease of measurement and accuracy of predictions, resulting in an average prediction error of only  $1.64 \pm 0.39$  mm. The ear height was not a good parameter, and including it actually decreased the prediction accuracy. This seems to indicate that the ear height has no correlation with the overall head shape, it might also be due to the limited fidelity of ear shape resulting from the shape modeling method.

Secondly, a number of methods were created to apply the statistical shape model in product design process. The shape model was used to create a (non-functional) one-size-fits-all BCI headset and to create a headset in three different sizes. For the one-size-fits-all prototype, the method was verified by comparing the electrode placement, stability during movement and repeatability of electrode positions to those of a current consumer-grade BCI headset. On average, the electrode positions differed from the ideal 10-20 locations by  $21.97 \pm 10.44$  mm, shifted by  $10.52 \pm 7.22$  mm after movement and deviated by  $11.28 \pm 6.11$  mm, which was comparable to the commercial device and within accepted values in EEG practice. While the prototypes resulting from product sizing were not systematically verified, they fit reasonably well in an initial fitting test, although assigning the product sizes based on a sizing table with anthropometric measurements was only correct in 14% of cases. On the other hand, assigning product sizes digitally based on the distance between electrode contact points and the user's head shape was much more reliable.

A number of conclusions could be drawn from these experiments. Using 3D anthropometry during the analysis phase results in a better, more robust understanding of head shape and in more accurate design specifications, eliminating the need for the intuition or previous

experience with similar products. However, the skill of the designer still plays an important role during the synthesis phase of the design process, e.g. during CAD design, in which creative solutions need to be found in order to conform to the product contact points derived from the shape analysis and at the same time still offer a pleasing aesthetic look (which, admittedly, was not entirely achieved for the prototypes produced in this work). Furthermore, contact points -or points of interest (POI)- were also found to play an important role in product sizing. Whenever possible, shape models and especially their derived manikins should be created for specific product applications, as opposed to relying on general manikins for multiple types of products. Taking regions and points of interest into account during shape modeling will greatly improve product design and will enable a correct fit in less design iterations. Finally -and perhaps surprisingly- 3D anthropometry should be considered as an advanced product design method that is not necessarily applicable for all types of products. It will mostly benefit products that require close contact with the body, such as products containing biometric sensors. For most other types of products, training designers to use 3D anthropometry during the entire product design process is not required and might even result in decreased productivity. However, even for 'simple' products, an analysis based on 3D anthropometry can support the definition of accurate design specifications. Therefore, shape models eliminate the need to perform large-scale measuring studies or to rely on limited and outdated anthropometric data.

In conclusion, this work shows that 3D anthropometry can be a valuable asset in multiple phases of the product design process. Using head shape models for the design of EEG measuring devices will result in better fitting and more convenient BCI headsets that can function in dynamic environments. If a user-centered design process is followed in the design of BCI applications, this will no doubt result in a resurgence of BCI research and real-world applications. By putting the user first, the coming decade might finally see the promise of brain-computer interfaces be fulfilled.



## BIBLIOGRAPHY

---

- [1] *Future BNCI Roadmap - A Roadmap for Future Directions in Brain/Neuronal Computer Interaction Research*. Roadmap. European Union Seventh Framework Programme [FP7/2007-2013] under grant agreement n°248320. Graz University of Technology et al., 2012.
- [2] Clemens Brunner, Niels Birbaumer, Benjamin Blankertz, Christoph Guger, Andrea Kübler, Donatella Mattia, José del R. Millán, Felip Miralles, Anton Nijholt, Eloy Opisso, Nick Ramsey, Patric Salomon, and Gernot R. Müller-Putz. „BNCI Horizon 2020: towards a roadmap for the BCI community.” en. In: *Brain-Computer Interfaces* (Feb. 2015), pp. 1–10. DOI: [10.1080/2326263X.2015.1008956](https://doi.org/10.1080/2326263X.2015.1008956).
- [3] Jonathan R. Wolpaw. „The BCI endeavor and the mission of this new journal.” en. In: *Brain-Computer Interfaces* 1.1 (Jan. 2014), pp. 2–4. DOI: [10.1080/2326263X.2014.884740](https://doi.org/10.1080/2326263X.2014.884740).
- [4] Minkyu Ahn, Mijin Lee, Jinyoung Choi, and Sung Jun. „A Review of Brain-Computer Interface Games and an Opinion Survey from Researchers, Developers and Users.” en. In: *Sensors* 14.8 (Aug. 2014), pp. 14601–14633. DOI: [10.3390/s140814601](https://doi.org/10.3390/s140814601).
- [5] *Applying Evidence-Based Design to Medical Product Design*. URL: <http://www.designingforhumans.com/idsa/2009/04/applying-evidencebased-design-to-product-design.html> (visited on 07/22/2016).
- [6] Erika Hall. *Let's Stop Doing Research\**. May 2016. URL: <https://medium.com/research-things/lets-stop-doing-research-48efcd7118c9#.jajqj2iijo> (visited on 07/22/2016).
- [7] Thomas E. Ward. „Hybrid Optical–Electrical Brain Computer Interfaces, Practices and Possibilities.” In: *Towards Practical Brain-Computer Interfaces*. Ed. by Brendan Allison, Stephen Dunne, Robert Leeb, José del R. Millán, and Anton Nijholt. Biological and Medical Physics, Biomedical Engineering. Berlin Heidelberg: Springer-Verlag, 2012, pp. 17–39.
- [8] Jacques J. Vidal. „Toward Direct Brain-Computer Communication.” In: *Annual Review of Biophysics and Bioengineering* 2.1 (1973), pp. 157–180. DOI: [10.1146/annurev.bb.02.060173.001105](https://doi.org/10.1146/annurev.bb.02.060173.001105).
- [9] Hilde Segers, Adrien Combaz, Nikolay V. Manyakov, Nikolay Chumerin, Katrien Vanderperren, Sabine Van Huffel, and M. M. Van Hulle. „Steady state visual evoked potential (SSVEP)-based brain spelling system with synchronous and asynchronous

- typing modes." In: *15th Nordic-Baltic Conference on Biomedical Engineering and Medical Physics (NBC 2011)*. Springer, 2011, pp. 164–167.
- [10] Connie C. Duncan, Robert J. Barry, John F. Connolly, Catherine Fischer, Patricia T. Michie, Risto Näätänen, John Polich, Ivar Reinvang, and Cyma Van Petten. „Event-related potentials in clinical research: Guidelines for eliciting, recording, and quantifying mismatch negativity, P300, and N400." en. In: *Clinical Neurophysiology* 120.11 (Nov. 2009), pp. 1883–1908. DOI: [10.1016/j.clinph.2009.07.045](https://doi.org/10.1016/j.clinph.2009.07.045).
- [11] H. Strasburger, H. Scheidler, and I. Rentschler. „Amplitude and phase characteristics of the steady-state visual evoked potential 6." In: *Applied Optics* 27.6 (1988), pp. 1069–1088.
- [12] M. Cheng, X. Gao, and D. Xu. „Design and implementation of a brain-computer interface with high transfer rates." In: *IEEE TBE* 49.10 (2002), pp. 1181–1186.
- [13] Y. Wang, R. Wang, X. Gao, B. Hong, and S. Gao. „A practical VEP-based brain-computer interface." In: *IEEE TNSRE* 14.2 (2006), pp. 234–240.
- [14] H. Segers, A. Combaz, N.V. Manyakov, N. Chumerin, K. Vanderperren, S. Van Huffel, and M.M. Van Hulle. „Steady-State Visual Evoked Potential (SSVEP) - based Brain Spellings System with Synchronous and Asynchronous Typing Modes." In: *15th Nordic-Baltic Conference on Biomedical Engineering and Medical Physics*. Aalborg, Denmark, 2011, pp. 164–167.
- [15] L. Farwell and E. Donchin. „Taking off the top of your head: toward a mental prosthesis utilizing event-related brain potentials." In: *Electroencephalography and Clinical Neurophysiology* 70.6 (1988), pp. 510–523.
- [16] F. Nijboer, E. Sellers, J. Mellinger, M. Jordan, T. Matuz, A. Furdea, S. Halder, U. Mochty, D. Krusienski, T. Vaughan, J. Wolpaw, N. Birbaumer, and A. Kübler. „A P300-based brain-computer interface for people with amyotrophic lateral sclerosis." In: *Clinical Neurophysiology* 119 (2008), pp. 1909–1916.
- [17] E. Sellers and E. Donchin. „A P300-based brain-computer interface: Initial test by ALS patients." In: *Clinical Neurophysiology* 117 (2006), pp. 538–548.
- [18] F. Piccione, F. Giorgi, P. Tonin, K. Priftis, S. Giove, S. Silvoni, G. Palmas, and F. Beverina. „P300-based brain-computer interface: Reliability and performance in healthy and paralysed participants." In: *Clinical Neurophysiology* 117 (2006), pp. 531–537.

- [19] U. Hoffman, E. T. Vesin, J.-M, and K. Diserens. „An efficient P300-based brain-computer interface for disabled subjects.” In: *Journal of Neuroscience Methods* 167 (2008), pp. 115–125.
- [20] N.V. Manyakov, N. Chumerin, A. Combas, A. Robben, M. van Vliet, and M.M. Van Hulle. „Decoding Phase-based Information from Steady-State Visual Evoked Potentials with Use of Complex-Valued Neural Network.” In: *12th International Conference on Intelligent Data Engineering and Automated Learning (IDEAL2011)*. Ed. by H. Yin, W. Wang, and V. Rayward-Smith. Lecture Notes in Computer Science (LNCS), 6936. Norwich, UK, 2011, pp. 135–143.
- [21] C. Duncan, R. Barry, J. Conolly, C. Fisher, P. Michie, and R. Naatanen. „Event-related potentials in clinical research: guidelines for eliciting, recording and quantifying mismatch negativity, P300 and N400.” In: *Clinical Neurology* 120 (2009), pp. 1883–1903.
- [22] Marta Kutas and Kara D. Federmeier. „Thirty Years and Counting: Finding Meaning in the N400 Component of the Event-Related Brain Potential (ERP).” en. In: *Annual Review of Psychology* 62.1 (Jan. 2011), pp. 621–647. ISSN: 0066-4308, 1545-2085. DOI: [10.1146/annurev.psych.093008.131123](https://doi.org/10.1146/annurev.psych.093008.131123). (Visited on 10/23/2016).
- [23] Valer Jurcak, Daisuke Tsuzuki, and Ippeita Dan. „10/20, 10/10, and 10/5 systems revisited: Their validity as relative head-surface-based positioning systems.” en. In: *NeuroImage* 34.4 (Feb. 2007), pp. 1600–1611. DOI: [10.1016/j.neuroimage.2006.09.024](https://doi.org/10.1016/j.neuroimage.2006.09.024).
- [24] George H. Klem, Hans Otto Lüders, H. H. Jasper, C. Elger, and others. „The ten-twenty electrode system of the International Federation.” In: *Electroencephalogr Clin Neurophysiol* 52.3 (1999).
- [25] William Speier, Aniket Deshpande, and Nader Pouratian. „A method for optimizing EEG electrode number and configuration for signal acquisition in P300 speller systems.” en. In: *Clinical Neurophysiology* 126.6 (June 2015), pp. 1171–1177. DOI: [10.1016/j.clinph.2014.09.021](https://doi.org/10.1016/j.clinph.2014.09.021).
- [26] W David Hairston, Keith W Whitaker, Anthony J Ries, Jean M Vettel, J Cortney Bradford, Scott E Kerick, and Kaleb McDowell. „Usability of four commercially-oriented EEG systems.” In: *Journal of Neural Engineering* 11.4 (Aug. 2014), p. 046018. DOI: [10.1088/1741-2560/11/4/046018](https://doi.org/10.1088/1741-2560/11/4/046018).
- [27] R. Yazicioglu, T. Torfs, P. Merken, J. Penders, V. Leonov, and R. Peurs. „Ultra-low power biopotential interfaces and their applications in wearable and implantable systems.” In: *Microelectronics Journal* 40.9 (2009), pp. 1313–1321.

- [28] *Geodesic Sensor Net*. URL: <https://www.egi.com/research-division/geodesic-eeg-system-components/geodesic-sensor-nets> (visited on 10/30/2016).
- [29] Tim Sheerman-Chase. *EEG Brain Scan*. URL: [https://www.flickr.com/photos/tim\\_uk/8135749317/](https://www.flickr.com/photos/tim_uk/8135749317/) (visited on 07/28/2016).
- [30] *Creative Commons Legal Code Attribution 2.0*. URL: <https://creativecommons.org/licenses/by/2.0/legalcode> (visited on 07/28/2016).
- [31] Samuel R. Atcherson, Herbert Jay Gould, Monique A. Pousson, and Tina M. Prout. „Variability of Electrode Positions Using Electrode Caps.” en. In: *Brain Topography* 20.2 (Oct. 2007), pp. 105–111. DOI: [10.1007/s10548-007-0036-z](https://doi.org/10.1007/s10548-007-0036-z).
- [32] Kristof Vaes. „Product Stigmaticity - Understanding, Measuring and Managing Product-Related Stigma.” PhD thesis. 2014, p. 227. ISBN: 97890-6562-3515.
- [33] Joshua I. Ekandem, Timothy A. Davis, Ignacio Alvarez, Melva T. James, and Juan E. Gilbert. „Evaluating the ergonomics of BCI devices for research and experimentation.” en. In: *Ergonomics* 55.5 (May 2012), pp. 592–598. DOI: [10.1080/00140139.2012.662527](https://doi.org/10.1080/00140139.2012.662527).
- [34] *EMOTIV Epoc - 14 Channel Wireless EEG Headset*. URL: <http://emotiv.com/epoc/> (visited on 07/31/2016).
- [35] Chrisshe. *English: Emotiv EPOC+*. June 2016. URL: [https://commons.wikimedia.org/wiki/File:Emotiv\\_EPOC%2B.png](https://commons.wikimedia.org/wiki/File:Emotiv_EPOC%2B.png) (visited on 07/29/2016).
- [36] Chrisshe. *English: Emotiv Insight*. June 2016. URL: [https://commons.wikimedia.org/wiki/File:Emotiv\\_insight.png](https://commons.wikimedia.org/wiki/File:Emotiv_insight.png) (visited on 07/29/2016).
- [37] *Creative Commons — Attribution-ShareAlike 4.0 International — CC BY-SA 4.0*. URL: <https://creativecommons.org/licenses/by-sa/4.0/legalcode> (visited on 07/29/2016).
- [38] Hatma Suryotrisongko and Febriliyan Samopa. „Evaluating OpenBCI Spiderclaw V1 Headwear’s Electrodes Placements for Brain-Computer Interface (BCI) Motor Imagery Application.” en. In: *Procedia Computer Science* 72 (2015), pp. 398–405. DOI: [10.1016/j.procs.2015.12.155](https://doi.org/10.1016/j.procs.2015.12.155).
- [39] Conor Russomanno. *Spiderclaw V1/V2 (deprecated)*. URL: <http://openbci.com/community/spiderclaw-v2-deprecated/> (visited on 07/31/2016).
- [40] *New EEG Headset From Imec to Compete Existing Brain-Reading Products*. URL: <http://neurogadget.net/2011/02/09/new-eeg-headset-from-imec-to-compete-existing-brain-reading-products/865> (visited on 08/14/2016).

- [41] Christoph Guger, Gunther Krausz, Brendan Z. Allison, and Guenter Edlinger. „Comparison of Dry and Gel Based Electrodes for P300 Brain–Computer Interfaces.” In: *Frontiers in Neuroscience* 6 (2012). DOI: [10.3389/fnins.2012.00060](https://doi.org/10.3389/fnins.2012.00060).
- [42] Femke Nijboer, Danny Plass-Oude Bos, Yvonne Blokland, René van Wijk, and Jason Farquhar. „Design requirements and potential target users for brain-computer interfaces – recommendations from rehabilitation professionals.” en. In: *Brain-Computer Interfaces* 1.1 (Jan. 2014), pp. 50–61. DOI: [10.1080/2326263X.2013.877210](https://doi.org/10.1080/2326263X.2013.877210).
- [43] Thomas C. Ferree, Phan Luu, Gerald S. Russell, and Don M. Tucker. „Scalp electrode impedance, infection risk, and EEG data quality.” In: *Clinical Neurophysiology* 112.3 (2001), pp. 536–544.
- [44] Ilkka Antero Hokajärvi. „Electrode contact impedance and biopotential signal quality.” PhD thesis. Tampere University of Technology, 2012.
- [45] J.F.M Molenbroek. *Op maat gemaakt*. Delft: Delftse Universitaire Pers, 1994.
- [46] Stephen Pheasant and Christine M. Haslegrave. *Bodyspace - Anthropometry, Ergonomics and the Design of Work*. Third Edition. United States of America: CRC Press, Taylor & Francis Group, 2006.
- [47] Peter R. M. Jones and Marc Rioux. „Three-dimensional Surface Anthropometry: Applications to the Human Body.” In: *Optics and Lasers in Engineering* 28 (1997), pp. 89–117.
- [48] International Ergonomics Association. *Definition and Domains of Ergonomics*. URL: <http://www.iea.cc/whats/index.html> (visited on 03/05/2017).
- [49] P Voskamp, P.A.M. van Scheijndel, and K.J. Peereboom, eds. *Handboek Ergonomie 2010*. Arbo. Alphen aan den Rijn: Kluwer, 2010.
- [50] Roger Ball. „SizeChina: a 3D anthropometric survey of the Chinese head.” English. PhD thesis. [Netherlands]: TUdelft, 2011.
- [51] *Anthropometric Source Book*. Vol. 1. NASA Scientific and Technical Information Office, 1978.
- [52] Blausen.com staff. *Blausen gallery 2014*. DOI: [10.15347/wjm/20014/010](https://doi.org/10.15347/wjm/20014/010). URL: [https://en.wikiversity.org/wiki/Wikiversity\\_Journal\\_of\\_Medicine/Medical\\_gallery\\_of\\_Blausen\\_Medical\\_2014](https://en.wikiversity.org/wiki/Wikiversity_Journal_of_Medicine/Medical_gallery_of_Blausen_Medical_2014) (visited on 07/28/2016).
- [53] Rudolf Martin. „Instrumentarium.” German. In: *Lehrbuch der Antropologie in Systematische Darstellung*. Vol. 1. Germany: Jena, 1928, pp. 122–137.

- [54] Kerstin Klipstein-Grobusch, Thomas Georg, and Heiner Boeing. „Interviewer variability in anthropometric measurements and estimates of body composition.” In: *International Journal of Epidemiology* 26.suppl 1 (1997), S174.
- [55] Stanley J. Ulijaszek and Deborah A. Kerr. „Anthropometric measurement error and the assessment of nutritional status.” In: *British Journal of Nutrition* 82.03 (1999), pp. 165–177.
- [56] Seth M. Weinberg, Nicole M. Scott, Katherine Neiswanger, and Mary L. Marazita. „Intraobserver error associated with measurements of the hand.” en. In: *American Journal of Human Biology* 17.3 (May 2005), pp. 368–371. DOI: [10.1002/ajhb.20129](https://doi.org/10.1002/ajhb.20129).
- [57] W.P. Yau, Anthony Leung, K.G. Liu, C.H. Yan, Lisa L.S. Wong, and K.Y. Chiu. „Interobserver and Intra-observer Errors in Obtaining Visually Selected Anatomical Landmarks During Registration Process in Non-Image-Based Navigation-Assisted Total Knee Arthroplasty.” en. In: *The Journal of Arthroplasty* 22.8 (Dec. 2007), pp. 1150–1161. DOI: [10.1016/j.arth.2006.10.010](https://doi.org/10.1016/j.arth.2006.10.010).
- [58] Ruben Beldé. „Anthropometrics 2.0.” Dutch. PhD thesis. University of Antwerp, 2013.
- [59] *Microscribe MX 3D Digitizer*. URL: <http://3d-microscribe.com/MX\%20Page.htm> (visited on 07/22/2016).
- [60] Kuang-Chao Fan, Fang Cheng, Weili Wang, Yejin Chen, and Jia-You Lin. „A scanning contact probe for a micro-coordinate measuring machine (CMM).” In: *Measurement Science and Technology* 21.5 (May 2010), p. 054002. DOI: [10.1088/0957-0233/21/5/054002](https://doi.org/10.1088/0957-0233/21/5/054002).
- [61] Karl Heinz Höhne and William A. Hanson. „Interactive 3D Segmentation of MRI and CT Volumes using Morphological Operations.” en. In: *Journal of Computer Assisted Tomography* 16.2 (Mar. 1992), pp. 285–294. DOI: [10.1097/00004728-199203000-00019](https://doi.org/10.1097/00004728-199203000-00019).
- [62] Wolfgang Boehler, Guido Heinz, and Andreas Marbs. „The potential of non-contact close range laser scanners for cultural heritage recording.” In: *International Archives of Photogrammetry, Remote Sensing, and Spatial Information Sciences* 34.5/C7 (2002), pp. 430–436.
- [63] CMPPC Rocchini, Paulo Cignoni, Claudio Montani, Paolo Pingi, and Roberto Scopigno. „A low cost 3 D scanner based on structured light.” In: *Computer Graphics Forum*. Vol. 20. 2001, pp. 299–308.
- [64] Godfrey N. Hounsfield. *Computed Medical Imaging (Nobel Lecture)*. 1979.

- [65] William Hollingworth, Christopher J. Todd, Matthew I. Bell, Qais Arafat, Simon Girling, Kanti R. Karia, and Adrian K. Dixon. „The Diagnostic and Therapeutic Impact of MRI: an Observational Multi-centre Study.” en. In: *Clinical Radiology* 55.11 (Nov. 2000), pp. 825–831. DOI: [10.1053/crad.2000.0546](https://doi.org/10.1053/crad.2000.0546).
- [66] Jan Ainali. *Philips MRI in Sahlgrenska Universitetsjukhuset, Gothenburg, Sweden*. Feb. 2008. URL: <https://commons.wikimedia.org/wiki/File:MRI-Philips.JPG> (visited on 07/29/2016).
- [67] *Creative Commons Legal Code - Attribution 3.0 Unported*. URL: <https://creativecommons.org/licenses/by/3.0/legalcode> (visited on 07/29/2016).
- [68] *3d Body Scanner - TC2labs*. URL: <http://www.tc2.com/tc2-19b-3d-body-scanner.html> (visited on 03/01/2017).
- [69] J. P. O. Evens, M. Robinson, S. X. Godber, and R. S. Petty. „The development of 3-D (stereoscopic) imaging systems for security applications.” In: *Security Technology, 1995. Proceedings. Institute of Electrical and Electronics Engineers 29th Annual 1995 International Carnahan Conference on*. IEEE, 1995, pp. 505–511.
- [70] Carrie L. Heike, Kristen Upson, Erik Stuhaug, and Seth M. Weinberg. „3D digital stereophotogrammetry: a practical guide to facial image acquisition.” In: *Head & face medicine* 6.1 (2010), p. 11.
- [71] *LONI Image Data Archive (IDA)*. URL: <https://ida.loni.usc.edu/login.jsp?project=ICBM> (visited on 04/25/2016).
- [72] *Open-Access Medical Image Repositories - aylward.org*. URL: <http://www.aylward.org/notes/open-access-medical-image-repositories> (visited on 07/22/2016).
- [73] C. E. McCulloch, B. Paal, and S. P. Ashdown. „An Optimisation Approach to Apparel Sizing.” In: *The Journal of the Operational Research Society* 49.5 (May 1998), p. 492. DOI: [10.2307/3009887](https://doi.org/10.2307/3009887).
- [74] C. Garneau and M. Parkinson. „Optimal product sizing through digital human models.” In: *Proc. of the SAE Digital Human Modeling Conferences*. 2008.
- [75] TU Delft. *DINED / Anthropometry in design*. URL: <http://dined.io.tudelft.nl/dined/full>.
- [76] J. M. Brewer, K. G. Davis, K. K. Dunning, and P. A. Succop. „Does ergonomic mismatch at school impact pain in school children?” In: *Work* 34.4 (2009), pp. 455–464.
- [77] James H. Gilmore and B. Joseph Pine. „The four faces of mass customization.” In: *Harvard business review* 75 (1997), pp. 91–101.

- [78] A. S. McIntosh, T. E. Andersen, R. Bahr, R. Greenwald, S. Kleiven, M. Turner, M. Varese, and P. McCrory. „Sports helmets now and in the future.” en. In: *British Journal of Sports Medicine* 45.16 (Dec. 2011), pp. 1258–1265. DOI: [10.1136/bjsports-2011-090509](https://doi.org/10.1136/bjsports-2011-090509).
- [79] Narayan Yoganandan and Frank A. Pintar. „Biomechanics of temporo-parietal skull fracture.” en. In: *Clinical Biomechanics* 19.3 (Mar. 2004), pp. 225–239. DOI: [10.1016/j.clinbiomech.2003.12.014](https://doi.org/10.1016/j.clinbiomech.2003.12.014).
- [80] Haiyan Li, Jesse Ruan, Zhonghua Xie, Hao Wang, and Wengling Liu. „Investigation of the critical geometric characteristics of living human skulls utilising medical image analysis techniques.” In: *International Journal of Vehicle Safety* 2.4 (2007), pp. 345–367.
- [81] Bart Depreitere, Carl Van Lierde, Jos Vander Sloten, Georges Van der Perre, Remy Van Audekercke, Christiaan Plets, and Jan Goffin. „Lateral Head Impacts and Protection of the Temporal Area by Bicycle Safety Helmets.” In: *The Journal of Trauma: Injury, Infection, and Critical Care* 62.6 (June 2007), pp. 1440–1445. DOI: [10.1097/01.ta.0000221472.68873.fb](https://doi.org/10.1097/01.ta.0000221472.68873.fb).
- [82] David R. Thom. „Comparison tests of motorcycle helmets qualified to international standards.” In: *Proceedings of the 2006 International Motorcycle Safety Conference*. 2006.
- [83] *Bicycle Helmet Standards*. URL: <http://www.bhsi.org/standard.htm> (visited on 07/22/2016).
- [84] Roger Ball. „3-D Design Tools from the SizeChina Project.” en. In: *Ergonomics in Design: The Quarterly of Human Factors Applications* 17.3 (July 2009), pp. 8–13. DOI: [10.1518/106480409X12487281219931](https://doi.org/10.1518/106480409X12487281219931).
- [85] K. M. Robinette and J. J. Whitestone. „The need for improved anthropometric methods for the development of helmet systems.” In: *Aviation, Space, and Environmental Medicine* (1994), pp. 95–99.
- [86] Pierre Meunier, David Tack, Angela Ricci, Linda Bossi, and Harry Angel. „Helmet accommodation analysis using 3D laser scanning.” In: *Applied Ergonomics* 31.4 (2000), pp. 361–369.
- [87] Charlie C.L. Wang. „Parameterization and parametric design of mannequins.” In: *Computer-Aided Design* 37.1 (Jan. 2005), pp. 83–98.
- [88] Nadia Magnenat-Thalmann, Hyewon Seo, and Frederic Cordier. „Automatic Modeling of Virtual Humans and Body Clothing.” In: *J. Comput. Sci. Technol.* 19.5 (Sept. 2004), pp. 575–584.
- [89] Brett Allen, Brian Curless, and Zoran Popović. „The space of human body shapes: reconstruction and parameterization from range scans.” In: *ACM Transactions on Graphics (TOG)*. Vol. 22. July 2003, 587–594.

- [90] Chih-Hsing Chu, Ya-Tien Tsai, Charlie C.L. Wang, and Tsz-Ho Kwok. „Exemplar-based statistical model for semantic parametric design of human body.” In: *Computers in Industry* 61.6 (Aug. 2010), pp. 541–549.
- [91] Seung-Yeob Baek and Kunwoo Lee. „Parametric human body shape modeling framework for human-centered product design.” In: *Computer-Aided Design* 44.1 (Jan. 2012), pp. 56–67.
- [92] Stefanie Wuhrer and Chang Shu. „Estimating 3D human shapes from measurements.” In: *Machine Vision and Applications* 24.6 (Dec. 2012), pp. 1133–1147.
- [93] Volker Blanz and Thomas Vetter. „A morphable model for the synthesis of 3D faces.” In: *Proceedings of the 26th annual conference on Computer graphics and interactive techniques*. 1999, 187–194.
- [94] Pengcheng Xi and Chang Shu. „Consistent parameterization and statistical analysis of human head scans.” In: *The Visual Computer* 25.9 (Mar. 2009), pp. 863–871.
- [95] Pierre Meunier and Shi Yin. „Performance of a 2D image-based anthropometric measurement and clothing sizing system.” In: *Applied Ergonomics* 31.5 (2000), pp. 445–451.
- [96] Jianwei Niu, Zhizhong Li, and Gavriel Salvendy. „Multi-resolution description of three-dimensional anthropometric data for design simplification.” In: *Applied Ergonomics* 40.4 (July 2009), pp. 807–810.
- [97] Pierre Meunier, Chang Shu, and Pengcheng Xi. „Revealing the internal structure of human variability for design purposes.” In: *Proceedings of the 17th World Congress on Ergonomics 2009*. 2009.
- [98] Ziqing Zhuang, Chang Shu, Pengcheng Xi, Michael Bergman, and Michael Joseph. „Head-and-face shape variations of U.S. civilian workers.” In: *Applied Ergonomics* 44.5 (Sept. 2013), pp. 775–784.
- [99] Yueh-Ling Lin and Mao-Jiun J. Wang. „Constructing 3D human model from front and side images.” In: *Expert Systems with Applications* 39 (2012), pp. 5012–5018.
- [100] Brendan Z. Allison, Stephen Dunne, Robert Leeb, José Del R. Millán, and Anton Nijholt. *Towards Practical Brain-Computer Interfaces, Bridging the Gap from Research to Real-World Applications*. Heidelberg: Springer, 2012.
- [101] Linda Capetillo-Cunliffe. *LONI: Laboratory of Neuro Imaging*. 2007.

- [102] Zhenhua Mai, Rudolf Hanel, Joost Batenburg, Marleen Verhoye, Paul Scheunders, and Jan Sijbers. „Bias field reduction by localized Lloyd-Max quantization.” In: *Magnetic Resonance Imaging* 29 (2011), pp. 536–545.
- [103] Michael B. Dillencourt, Hannan Samet, and Markku Tamminen. „A General Approach to Connected-Component Representations Labeling for Arbitrary Image Representations.” In: *Journal of the Association for Computing Machinery* 39.2 (Apr. 1992), pp. 253–280.
- [104] M Lepage and J C Gore. „Contrast mechanisms in magnetic resonance imaging.” In: *Journal of Physics: Conference Series* 3 (Jan. 2004), pp. 78–86.
- [105] Andrew Simmons, Paul S. Tofts, Gareth J. Barker, and Simon R. Arridge. „Sources of intensity nonuniformity in spin echo images at 1.5 T.” In: *Magnetic Resonance in Medicine* 32.1 (1994), 121–128.
- [106] Ron Kimmel and James A. Sethian. „Computing geodesic paths on manifolds.” In: *Proceedings of the National Academy of Sciences* 95.15 (1998), pp. 8431–8435.
- [107] Toon Huysmans, Jan Sijbers, and Verdonk Brigitte. „Automatic construction of correspondences for tubular surfaces.” In: *IEEE Transactions on Pattern Analysis and Machine Intelligence* 32.4 (2010), 636–651.
- [108] Michael S. Floater. „Parametrization and smooth approximation of surface triangulations.” In: *Computer-Aided Design* 14 (1997), pp. 231–250.
- [109] Michael S. Floater. „Mean value coordinates.” In: *Computer Aided Geometric Design* 20.1 (Mar. 2003), pp. 19–27.
- [110] Rudolf Martin and Karl Saller. *Lehrbuch der Anthropologie, in systematischer Darstellung*. Germany: Stuttgart, Fischer, 1957.
- [111] Yuan Cheng, Wee Kheng Leow, and Thiam Chye Lim. „Automatic identification of frankfurt plane and mid-sagittal plane of skull.” In: *Applications of Computer Vision (WACV), 2012 IEEE Workshop on*. IEEE, 2012, 233–238.
- [112] Makiko Kouchi, Masaaki Mochimaru, Kazuyo Tsuzuki, and Takashi Yokoi. „Interobserver Errors in Anthropometry.” In: *Journal of Human Ergol.* 28 (1999), pp. 15–24.
- [113] Makiko Kouchi and Masaaki Mochimaru. „Errors in landmarking and the evaluation of the accuracy of traditional and 3D anthropometry.” In: *Applied Ergonomics* 42.3 (Mar. 2011), pp. 518–527.

- [114] A. Yu, K.L. Yick, S.P. Ng, and J. Yip. „2D and 3D anatomical analyses of hand dimensions for custom-made gloves.” In: *Applied Ergonomics* 44.3 (May 2013), pp. 381–392.
- [115] Domenico Formica and Sergio Silvestri. „Biological effects of exposure to magnetic resonance imaging an overview.” In: *BioMedical Engineering OnLine* (Apr. 2004).
- [116] Roger Ball, Chang Shu, Pengcheng Xi, Marc Rioux, Yan Luximon, and Johan Molenbroek. „A comparison between Chinese and Caucasian head shapes.” In: *Applied Ergonomics* 41.6 (Oct. 2010), pp. 832–839.
- [117] G.H. Golub and Van Loan. C.F. *Matrix Computations*, 3rd ed. Baltimore: Johns Hopkins, 1996.
- [118] Z. Zhuang, D. Landsittel, S. Benson, R. Roberge, and R. Shaffer. „Facial Anthropometric Differences among Gender, Ethnicity, and Age Groups.” In: *Annals of Occupational Hygiene* 54.4 (June 2010), pp. 391–402.
- [119] Matthew K. Lee, Osamu Sakai, and Jeffrey H. Spiegel. „CT measurement of the frontal sinus – Gender differences and implications for frontal cranioplasty.” In: *Journal of Cranio-Maxillofacial Surgery* 38.7 (Oct. 2010), pp. 494–500.
- [120] Ese Anibor, Dennis EO Eboh, and Mabel O. Etetafia. „A study of craniofacial parameters and total body height.” In: *Pelagia Research Library, Advances in Applied Science Research* 2 (2011), pp. 400–405.
- [121] P Brunner, I Bianchi, C Guger, F Cincotti, and G Schalk. „Current trends in hardware and software for brain-computer interfaces (BCIs).” In: *Journal of Neural Engineering* 8 (Mar. 2011), 7pp.
- [122] Dassault Systèmes SOLIDWORKS Corp. *3D CAD Design Software SolidWorks*. 2014.
- [123] Naomi Christis. „Anthropometrics 2.0.” PhD thesis. Universiteit Antwerpen, 2013.
- [124] Robert Oostenveld and Peter Praamstra. „The five percent electrode system for high-resolution EEG and ERP measurements.” In: *Clinical neurophysiology* 112.4 (2001), 713–719.
- [125] Michal Teplan. „Fundamentals of EEG measurement.” In: *Measurement science review* 2.2 (2002), pp. 1–11.
- [126] Cornelia Kranczioch, Catharina Zich, Irina Schierholz, and Annette Sterr. „Mobile EEG and its potential to promote the theory and application of imagery-based motor rehabilitation.” en. In: *International Journal of Psychophysiology* 91.1 (Jan. 2014), pp. 10–15. ISSN: 01678760. DOI: [10.1016/j.ijpsycho.2013.10.004](https://doi.org/10.1016/j.ijpsycho.2013.10.004). (Visited on 07/03/2015).

- [127] Christian Mühl, Brendan Allison, Anton Nijholt, and Guillaume Chanel. „A survey of affective brain computer interfaces: principles, state-of-the-art, and challenges.” en. In: *Brain-Computer Interfaces* 1.2 (Apr. 2014), pp. 66–84. DOI: [10.1080/2326263X.2014.912881](https://doi.org/10.1080/2326263X.2014.912881).
- [128] Vernon L. Towle, José Bolaños, Diane Suarez, Kim Tan, Robert Grzeszczuk, David N. Levin, Raif Cakmur, Samuel A. Frank, and Jean-Paul Spire. „The spatial location of EEG electrodes: locating the best-fitting sphere relative to cortical anatomy.” In: *Electroencephalography and clinical Neurophysiology* 86 (1993), pp. 1–6.
- [129] „Guideline 5: Guidelines for Standard Electrode Position Nomenclature.” In: *American Journal of Electroneurodiagnostic Technology* 46.3 (2006), pp. 222–225. DOI: [10.1080/1086508X.2006.11079580](https://doi.org/10.1080/1086508X.2006.11079580).
- [130] Emotiv. *Emotiv Epoc User Manual*. [https://emotiv.zendesk.com/hc/en-us/article\\_attachments/200343895/EPOCUserManual2014.pdf](https://emotiv.zendesk.com/hc/en-us/article_attachments/200343895/EPOCUserManual2014.pdf).
- [131] Jianwei Niu and Zhizhong Li. „Using Three-Dimensional (3D) Anthropometric Data in Design.” en. In: *Handbook of Anthropometry*. Ed. by Victor R. Preedy. New York, NY: Springer New York, 2012, pp. 3001–3013. ISBN: 978-1-4419-1787-4 978-1-4419-1788-1. (Visited on 07/20/2015).
- [132] J. Chang, K. Jung, J. Hwang, Y. Kang, S. Lee, and A. Freivalds. „Determination of Bicycle Handle Diameters considering Hand Anthropometric Data and User Satisfaction.” en. In: *Proceedings of the Human Factors and Ergonomics Society Annual Meeting* 54.20 (Sept. 2010), pp. 1790–1793. DOI: [10.1177/154193121005402010](https://doi.org/10.1177/154193121005402010).
- [133] Ameersing Luximon, Yifan Zhang, Yan Luximon, and Ma Xiao. „Sizing and grading for wearable products.” en. In: *Computer-Aided Design* 44.1 (Jan. 2012), pp. 77–84. DOI: [10.1016/j.cad.2011.07.004](https://doi.org/10.1016/j.cad.2011.07.004).
- [134] Mercedes de Onis, Adelheid W. Onyango, Jan Van den Broeck, Wm. Cameron Chumlea, and Reynaldo Martorell. „Measurement and standardization protocols for anthropometry used in the construction of a new international growth reference.” In: *Food and Nutrition Bulletin* 25.1 (2004), S27–S36.
- [135] Daniël Lacko, Toon Huysmans, Paul M. Parizel, Guido De Bruyne, Stijn Verwulgen, Marc M. Van Hulle, and Jan Sijbers. „Evaluation of an anthropometric shape model of the human scalp.” en. In: *Applied Ergonomics* 48 (May 2015), pp. 70–85. ISSN: 00036870. DOI: [10.1016/j.apergo.2014.11.008](https://doi.org/10.1016/j.apergo.2014.11.008).

- [136] Yong-Jin Liu, Dong-Liang Zhang, and Matthew Ming-Fai Yuen. „A survey on CAD methods in 3D garment design.” en. In: *Computers in Industry* 61.6 (Aug. 2010), pp. 576–593. ISSN: 01663615. DOI: [10.1016/j.compind.2010.03.007](https://doi.org/10.1016/j.compind.2010.03.007).
- [137] Chang Shu, Pengcheng Xi, Zouhour Ben Azouz, and Pierre Meunier. „Geometry processing and statistical shape analysis of 3-D anthropometry data.” In: *Proceedings of the 17th World Congress on Ergonomics*. 2009.
- [138] Hong Liu, Zhizhong Li, and Li Zheng. „Rapid preliminary helmet shell design based on three-dimensional anthropometric head data.” en. In: *Journal of Engineering Design* 19.1 (Feb. 2008), pp. 45–54. ISSN: 0954-4828, 1466-1837. DOI: [10.1080/09544820601186088](https://doi.org/10.1080/09544820601186088). (Visited on 06/03/2015).
- [139] Chih-Hsing Chu, Szu-Hao Huang, Chih-Kai Yang, and Chun-Yang Tseng. „Design customization of respiratory mask based on 3D face anthropometric data.” en. In: *International Journal of Precision Engineering and Manufacturing* 16.3 (Mar. 2015), pp. 487–494. ISSN: 2234-7593, 2005-4602. DOI: [10.1007/s12541-015-0066-5](https://doi.org/10.1007/s12541-015-0066-5).
- [140] Vincent G. Duffy, ed. *Digital human modeling: second international conference, ICDHM 2009*. Lecture notes in computer science 5620. Berlin; New York: Springer, July 2009. ISBN: 978-3-642-02808-3.
- [141] William Trochim. *The Research Methods Knowledge Base, 2nd Edition*. <http://www.socialresearchmethods.net/kb/>. 2006.
- [142] Vernon L. Towle, José Bolaños, Diane Suarez, Kim Tan, Robert Grzeszczuk, David N. Levin, Raif Cakmur, Samuel A. Frank, and Jean-Paul Spire. „The spatial location of EEG electrodes: locating the best-fitting sphere relative to cortical anatomy.” In: *Electroencephalography and Clinical Neurophysiology* 86.1 (1993), pp. 1–6. ISSN: 0013-4694. DOI: [http://dx.doi.org/10.1016/0013-4694\(93\)90061-Y](http://dx.doi.org/10.1016/0013-4694(93)90061-Y).
- [143] Robert McNeel and Associates. *Rhinoceros*. <http://www.rhino3d.com/>.
- [144] Hervé Abdi and Lynne J. Williams. „Principal component analysis.” en. In: *Wiley Interdisciplinary Reviews: Computational Statistics* 2.4 (2010), pp. 433–459. ISSN: 19395108. DOI: [10.1002/wics.101](https://doi.org/10.1002/wics.101).
- [145] Yan Luximon, Roger Ball, and Lorraine Justice. „The 3D Chinese head and face modeling.” en. In: *Computer-Aided Design* 44.1 (Jan. 2012), pp. 40–47. DOI: [10.1016/j.cad.2011.01.011](https://doi.org/10.1016/j.cad.2011.01.011).

- [146] Seung-Yeob Baek and Kunwoo Lee. „Parametric human body shape modeling framework for human-centered product design.” en. In: *Computer-Aided Design* 44.1 (Jan. 2012), pp. 56–67. ISSN: 00104485. DOI: [10.1016/j.cad.2010.12.006](https://doi.org/10.1016/j.cad.2010.12.006).
- [147] Stefanie Wuhrer, Chang Shu, and Prosenjit Bose. „Automatically creating design models from 3D anthropometry data.” In: *Journal of Computing and Information Science in Engineering* 12.4 (2012), p. 041007.
- [148] Dorit S. Hochbaum and Wolfgang Maass. „Approximation schemes for covering and packing problems in image processing and VLSI.” In: *Journal of the ACM (JACM)* 32.1 (1985), pp. 130–136.
- [149] Dorit S. Hochbaum and Wolfgang Maass. „Fast Approximation Algorithms for a Nonconvex Covering Problem.” In: *Journal of Algorithms* 8 (1987), pp. 305–323.
- [150] Jianwei Niu, Zhizhong Li, and Song Xu. „Block Division for 3D Head Shape Clustering.” In: *Digital Human Modeling*. Springer, 2009, pp. 64–71. (Visited on 01/19/2016).
- [151] Jianwei Niu, Zhizhong Li, and Gavriel Salvendy. „Multi-resolution shape description and clustering of three-dimensional head data.” en. In: *Ergonomics* 52.2 (Feb. 2009), pp. 251–269. DOI: [10.1080/00140130802334561](https://doi.org/10.1080/00140130802334561).
- [152] Jianwei Niu, Zhizhong Li, and Gavriel Salvendy. „Multi-resolution shape description and clustering of three-dimensional head data.” en. In: *Ergonomics* 52.2 (Feb. 2009), pp. 251–269. ISSN: 0014-0139, 1366-5847. DOI: [10.1080/00140130802334561](https://doi.org/10.1080/00140130802334561).
- [153] Seung-Yeob Baek and Kunwoo Lee. „Statistical foot-shape analysis for mass-customisation of footwear.” In: *International Journal of Computer Aided Engineering and Technology* 8.1-2 (2016), pp. 80–98.
- [154] Peter Hammond, Tim J. Hutton, Judith E. Allanson, Bernard Buxton, Linda E. Campbell, Jill Clayton-Smith, Dian Donnai, Annette Karmiloff-Smith, Kay Metcalfe, Kieran C. Murphy, and others. „Discriminating power of localized three-dimensional facial morphology.” In: *The American Journal of Human Genetics* 77.6 (2005), pp. 999–1010. URL: <http://www.sciencedirect.com/science/article/pii/S0002929707633849>.
- [155] Chih-Hsing Chu, Ya-Tien Tsai, Charlie C.L. Wang, and Tsz-Ho Kwok. „Exemplar-based statistical model for semantic parametric design of human body.” en. In: *Computers in Industry* 61.6 (Aug. 2010), pp. 541–549. ISSN: 01663615. DOI: [10.1016/j.compind.2010.03.004](https://doi.org/10.1016/j.compind.2010.03.004).
- [156] M.P. Reed, U. Raschke, R. Tirumali, and M.B. Parkinson. „Developing and implementing parametric human body shape models in ergonomics software.” In: 2014.

- [157] L.T. Jolliffe. *Principal Component Analysis*. 2nd ed. Springer, 2002.
- [158] Hae-Sang Park and Chi-Hyuck Jun. „A simple and fast algorithm for K-medoids clustering.” en. In: *Expert Systems with Applications* 36.2 (Mar. 2009), pp. 3336–3341. ISSN: 09574174. DOI: [10.1016/j.eswa.2008.01.039](https://doi.org/10.1016/j.eswa.2008.01.039).
- [159] Christian Bauckhage. *Numpy/scipy Recipes for Data Science: k-Medoids Clustering*. Tech. rep. Technical Report, University of Bonn, 2015. URL: [https://www.researchgate.net/profile/Christian\\_Bauckhage/publication/272351873\\_NumPy\\_SciPy\\_Recipes\\_for\\_Data\\_Science\\_k-Medoids\\_Clustering/links/54e244d10cf29666379649bc.pdf](https://www.researchgate.net/profile/Christian_Bauckhage/publication/272351873_NumPy_SciPy_Recipes_for_Data_Science_k-Medoids_Clustering/links/54e244d10cf29666379649bc.pdf) (visited on 12/19/2016).
- [160] Siddheswar Ray and Rose H. Turi. „Determination of number of clusters in k-means clustering and application in colour image segmentation.” In: *Proceedings of the 4th international conference on advances in pattern recognition and digital techniques*. India, 1999, pp. 137–143.
- [161] Bernard Desgraupes. „Clustering Indices.” In: *University of Paris Ouest-Lab Modal'X* (2013), pp. 1–34. URL: <ftp://apache.cs.uu.nl/mirror/CRAN/web/packages/clusterCrit/vignettes/clusterCrit.pdf> (visited on 10/06/2015).
- [162] „Continuous Saturation of Curved Surfaces.” In: *IEEE Transactions on Computers* 20.6 (1971).
- [163] *ISO20685: 3-D scanning methodologies for internationally compatible anthropometric databases*. 2010. URL: <http://www.518578.com/Doc/WebNote/201104/Y2011M04D25H12m18s57/bs20iso2010298-201020u6C14u4F53u6216u6DF7u5408u6C14u4F53u7684u6BD2u6027u6D4Bu5B9A.pdf> (visited on 08/03/2016).
- [164] Claire C. Gordon, Thomas Churchill, Charles E. Clauser, Bruce Bradtmiller, and John T. McConville. *Anthropometric survey of US army personnel: methods and summary statistics 1988*. Tech. rep. DTIC Document, 1989.
- [165] Ziqing Zhuang and Bruce Bradtmiller. „Head-and-Face Anthropometric Survey of U.S. Respirator Users.” en. In: *Journal of Occupational and Environmental Hygiene* 2.11 (Nov. 2005), pp. 567–576. DOI: [10.1080/15459620500324727](https://doi.org/10.1080/15459620500324727).
- [166] R. Motmans. *DINBelg 2005 - anthropometry table*. URL: <http://www.dinbelg.be/anthropometry.htm>.
- [167] Yuewei Liu, Pengcheng Xi, Michael Joseph, Ziqing Zhuang, Chang Shu, Luman Jiang, Michael Bergman, and Weihong Chen. „Variations in Head-and-Face Shape of Chinese Civilian Workers.” en. In: *Annals of Occupational Hygiene* 59.7 (Aug. 2015), pp. 932–944. DOI: [10.1093/annhyg/mev026](https://doi.org/10.1093/annhyg/mev026).

- [168] M. Jahanshahi, M. J. Golalipour, and K. Heidari. „The effect of ethnicity on facial anthropometry in Northern Iran.” In: *Singapore medical journal* 49.11 (2008), p. 940.
- [169] Ziqing Zhuang, Douglas Langsittel, Stacey Benson, and Ronald Roberge Raymond an Shaffer. „Facial Anthropometric Differences among Gender, Ethnicity, and Age Groups.” In: *The Annals of Occupational Hygiene* (Mar. 2010). DOI: [10.1093/annhyg/meq007](https://doi.org/10.1093/annhyg/meq007).
- [170] Leonard S. Mark, John B. Pittenger, Helen Hines, Claudia Carello, Robert E. Shaw, and James T. Todd. „Wrinkling and head shape as coordinated sources of age-level information.” In: *Perception & Psychophysics* 27.2 (1980), pp. 117–124.
- [171] April J. Chambers, Alison L. Sukits, Jean L. McCrory, and Rakié Cham. „The effect of obesity and gender on body segment parameters in older adults.” en. In: *Clinical Biomechanics* 25.2 (Feb. 2010), pp. 131–136. DOI: [10.1016/j.clinbiomech.2009.10.015](https://doi.org/10.1016/j.clinbiomech.2009.10.015).
- [172] N.F.M. Roozenburg and J. Eekels. *Productontwerpen, structuur en methoden*. Dutch. Boom Lemma Uitgevers, 2002. ISBN: 978-90-5189-706-7.
- [173] Eva Xantippe Plaetinck. „HelmAid: verbetering fysiek comfort van fietshelmen.” PhD thesis. University of Antwerp, 2016.
- [174] Laureen Ratinckx. „Geoptimaliseerd zuurstofmasker bestemd voor pateiënten met een discontinue zuurstoftoediening.” PhD thesis. University of Antwerp, 2016.
- [175] Alper Comert, Markku Honkala, and Jari Hyttinen. „Effect of pressure and padding on motion artifact of textile electrodes.” In: *Biomedical engineering online* 12.1 (2013), p. 1.
- [176] P. Salvo, R. Raedt, E. Carrette, D. Schaubroeck, J. Vanfleteren, and L. Cardon. „A 3D printed dry electrode for ECG/EEG recording.” In: *Sensors and Actuators A: Physical* 174 (Feb. 2012), pp. 96–102. DOI: [10.1016/j.sna.2011.12.017](https://doi.org/10.1016/j.sna.2011.12.017).
- [177] Catharina Zich, Maarten De Vos, Cornelia Kranczioch, and Stefan Debener. „Wireless EEG with individualized channel layout enables efficient motor imagery training.” In: *Clinical Neurophysiology* 126.4 (Apr. 2015), pp. 698–710. DOI: [10.1016/j.clinph.2014.07.007](https://doi.org/10.1016/j.clinph.2014.07.007).
- [178] Scott E. Kerick, Kelvin S. Oie, and Kaleb McDowell. *Assessment of EEG signal quality in motion environments*. Tech. rep. DTIC, 2009.

- [179] Arthur C. Grant, Samah G. Abdel-Baki, Ahmet Omurtag, Richard Sinert, Geetha Chari, Schweta Malhotra, Jeremy Weedon, Andre A. Fenton, and Shahriar Zehtabchi. „Diagnostic accuracy of microEEG: A miniature, wireless EEG device.” en. In: *Epilepsy & Behavior* 34 (May 2014), pp. 81–85. DOI: [10.1016/j.yebeh.2014.03.015](https://doi.org/10.1016/j.yebeh.2014.03.015).
- [180] Rebeca Corralejo, Luis F. Nicolás-Alonso, Daniel Álvarez, and Roberto Hornero. „A P300-based brain–computer interface aimed at operating electronic devices at home for severely disabled people.” en. In: *Medical & Biological Engineering & Computing* 52.10 (Oct. 2014), pp. 861–872. DOI: [10.1007/s11517-014-1191-5](https://doi.org/10.1007/s11517-014-1191-5).
- [181] CADANS - Computer-aided design plugin for 3D statistic anthropometric design. URL: <http://cadans.uantwerpen.be/> (visited on 07/22/2016).



## COLOPHON

This document was typeset using the typographical look-and-feel `classicthesis` developed by André Miede. The style was inspired by Robert Bringhurst's seminal book on typography "*The Elements of Typographic Style*". `classicthesis` is available for both  $\text{\LaTeX}$  and  $\text{\LyX}$ :

<https://bitbucket.org/amiede/classicthesis/>

Happy users of `classicthesis` usually send a real postcard to the author, a collection of postcards received so far is featured here:

<http://postcards.miede.de/>

*Final Version* as of March 6, 2017 (`classicthesis` version 0.1).